Application of Advanced Linear Algebra Techniques to Array Signal Processing

博 士 学 位 論 文

Doctoral Dissertation

Application of Advanced Linear Algebra Techniques

to Array Signal Processing

（先進的な線形代数のアレイ信号処理への応用に関する研究）

東北大学大学院環境科学研究科

Graduate School of Environmental Studies, Tohoku University

Department of Environmental Studies for Advanced Society	**専攻** major / **コース** course
学籍番号 Student ID No.	C0GD1505
氏　名 Name	周　昶宇

指　導　教　員 Supervisor at Tohoku Univ.	Professor SATO Motoyuki	
研 究 指 導 教 員 Research Advisor at Tohoku Univ.		
審　査　委　員 （○印は主査） Dissertation Committee Members Name marked with “○” is the Chief Examiner	○ Professor SATO Motoyuki	
	1 Professor TAKAHASHI Hiroshi	2 Professor OKAMOTO Atsushi
	3 Professor CHEN Qiang (Graduate School of Engineering)	4 Professor YAMADA Hiroyoshi (Niigata University)

Ph.D. Thesis

Application of Advanced Linear Algebra Techniques to Array Signal Processing
先進的な線形代数のアレイ信号処理への応用に関する研究

Submitted to
Graduate School of Environmental Studies
Tohoku University

by

周 昶宇
Changyu Zhou

C0GD1505

Supervised by

Prof. Motoyuki Sato

Dissertation committee:

Prof. Hiroshi Takahashi

Prof. Atsushi Okamoto

Prof. Qiang Chen

Prof. Hiroyoshi Yamada

Abstract

Array signal processing has a rich history that dates back to a century ago. Despite its long-standing existence, the demand for its study has only increased due to the need for continuous development in multiple fields. The objective of this work is to enhance the existing subspace method in array signal processing to tackle two significant problems. Firstly, compensating for the arrival time and phase errors. Secondly, reducing complexity for certain subspace techniques. These issues pose a challenge for accurate signal processing and require novel solutions to achieve optimal results. Therefore, the proposed improvements to the subspace method will contribute to the advancement of array signal processing and its applications in various domains.

To solve the first problem, this work uses an enumeration to process all possible combinations of the arrival time from each channel. Then, near field MUltiple SIgnal Classification (MUSIC) algorithms are used to generate super-resolution spectra, where the data with fewer phase errors will have much more focused results than others. This method has obvious advantages and disadvantages; the advantage is that the hidden information can be revealed, and the accuracy of the proposed method is much higher than the conventional method. However, because all the stationary points are considered to be related to the possible arrival time, the computation complexity is extremely high. Thus, the second problem appears. To tackle this problem, optimization techniques are applied to replace the two-dimensional scan process in the near field MUSIC into gradient based optimization.

Besides, the work discussed advanced matrix decomposition Generalized Singular Value Decomposition (GSVD),and Generalized EigenValue Decomposition(GEVD) as possible alternative approaches for the first problem. In addition, the resolution of the near field MUSIC is discussed. The calculation shows that , under the assumptions this work made, the resolution has no upper limit if the arrival time information is precisely evaluated. Thus, it has great potential that super-resolution imaging can be achieved by using relatively weaker hardware platform, as proof, we bring an SDR array experiment to verify the idea, which shows the feasibility of the study.

This work also introduced a modified near field Estimation of Signal Parameters via Rotational Invariant Technique (ESPRIT), unlike previous studies, the work focuses on the Least Square (LS) method, and reconstruct the problem from the non-constrained optimizations to the constrained ones. The Lagrange multiplier is introduced to solve the Total Least Square(TLS) based ESPRIT for the special linear system caused by the error in the covariance matrix. A classical sphere reflector experiment is conducted and the results show that the proposed method is more efficient and accurate than SAR imaging in terms of localization purposes.

In the last part, this work continues the constrained optimization techniques mentioned previously, presenting subspace tracking techniques. This work introduces a recent trending technique, low-rank matrix recovery to solve the conventional subspace tracking problem for the DOA estimation. Because the kernel iterations of the ALM based low rank matrix recovery process is similar to the subspace tracking. Numerical simulations are carried out, and they show the potential of the ALM-based algorithm. Besides, as a bonus work, we use edge detection techniques to reduce the rank of the GPR profile, and it allows the implementation of the proposed method not only for the array signal processing but for more universal uses.

Keywords: Direction Of Arrival (DOA), Multiple Signal Classification (MUSIC), Estimation of Signal Parameters via Rotational Invariant Technique (ESPRIT), Subspace tracking, GPR, RF localization, low-rank matrix recovery, Optimization.

Table of contents

List of Figures

List of Tables

List of Abbreviations

Augmented Lagrange Multiplier:	ALM
Conventional Beam Forming:	CBF
Direction Of Arrival:	DOA
Estimation of Signal Parameters via Rotational Invariance Techniques:	ESPRIT
Gradient Descent:	GD
Incoherent Signal Subspace method:	ISSM
Karush–Kuhn–Tucker:	KKT
Least Square:	LS
Minimum Mean Square Error:	MMSE
Multiple Input Multiple Output:	MIMO
MUltiple SIgnal Classification:	MUSIC
Hybrid Beamforming:	HB
Spatial Covariance matrix:	SCM
Total Least Square:	TLS

Chapter 1 Introduction

1.1 Research background

A linear array radar system is a type of radar system that uses a linear array of antenna elements to transmit and receive electromagnetic signals. These systems are used in various applications, including infrastructure engineering, archaeology science, and military surveillance [1~5].

In a linear array radar system, the antenna elements are arranged in a straight line. Initially, the design aims to transmit a focused signal beam that could be directed in a specific direction. Many may think linear array radar systems have the capability of high resolution and accuracy, making them well-suited for various applications [6][7]. However, the systems can only partially determine the resolution and accuracy capability; the algorithm is also a significant part that contributes to the results. In speaking of the algorithm, this work emphasizes the Direction Of Arrival (DOA) estimation. DOA estimation is a technique used to determine the direction from which a signal arrives at a sensor or array of sensors, which is used in many kinds of fields, including radar, sonar, wireless communication, and speech processing [7~12].

There are three main approaches to estimating the DOA of a signal, including beamforming, Multiple Signal Classification (MUSIC), Estimation of Signal Parameters via Rotational Invariance Techniques (ESPRIT), and others. These methods originally and typically involve linear array systems to achieve better performance by utilizing all elements of the systems rather than one. In the next few sections, a short history of these methods is briefly reviewed.

1.2 History of beamforming

Beamforming is a classical approach to solving DOA problems. It is a technique used to steer a beam of electromagnetic waves in a specific direction. It has a long history dating back to the early days of radar and radio communications. One of the earliest forms of beamforming was using mechanically steerable antenna arrays, which used motors or other mechanical devices to move the antenna elements to steer the beam physically. This type of beamforming was used extensively during World War II in radar systems to detect enemy aircraft.

In the 1950s and 60s, electronic beamforming techniques began to be developed, which used electronic circuitry to adjust the phase of the signals transmitted by each antenna element to steer the beam. These techniques allowed for much more agile and precise beam steering and are still widely used today [13][14]. More recently, advances in digital signal processing have led to the development of digital beamforming techniques, which use software algorithms to adjust the phase and amplitude of the transmitted signals to steer the beam. These techniques are widely used in modern radar and communication systems. The resolution of the conventional beamforming technique is not satisfactory in some cases; thus, many developments have been made to it. Nowadays, modern beamforming techniques are not a bad option for some DOA purposes that require high resolution and some times better approach among all solutions[16~18].

1.3 History of subspace methods

The Subspace method basically contains three parts. The first one is MUSIC and its variant. The studies have been made since 1975. Schmidt, Van Loan and Speiser raised and gave many modifications to the original MUSIC [19~21]. Mathematically, the MUSIC algorithm works by calculating the eigenvectors of the covariance matrix of the received signals at the antenna array. These eigenvectors correspond to the signal subspaces of the received signals, and particular operations can estimate the DOA of the signals. One of the key advantages of the MUSIC algorithm is that it can provide very high-resolution DOA estimates, even in the presence of noise and interference. It is also relatively simple to implement, contributing to its widespread use in many fields.

The second part is about ESPRIT methods; different from the MUSIC, ESPRIT methods directly use the Eigen Value Decomposition (EVD), Singular Value Decomposition (SVD) or Generalized Value Decomposition (GSVD) to present solutions to the unknown parameters in the rotation matrix. ESPRIT is around 40 years old. It was developed in the 1980s and is a widely used method for DOA estimation [22,23]. Mathematically, the ESPRIT algorithm works by diagonalizing the results from the covariance matrices of the subarrays of the system.

The third one is called subspace tracking. The idea is to use some matrix operations, especially decomposition techniques, to renew the subspaces iteratively. One of the earliest subspace tracking algorithms was developed by E. Oja in the 1980s [23]. The method is developed in the 1980s and 1990s, building on earlier work in the field of subspace methods for signal processing[24,25]. Several different subspace tracking algorithms have been developed over the years, including the R-Method, the Adaptive Space-Time Processing (STAP) algorithm, the Projection-Approximation Subspace Tracking (PAST) algorithm, and others[24,26]. The idea is to use some matrix operations, especially decomposition techniques, to renew the subspaces iteratively.

1.4 Motivations and novelties

Significant progress has been made in linear array signal processing, especially, for DOA purposes, an increasing number and complexity of research have been conducted in recent years. However, there are still questions and challenges that need to be addressed. In particular, applying these subtle algorithms to some hardware with limitations has attracted attention. Because most of the algorithms are too abstract and can hardly be implemented in accessible systems. However, current approaches to studying [specific topic] have several limitations that prevent further advancement.

This dissertation address some of these limitations and tries to contribute to the field by using some mathematical technologies. The research is motivated by the belief that advanced linear algebra techniques such as matrix decomposition, and linear optimization can handle the input data with noise and be applied to the hardware platform under certain conditions that can be relatively easily achieved practically.

In addition to its practical significance, this work is also motivated by the theoretical importance following the previous study on the far field of DOA. By summarizing and extracting the current literature, this dissertation attempts to rephrase the theoretical understanding of DOA algorithms to the near field form.

The novelty of this dissertation can be considered as the following two aspects: first, it provides a novel approach to solving the problem of near field localization problem by using technologies with less computational complexity.

Second, In this work, proposed algorithms have been tested on a wide range of data sets; some have consistently outperformed existing methods in accuracy and efficiency. However, some other algorithms are theoretically proven accurate but need to be adjusted accordingly to achieve the full implementation in the experimental condition. We can shed light on the underlying factors contributing to the algorithm's effectiveness and provide insights into how it can be further improved.

Overall, this dissertation contributes to developing the near field DOA estimation by providing some solutions to the existing problems and trying to involve multiple kinds of factors that influence the performance of this solution.

1.5 Structure of thesis

This work is organized as follows:

Chapter 2 introduces the basic mathematical knowledge required for the later chapters. In addition, many assumptions are made to ensure the proposed algorithm is self-consistent. This chapter gives a brief introduction to the phase error problem that we will encounter in the next few chapters.

Chapter 3 is a brief introduction to modern beamforming. The chapter describes some advanced beamforming techniques, revealing that the border between the beamforming and subspace methods has been blurred in the last half-century. Using such approaches as covariance matrices, optimization and eigenvalue decompositions are no more uniquely used in the subspace methods. Thus, the chapter is presented, even though this work is not emphasizing the beamforming problems.

Chapter 4 studies the near field of MUSIC and its variants. As we know some of the universal approaches to solve the DOA problems in the last chapter in the far field, this chapter transforms the far field problem into a near field one, and then tries to reduce the computational load by using music algorithm and its variants. Computation acceleration is so emphasized because we are using local maxima as a judgment for computers. Almost all of the combinations of different maxima of different channels will be the input for the enumeration which generates a tremendous amount of loops in code, where near field MUSIC itself is an O(2) complexity algorithm. Besides, avoiding manual arrival time selection is essential in this study, as the experiments show that under the high attenuation condition, the arrival time decided by the bare eye and the global maxima judgment is no longer reliable.

Chapter 5 can be considered as an extensional study of Chapter 4; though we name the method ESPRIT the kernel step is still as same as the MUSIC. However, this chapter introduces the least square problem for

solving the linear system; the constrained optimization problem is introduced in this chapter. and we also move our focus from the GPR cases to a classical and experimental MIMO system localization.

Chapter 6 is a fundamental study of the subspace tracking method for linear array DOA estimation. However, the conventional method could be better-suited to our cases, thus, low-ranked matrix-related algorithms are applied. This kind of algorithm was trending around 15 years ago and achieved significant success in the imaging process research; however, it is not heavily used in GPR signal processing for many reasons. Moreover, as an extension, this chapter also offers an idea for handling GPR profiles (might not be array signals) by using the proposed techniques.

References

[1] L. Yi, L. Zou, K. Takahashi and M. Sato, "High-Resolution Velocity Analysis Method Using the ℓ-1 Norm Regularized Least-Squares Method for Pavement Inspection," *in IEEE J. Sel. Top Appl Earth Obs Remote Sens.*, vol. 11, no. 3, pp. 1005-1015, March 2018.

[2] L. Yi, K. Takahashi and M. Sato, "Large-scale subsurface velocity estimation with Yakumo GPR array system," in *URSI Radio Sci. Bull.*, vol. 2016, no. 356, pp. 24-31, March 2016.

[3] L. Zou, L. Yi and M. Sato, "On the Use of Lateral Wave for the Interlayer Debonding Detecting in an Asphalt Airport Pavement Using a Multistatic GPR System," *in IEEE Trans. Geosci. Remote Sens.*, vol. 58, no. 6, pp. 4215-4224, June 2020 .

[4] D. J. Daniels, Ed., Ground Penetrating Radar, 2nd ed. London, U.K.: Inst. Electr. Eng., 2004.

[5] X. Feng and M. Sato, "Pre-stack migration applied to GPR for landmine detection," in *Inv. Probl*., vol. 20, no. 6, pp. S99–S115, Dec. 2004.

[6] H. Cox, R. Zeskind and M. Owen, "Robust adaptive beamforming," in *IEEE Trans. Acoust. Speech Signal Process*., vol. 35, no. 10, pp. 1365-1376, Oct. 1987.

[7] P. Stoica and A. Nehorai, "MUSIC, maximum likelihood, and Cramer-Rao bound," in *IEEE Trans. Acoust. Speech Signal Process.,* vol. 37, no. 5, pp. 720-741, May 1989.

[8] L. C. Godara, "Application of antenna arrays to mobile communications. II. Beam-forming and direction-of-arrival considerations," *Proc. of the IEEE,* vol. 85, no. 8, pp. 1195-1245, Aug. 1997.

[9] P. Pal and P. P. Vaidyanathan, "Nested Arrays: A Novel Approach to Array Processing With Enhanced Degrees of Freedom," in *IEEE Trans. Signal Process.*, vol. 58, no. 8, pp. 4167-4181, Aug. 2010.

[10] S. Qin, Y. D. Zhang and M. G. Amin, "Generalized Coprime Array Configurations for Direction-of-Arrival Estimation," in *IEEE Trans. Signal Process.*, vol. 63, no. 6, pp. 1377-1390, March15, 2015.

[11] P. Stoica, P. Babu and J. Li, "SPICE: A Sparse Covariance-Based Estimation Method for Array Processing," in *IEEE Trans. Signal Process.*, vol. 59, no. 2, pp. 629-638, Feb. 2011.

[12] F. Shu et al., "Low-Complexity and High-Resolution DOA Estimation for Hybrid Analog and Digital Massive MIMO Receive Array," in *IEEE Trans Commun.*, vol. 66, no. 6, pp. 2487-2501, June2018.

[13] D. C. Beste and E. N. Leith, "An Optical Technique for Simultaneous Beamforming and Cross-Correlation," in *IEEE Trans. Aerosp. Electron. Syst.*, vol. AES-2, no. 4, pp. 376-384, July 1966

[14] S. Pasupathy, "Array detection of active sonar signals," *Proc.* of *IEEE Ocean '74* -, Halifax, NS, Canada, 1974, pp. 299-303.

[15] L. Griffiths, "Time-domain adaptive beamforming of HF backscatter radar signals," in *IEEE Trans. Antennas Propag.*, vol. 24, no. 5, pp. 707-720, Sep. 1976.

[16] L. Zhang, Y. -C. Liang and Y. Xin, "Joint Beamforming and Power Allocation for Multiple Access Channels in Cognitive Radio Networks," in *IEEE J. Sel. Areas Commun.*, vol. 26, no. 1, pp. 38-51, Jan. 2008.

[17] P. Kasemir, N. Sutton, M. Radway, B. Jeong, T. Brown, and D. S. Filipovic, "Wideband analog and digital beamforming," *Proc.* of *9th Int. Conf. Telecommun. Mod. Satell., Cable, Broadcast. Services*, Niš, Serbia, Oct. 2009, pp. 372–375.

[18] O. E. Ayach, S. Rajagopal, S. Abu-Surra, Z. Pi and R. W. Heath, "Spatially Sparse Precoding in Millimeter Wave MIMO Systems," in *IEEE Trans. Wirel. Commun.*, vol. 13, no. 3, pp. 1499-1513, March, 2014.

[19] R. Schmidt, "Multiple emitter location and signal parameter estimation," in *IEEE Trans. Antennas Propag.*, vol. 34, no. 3, pp. 276-280, March,1986.

[20] B. D. Rao and K. V. S. Hari, "Performance analysis of Root-Music," in *IEEE Trans. Acoust. Speech Signal Process*., vol. 37, no. 12, pp. 1939-1949, Dec. 1989.

[21] Van Loan, C. “Computing the CS and the generalized singular value decompositions,” in *Numer. Math.* vol.46, 479–491,1985.

[22] Q. Wu and J. P. Reilly, "Extension of ESPRIT method to unknown noise environments," *Proc. of ICASSP 91, Toronto, ON, Canada, 1991, pp. 3365-3368 vol.5.*

[23] E. Oja, “Simplified neuron model as a principal component analyzer,” in *J. Math. Biol*., vol. 15, no. 3, pp. 267–273, 1982.

[24] Bin Yang, "Projection approximation subspace tracking," in *IEEE Trans. Signal Process*., vol. 43, no. 1, pp. 95-107, Jan. 1995.

[25] J. Zhuang, T. Tan, D. Chen and J. Kang, "DOA Tracking Via Signal-Subspace Projector Update," *Proc. of ICASSP 2020,* Barcelona, Spain, 2020, pp. 4905-4909.

[26] E. C. Real, D. W. Tufts and J. W. Cooley, "Two algorithms for fast approximate subspace tracking," in *IEEE Trans. Signal Process.*, vol. 47, no. 7, pp. 1936-1945, July 1999.

Chapter 2 Basic Knowledge and Assumptions About Signal Mode and Linear Algebra

In this chapter, some basic terminologies and linear algebra knowledge will be introduced. Especially some theorems of covariance matrix decomposition will be given. Signal mode is another issue, and some assumptions are made to simplify the mathematic procedure in the later chapters.

2.1 Covariance matrix

The original representation of the covariance matrix is defined as

$$R = E\left[(X(t) - E(x(t)))(X(t) - E(x(t)))^* \right] . \tag{2.1.1}$$

The noise term should follow the Gaussian process, which means the expect value of noise is 0 , the noise has no correlation and the power of noise σ^2 follows

$$E[N(t)N^*(t)] = \sigma^2 I . \tag{2.2.2}$$

In this case, the covariance matrix can be represented by using a steering matrix and a reference channel

$$R = AE\left[x(t)x^*(t) \right] A + \sigma^2 I . \tag{2.2.3}$$

or

$$R = AR_x A + \sigma^2 I \tag{2.2.4}$$

However, because of the limited length of the acquired data, we can only calculate an approximation of the signal covariance matrix , which is marked as $\hat{R}$

$$\hat{R} = \frac{1}{L} X(t)X^*(t) . \tag{2.2.5}$$

The covariance matrices in the later chapters are all actually $\hat{R}$ unless it is specifically noted.

2.2 Toeplitz and Hermitian

There are two types of matrices that will be often used later: the Toeplitz matrix and the Hermitian matrix. If a matrix A is Toeplitz, it can be written as

$$A=\begin{bmatrix} a_0 & a_1 & a_2 & \cdots & a_{n-1} \\ a_{-1} & a_0 & \ddots & \ddots & \vdots \\ a_{-2} & \ddots & a_0 & \ddots & a_2 \\ \vdots & \ddots & a_{-1} & \ddots & a_1 \\ a_{1-n} & \cdots & a_{-2} & a_{-1} & a_0 \end{bmatrix}. \tag{2.2.1}$$

It means that the elements are systematical along the main diagonal and the elements parrel along the main diagonal are equal. The information of the matrix are determined by the first row and the first column, totally 2n-1 elements[1]. Another one is the Hermitian matrix. The feature of a Hermitian matrix is $A = A^H$.

2.3 Matrix Decompositions

Matrix decompositions are fundamental analysis methods for revealing further information from the data matrix[2,4,5]. Primarily, modern DOA estimation methods heavily rely on the subspace generated by the decompositions. In this case, typical decompositions are introduced in this section to have a regulated mathematical form for the later chapters.

2.3.1 Eigenvalue decomposition

Let $A \in C^{N\times N}$ and $x \in C^{N\times 1}$, the EigenValue Decomposition(EVD) can be defined as

$$Ax = \lambda x \tag{2.3.1}$$

where λ is a scalar named eigenvalue and x is its corresponding Eigenvector. Note that the eigen value can be zero but eigenvectors are always non-zero[3].

2.3.2 Singular value decomposition

Unlike EVD, Singular Value Decomposition (SVD)does not need to be performed in a square matrix. Let , the SVD of A can be written as

$$A = U\Sigma V^H \tag{2.3.2}$$

where $U \in C^{M\times M}$ and $V \in C^{N\times N}$ are unitary. And the singular value matrix $\Sigma \in C^{M\times N}$ is the singular value which has a form

$$\Sigma=\begin{bmatrix} \sqrt{\lambda_i} & & & & \\ & \ddots & & & \\ & & \sqrt{\lambda_r} & & \\ & & & 0 & \\ & & & & \ddots \\ & & & & & 0 \end{bmatrix} \tag{2.3.3}$$

where r is arbitrary[3].

2.4 Subspaces

Covariance matrix R can be described as a summation of signal covariance matrix S and noise covariance matrix N:

$$R = S + N \tag{2.4.1}$$

where

$$S = \sum_{k=1}^{d} A_k s_k s_k^H \tag{2.4.2}$$

and

$$N = \sigma^2 I \tag{2.4.3}$$

where R, S and N are all square matrices of size $N \times N$. Note that rank(S) = d if $N > d$, this situation is very typical in radar signal processing, because the number of sinusoidal waves is not as many as the length of the signal. In this case, N is a full rank matrix, rank(N)=M. Now, perform EVD on S in a vector form

$$S = \sum_{k=1}^{d} \lambda_k v_i v_i^H \ . \tag{2.4.4}$$

Because rank(S) =d, the amount of none-zero eigenvalues of S is $M - d$. Thus above can be written as

$$S = \sum_{i=1}^{d} \lambda_i v_i v_i^H \ . \tag{2.4.5}$$

Eigenvalues $\lambda_1,\ldots, \lambda_d$ are defined as principal eigenvalues, correspondingly, $v_1,\ldots, v_d$ are called principal eigenvectors. Because v_i is the an eigen vector of S, then

$$S v_i = \lambda_i v_i \tag{2.4.6}$$

substituting S in (2.8.9) by (2.8.5a)

$$\sum_{k=1}^{d} A_k s_k s_k^H v_i = \lambda_i v_i \ . \tag{2.4.7}$$

The above equation means that for any v_i, it can be expressed as a linear combination of signal vectors, s_k. A more important equation can be drawn by using the orthogonality of v_i

$$I = \sum_{i=1}^{M} v_i v_i^H \quad . \tag{2.4.8}$$

Then R can be rewritten by

$$R = \sum_{i=1}^{d} \lambda_i v_i v_i^H + \sigma^2 \sum_{i=1}^{M} v_i v_i^H \tag{2.4.9}$$

Note that $M > d$, (2.4.9) can be written by changing the index of summation.

$$R = \sum_{i=1}^{d} (\lambda_i + \sigma^2) v_i v_i^H + \sum_{i=d+1}^{M} \sigma^2 v_i v_i^H \ . \tag{2.4.10}$$

From this equation, two important features can be drawn. The first one is related to the smallest Eigen value of R, the inequation shown below describes

$$\lambda_1 > \lambda_2 > \ldots > \lambda_d > \lambda_{d+1} = \lambda_M = \sigma^2 \ . \tag{2.4.11}$$

Secondly, column vector of R is orthogonal to Eigen vectors of smallest Eigenvalues [4][5]

$$\{s_1, \ldots, s_d\} \perp \{v_{d+1}, \ldots, v_M\} . \tag{2.4.12}$$

As principal Eigen values and Eigen vectors are defined, here, correspondingly, $\lambda_{d+1}, \ldots, \lambda_M$ and $v_1, \ldots, v_d$ are defined as secondary Eigen values and Eigen vectors. In the field of signal processing, (λ_i , v_i) , $i=1,\ldots,d$ are called signal characteristic pair (signal characteristic values and signal characteristic vectors). Also, (λ_i , v_i) , $i=d+1,\ldots,M$ are called noise characteristic pair (noise characteristic values and noise characteristic vectors).

Above concepts are basis of subspace analysis, signal subspace can be defined as

$$V_S = [v_1, \ldots v_d] \ . \tag{2.4.13}$$

And noise subspace can be defined as

$$V_N = [v_{d+1}, \ldots v_M] \tag{2.4.14}$$

Or

$$\text{span}\{V_N\} = [v_{d+1}, \ldots v_M] . \tag{2.4.15}$$

2.5 Signal mode

Practically, the propagation of electromagnetic waves is usually complicated and cannot be explicitly described. It is necessary to have an abstract and simplified form of the signal mode for convenience. The following assumptions are made to all algorithms introduced and discussed in this dissertation.

- The antenna elements (transmitters and receivers) are all omnidirectional.;
- The transmission medium is isotropy and homogenous.

- The EM wave propagates in a straight line.
- There is only one signal source/ target.
- The target and the system are located on the same plane (2D processing only)
- Only time delay can cause the signal phase shift.
- The target is ideal.

Unlike many related studies[7~9], the last assumption is not equivalent to the assumption that all signals are narrowband. Under a common narrowband assumption, the frequency bandwidth B is much larger than the center frequency f_c, which is described as

$$\frac{B}{f_c} < \frac{1}{10} \ . \tag{2.5.1}$$

However, we use wideband SFCW systems in the following chapters to conduct the experiments and simulations. It relates to a fundamental problem: what is used to determine the signal delay?

If we are using the SFCW system, the time domain signal can be written explicitly as:

$$s(t) = 2\frac{\sin(\frac{B}{2}(t-\tau))}{(t-\tau)} e^{j\omega_c(t-\tau)} \tag{2.5.2}$$

where ω_c is center angular frequency and τ is the arrival time or delay. It apparently shows the feasibility of directly assuming the global maximum of the time domain signal indicates the arrival time, though the system is wideband.

A simulated example is shown below by using an SFCW signal source B=1.5GHz and f_c =0.75Ghz with a delay of 3.4ns. It is seen that both maxima of real part and the absolute value of the signal are located at the delay time/

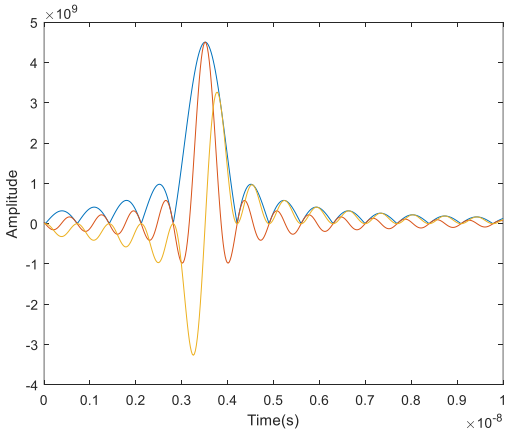

Fig.2.5.1.Simulation of a trace of SFCW signal in time domain

In this dissertation, assumptions are made to have a very extreme condition, while the mathematic form of the array received signal $S(t) \in C^{M \times L}$ still follows

$$S(t) = Ax(t) \tag{2.5.3}$$

where $A \in C^{M\times 1}$ is the steering matrix and $x(t) \in C^{1\times L}$ is the signal of the reference channel, and it has a pure phase representation.

$$x(t) = e^{-i\omega(t-\tau)} \ . \tag{2.5.4}$$

Note that the noise term and the amplitude information are not added because we assume that we can directly acquire the delay information of each channel in the received signal. In other words, we assume that the information given by the global or local maxima has no error. The example of SFCW in Fig2.5.1 proves this assumption's mathematical correctness if there is only a signal source. And an example is given below to demonstrate how to transform the signal to a phase-only mode.

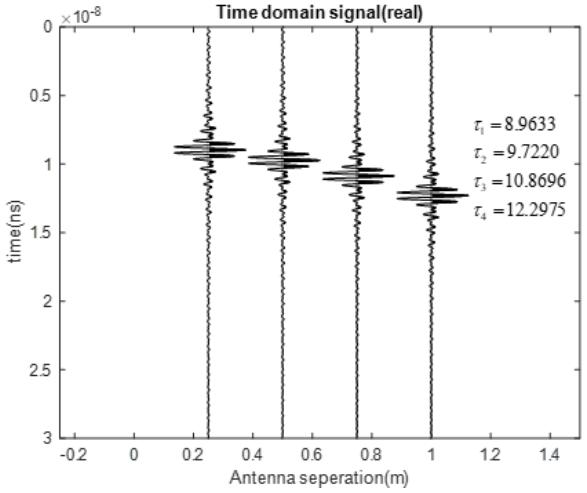

Fig.2.5.2. Simulation of time domain SFCW signal received by a 4 element array.

If an SFCW signal is received as in Fig.2.5.2., we can directly acquire the arrival time information from the global maximum. And for the first channel, the phase signal should be $x_1(t) = e^{-i\omega(t-\tau_1)}$, and these signals only have phase difference with the same waveform.

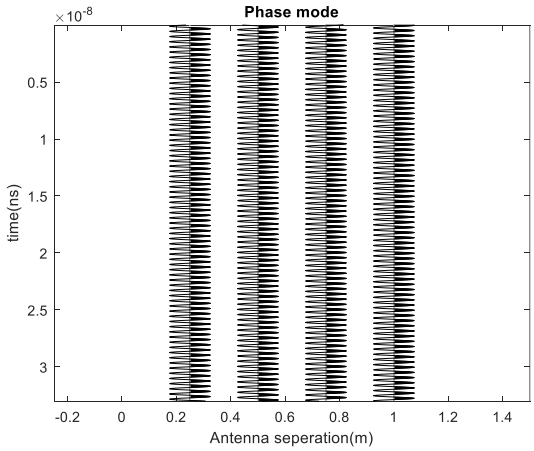

Fig.2.5.3. phase mode of the simulation.

Along with the signal mode, the antenna configuration is also a factor influencing the received signal. The configuration of the Uniform Linear Array (ULA) is plotted.

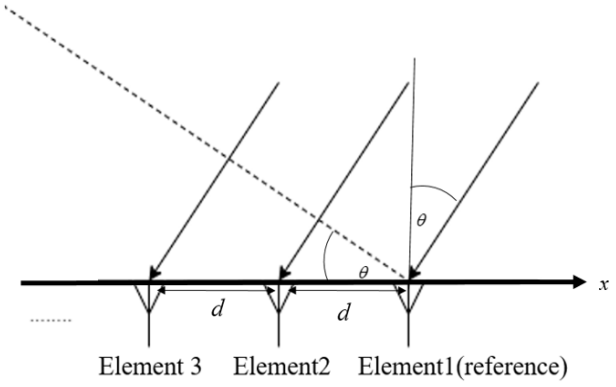

Fig.2.5.4. Far field ULA configuration.

We use the elements on the very right to be our signal if there is no notation in the following chapters. But practically, the error occurred while we selected the arrival time manually or automatically because there is not possible to have such a precise signal as shown previously. What we can do is to have some close estimations of the delay times for each signal and perform a series of processing to compare their results. The detailed content of arrival or delay time selection will be discussed in the later chapters.

2.6 Summary

In this chapter, the use of mathematical operations and the signal mode have been introduced for further purposes. The signal mode has been emphasized because of the extreme conditions that were assumed. It should be noted that transforming the received signal into a pure phase mode is not unique to this work. In fact, many algorithms employ such a process to ensure that the input to the kernel processor is suitable for processing. However, in practice, even the input signal is mathematically correct, it is not always possible to achieve this due to floating-point errors in computer calculations and other issues. In such cases, works that are based on these assumptions are meaningful mathematically.

References

[1] C.Eckart and G. Marion Young. “A principal axis transformation for non-hermitian matrices.”in *Bull. Am. Math*., 1939, vol.45, pp. 118-121.

[2] Y. Wang and L. Zhu, "Research and implementation of SVD in machine learning,” *Proc. of 2017 ICIS*, Wuhan,China, 2017, pp. 471-475.

[3] G. H. Golub and C. F. Van Loan, *Matrix Computations*, 3rd edition, Johns Hopkins University Press, 1996.

[4] V. F. Pisarenko, "The Retrieval of Harmonics from a Covariance Function, " in *Geophys. J. Int.*, 1973, vol. 33, pp.347–366.

[5] T. Shan, M. Wax and T. Kailath, "On spatial smoothing for direction-of-arrival estimation of coherent signals," in *IEEE Trans. Signal Process.*, vol. 33, no. 4, pp. 806-811. Aug.1985.

[6] R. Schmidt, "Multiple emitter location and signal parameter estimation," in *IEEE Trans. Antennas Propag*., vol. 34, no. 3, pp. 276-280, March 1986.

[7] M. A .Thomas. *Modern Antenna Design, 2nd Ed*. John Wiley & Sons.2005.

[8] V. J. Hubregt. *Array and Phased Array Antenna Basics*. John Wiley & Sons. 2006.

[9] F.T. Ulaby and D.G. Long. *Microwave Radar and Radiometric Remote Sensing.* University of Michigan Press, 2014.

Chapter 3 Modern Beamforming

As mentioned, beamforming techniques has the longest history in all DOA methods, it is still a popular topic in the various field. In last 5 years, the beamforming technology are developed for multiple kinds of hardware platform; however, the technology itself is improved slightly for purposes. For example, Capon beamformer will suffer from performance degradation due to the steering vector error dominated by large DOA mismatch. To solve this, a new robust Capon beamforming approach is proposed by Hao et. al., 2019[1]. A low-complexity yet effective DOA estimation algorithm and the corresponding hardware accelerator chip design are presented by Chen et. al. [2]. Zhu et. al., presents a novel Hybird Beamforming (HB) algorithm based on the spatial covariance matrix (SCM) knowledge of all UEs ,which is proposed for a large scale MIMO-OFDM system to support multiple groups of single user equipment[3]. Xiao et. Al., combined UAV and beamforming for the positioning and communication applications [4].In addition, Zhao et. al., proposed a novel and related DOA estimation algorithm to predict angle variations during the intervals, which achieves high precision even when UAVs are at high mobility [5].

3.1 Definition of beamforming

The beamforming problem can be described in such a way: adjusting the weights on received signal of channels to have a maximum array output. Mathematically, under the assumption of the far field and narrow band signal, the array output follows

$$X(t) = W(\theta)X(t) \tag{3.1.1}$$

where $W(\theta)$ is the weight function, under an extreme condition as assumed: there is only one source, $W(\theta)$ is equivalent to matrix . In this case the expected output power is

$$P_{\mathrm{CBF}}(\theta) = E[X(t)^2] = A(\theta)R_x A^*(\theta) \tag{3.1.2}$$

In the case $P_{\mathrm{CBF}}(\theta)$ is so-called a spatial spectrum function. Because this kind of spectra will be closely related to the rest part of the work, an example is given to introduce rule that the work will follow to plot the related spatial spectra.

According to Fig.3.1.1, The horizontal axis is the arrival angle, and we always use the degree as unit. There is two different range of horizontal axis, one is as shown from -90° to 90° and another one is from 0° to180 °, which is typically used in the near field spatial spectrum cases. The vertical axis is the amplitude, the unit may vary according to the output power. Because in the later chapters, there are many level of peaks on the spectra are not dB scale higher than the background noise level, thus the vertical axis will be in a normalized scale or just the calculated result of the spectrum function unless notation presented.

Apparently, the output power is only related to the signal DOA θ. So, it is also considered as a filter in the spatial domain; meanwhile the method is different from the conventional time domain filters. It mainly uses the phase difference generated by the antenna configurations rather than the amplitude information of the envelope of the signal in the time domain.

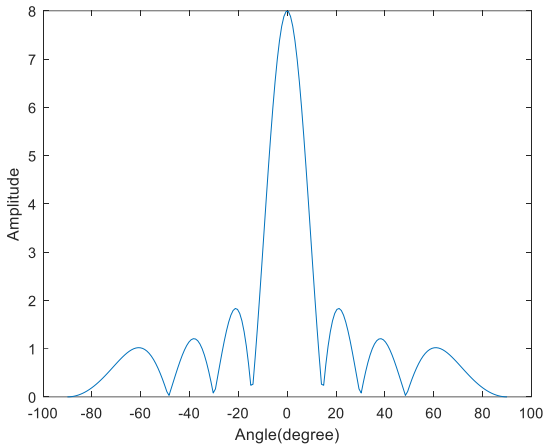

Fig.3.1.1 An example of showing the DOA estimation by using CBF

3.2 Standards and cost functions of beamforming

The method introduced in the above section is not often used in modern beamforming because of its precision. In recent decades, the design of the cost functions because the signal processing techniques of beamforming is a popular topic. In this work, we introduce two fundamental standards and cost functions to demonstrate its related beamforming method and reveal the uses of the subspaces.

As previously mentioned, $P_{\mathrm{CBF}}(\theta)$ is the expected output power, we may want to adjust the steering matrix in (3.1.1) to have a cost function that has the Minimum Mean Square Error(MMSE), and the cost function can be written as

$$J(w) = E\left[\left|wx(t) - X(t)\right|^2\right] \tag{3.2.1}$$

where *w* is the weight vector containing DOA information. MMSE is achieved when the estimated DOA is equal to the ground truth. Consequently, this method is called MMSE beamforming[7,8]. The solution to the cost function is straightforward. Firstly, we assume that there is only one signal source, as we did previously. Then the partial derivative of the weight function can be written as

$$\frac{\partial J(w)}{\partial w} = 2E[x(t)x^*(t)]w - 2E[(x(t)X^*(t))]\,. \tag{3.2.2}$$

Let the self-correlation matrix of $x(t)$ be R_x, and let cross-correlation matrix of the reference signal and received signal $X(t)$ be r_x. Then the equation above can be simplified as

$$\frac{\partial J(w)}{\partial w} = 2R_x w - 2r_x \tag{3.2.3}$$

when the derivative is zero, the stationary point appears which means the MMSE is achieved and the weight vector or the steering vector is

$$w = R_x^{-1} r_x \,. \tag{3.2.4}$$

It is resulted to the ideal form of the Wiener filter, and it is also called the Wiener-hopf equation [6]. This method. In previous chapter, we mentioned subspaces, and we notice that the relationship among the eigenvalue, subspaces, and the signal covariance matrices. Under such circumstances, it is very natural to have a standard or to establish a cost function to evaluate the DOA. Typical Minimum SNR (MSNR) cost function can be written as

$$J(w) = \frac{wR_s w}{wR_N w} \tag{3.2.5}$$

where R_s is the covariance matrix of the signal subspace and R_N is the covariance matrix of the noise subspace [8]. The two methods introduced above has their own advantages and disadvantages, and they are both widely used for the various purposes. Based on these two methods, modern beamforming techniques have been developed for decades.

3.3 Subspace and optimization techniques in beamforming

Optimization and subspace techniques are very often used in modern beamforming techniques because the weight vector must be adjusted accordingly. For example, in self adaptive weight vector beamforming, Gradient Descent (GD) method will be used to update the weight vector. In this section, the cost function is modified to conduct the summation on the array received signal in each snapshot. In gradient based optimization numerical methods, a typical iteration can be written as

$$d(k+1) = d(k) - u\nabla \tag{3.3.1}$$

where *d* is an arbitrary vector and *u* is a scalar that controls the search speed. In our particular cases, the gradient is apparently partial derivative of weight vector. Note that in the beamforming problem, the iterations are performing along the snapshot. In other words, the weight vector will be adjusted according to the weight vector in the previous snapshot. So, the above equation can be reformulated into

$$\nabla = R_x w(t) - r_x \approx x(t)[w(t)x(t) - X(t)] \,. \tag{3.3.2}$$

Note that the $x(t)$, $w(t)$ and $X(t)$ are all instantaneous. Sometimes, we let the term $[w(t)x(t) - X(t)] = e(t)$ are written as a noise term, and the iteration can be modified to

$$w(t+1) = w(t) - ux(t)e(t) \,. \tag{3.3.3}$$

The above procedure is called the self-adaptive weight vector updating. A significant advantage of this method is the computation speed, if the signal is stationary, the converge speed will be extremely fast, while the accuracy will not be sacrificed. Here, we use a same narrow band signal emitted at 0°to demonstrate the performance of the method above. The figure shown below are the comparison between the CBF and the self-adaptive method.

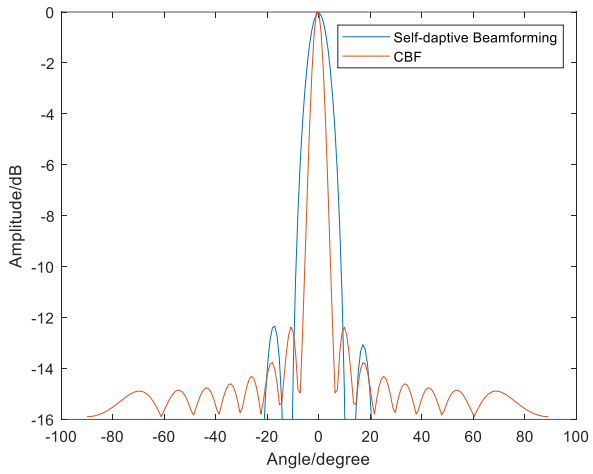

Fig.3.3.1.The comparison between simulation result of the CBF and the self-adaptive beamforming

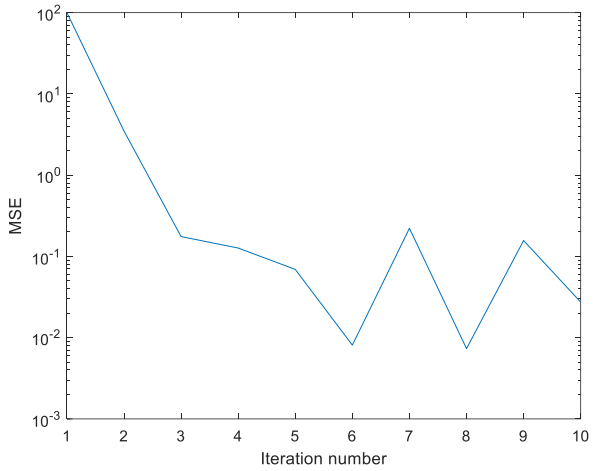

Fig.3.3.2. Convergence of the algorithm

The self-adaptive method is converged within 10 iteration and the accuracy of the estimation is the almost same, but the computational speed is much faster. A very intuitive explanation can be given, as some of the signature of the signal can be captured within a few snapshots, the processing can be done by only using this instantaneous information rather than the whole time series. Consequently, the large size matrix and vector multiplication can be avoided which leads to the improvement of the computational speed. These beamforming techniques are introduced in purpose because in the next section, the method is in serious demand of reducing the computational complexity.

3.6 Summary

In this chapter, mathematical operation and the signal mode are introduced for the further purposes. The signal mode is emphasized in this chapter because the extreme condition we assumed. Note that

transforming the receive signal in a pure phase mode is not only existing in this work, in fact, many algorithms has such an process to make sure that the input to the kernel processor is processable enough; however, sometimes, this cannot be done practically due to the floating calculation of the computer and other issues. In this case, the work based on such assumptions are meaningful mathematically.

References

[1] Y. Hao, N. Zou, and G. Liang, “Robust Capon Beamforming against Steering Vector Error Dominated by Large Direction-of-Arrival Mismatch for Passive Sonar,”in *J. Mar. Sci. Eng.*, vol. 7, no. 3, p. 80, Mar. 2019.

[2] F. Sun, B. Gao, L. Chen, and P. Lan, “A Low-Complexity ESPRIT-Based DOA Estimation Method for Co-Prime Linear Arrays,” in *Sensors*, vol. 16, no. 9, p. 1367, Aug. 2016.

[3] Z. Xiao, L. Zhu and X. -G. Xia, "UAV communications with millimeter-wave beamforming: Potentials, scenarios, and challenges," in *China Commun., 2020*, vol. 17, no. 9, pp. 147-166, Sept. 2020.

[4] D. Zhu, B. Li and P. Liang, "A Novel Hybrid Beamforming Algorithm With Unified Analog Beamforming by Subspace Construction Based on Partial CSI for Massive MIMO-OFDM Systems," in *IEEE Trans Commun.*, vol. 65, no. 2, pp. 594-607, Feb. 2017.

[5] T.Zhao, C.luo., J.Zhou,D.GUO, N.Chen. and P. Casaseca-de-la-Higuera, “*DOA prediction based beamforming with low training overhead for highly-mobile UAV communication with cellular* networks”, in *Appl. Sci.*, vol.10,10, no. p.4420-4426.Jan. 2020.

[6] F. Sun and E. de Carvalho, "A Leakage-Based MMSE Beamforming Design for a MIMO Interference Channel," in *IEEE Signal Process. Lett.*, vol. 19, no. 6, pp. 368-371, June 2012.

[7] Z. Wang, Y. Wu, Y. Cai, J. Wang and G. Yue, "Robust MMSE-Based Beamforming for Massive MIMO Multi-Pair Two-Way Relay Systems with Low-Resolution ADCs/DACs," *2021 13th International Conference on Wireless Communications and Signal Processing*, Changsha, China, 2021, pp. 1-6.

[8] F. Alam, Donghee Shim and B. D. Woerner, "Comparison of low complexity algorithms for MSNR beamforming," *Proc. of. IEEE 55th Vehicular Technology Conference. VTC Spring 2002,* Birmingham, USA.2002, pp. vol.41776-1780.

[9] T. Kailath, "Fredholm resolvents, Wiener-Hopf equations, and Riccati differential equations," in , vol. 15, no. 6, pp. 665-672, Nov.1969.

Chapter 4 Multiple Signal Classifications

MUSIC algorithm is widely used in array signal processing mainly because of its resolution capability compared to conventional beamforming techniques. [1] By using the orthogonality of the signal subspace and noise subspace, the signal source can be magnificently emphasized from the background. [2]

In recent years, Li et. al., proposed unitary root MUSIC by using a modified array system[3]. Using the noiseless cross-covariance matrix which is obtained by utilizing the spatial cross-correlation technique., F. Wen presented a method for DOAs estimation via reduced-dimension multiple signal classification (RD-MUSIC)[4].Huang et. al., considered an extreme condition that covariance matrix is "one-bit" quantized[5].Zheng et. al uses subarrays to perform both near field and far field localization by using spatial smoothing MUSIC and its modified algorithms[6].Osman et. al., introduce a new two-dimensional direction of arrival (DOA) elevation and azimuth angles estimation technique for global positioning system (GPS) jamming signals in challenging environments based on the fast orthogonal search (FOS) method[7].

Nonetheless, original MUSIC algorithm only fits the condition where the signal sources located in the far field, so that the phase differences of the array receiving signal can be expressed by using only one angle parameter. In practical, such a condition can be hardly suited while the signal source is not located very distant from the receiver. It is due to the geometry of the signal source and the array elements, for example, uniform linear array always requires both range and angle parameters to set a completed phase expression for each array element. Adding a new parameters range is so called 2D MUSIC; however, it also has one more enumeration process along the range dimension, which is time-consuming.

4.1 The original MUSIC and its near field form

The original MUISC algorithm is designed for the far field condition, in this case ,we can directly use (2.2.3),(2.2.5) and (2.31) to have the following equation

$$\sigma^2 v_i = (AR_s A^* + \sigma^2 I)v_i \tag{4.1.1}$$

where a is a steering matrix, in the case of this work, a steering vector that has the following formulation according to Fig.2.5.4.

$$A = [1, e^{j\omega d \sin\theta/c} ..., e^{j\omega(M-1)d\sin\theta/c}]. \tag{4.1.2}$$

Knowing that $AR_s A$ and R_s are positive defined, we can have the orthogonality established as below

$$Av_i = 0. \tag{4.1.3}$$

Following the previous section if the target is located in the near field, the received signal can be rewritten as

$$X(t) = A(\theta, r)x(t) + N \tag{4.1.4}$$

where $X(t)$ is the received signal of the reference element in time domain, steering matrix $A(\theta,r)$ contains two unknown range r and angle θ, and can be explicitly written. $X(t)$ is the received signal matrix for all channels and, N is a noise matrix.

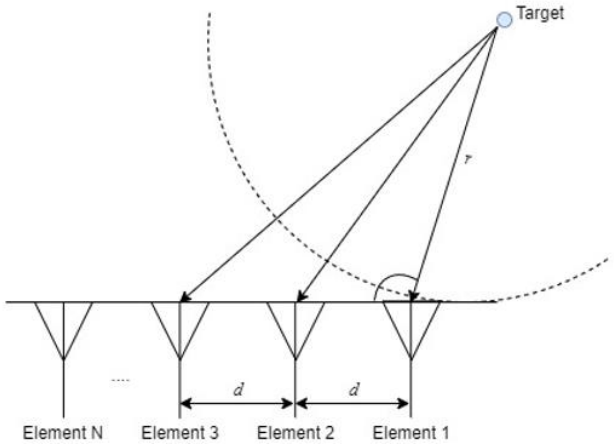

Fig.4.1.1 Antenna configuration in the near field

A spectrum or sometimes named as spatial spectrum P contains both range and angle parameters are given to estimate the signal source location following the same procedure in section 4.1.1.

$$P(\theta,r)=\frac{1}{A(\theta,r)E_N^*E_N A(\theta,r)^*} \tag{4.1.5}$$

4.2 The arrival time selection

MUSIC algorithm is unstable, in other words, the algorithm is sensitive in term of the arrival time inputs. But due to many reasons, it is impossible to pick an arrival time vector manually. The most common way is to pick the maxima of the received signal from the different channel and considered they are the first arrival times. This approximation is not always correct because of the signal deformation, the global maxima are not always indicating the arrival times and the local maxima are too many.Fig.4.2.1 are acquired data from the SFCW system, we can see that the arrival time can be merely determined especially in the GPR cases.

If we pick arrival time input without any error, the covariance matrix can be expressed as

$$R_{xx}=\begin{bmatrix} 1 & e^{j\omega_c(\tau_2-\tau_1)} & \cdots & e^{j\omega_c(\tau_n-\tau_1)} \\ e^{j\omega_c(\tau_1-\tau_2)} & 1 & & \\ \vdots & & \ddots & \\ e^{j\omega_c(\tau_1-t_n)} & & & 1 \end{bmatrix}. \tag{4.2.1}$$

But as mentioned the arrival time selection inevitably contains phase errors, which makes the covariance matrix of the received signal matrix as shown in (4.2.2). The goal of the thesis is to handle such a problem:

performing DOA estimations with the covariance matrix that has non-additive phase noise, or in other words, recovery (4.2.1) from (4.2.2)

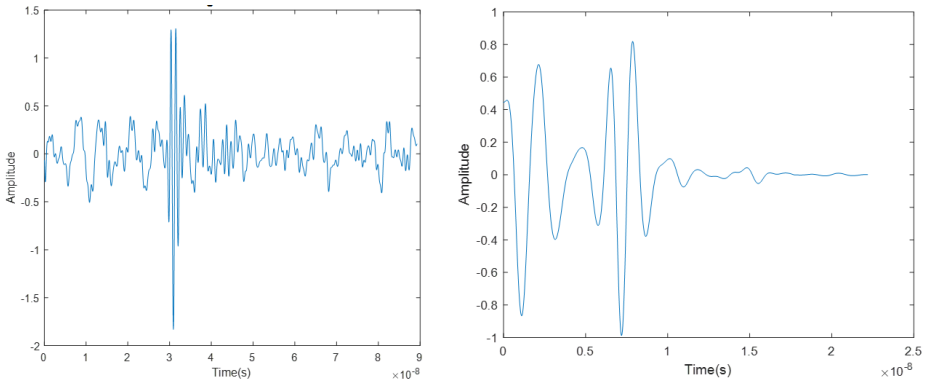

(a) SFCW signal in SAR measurement (b) SFCW signal in GPR measurement

Fig.4.2.1 Real SFCW signal (a) in SAR measurement (signal transmitted in the air)(b) in GPR measurement (signal transmitted in the subsurface)

Note that even as mentioned, MUSIC algorithms are sensitive to the inputs, it does not mean that the algorithm cannot function if there are errors, we are still going to use MUSIC algorithms in the next sections without any modification of the covariance matrix unless noted.

$$\bar{R}_{xx} = \begin{bmatrix} 1 & e^{j\omega_c(\tau_2-\tau_1+\Delta\tau_{2,1})} & \cdots & e^{j\omega_c(\tau_n-\tau_1+\Delta\tau_{n,1})} \\ e^{j\omega_c(\tau_1-\tau_2-\Delta\tau_{2,1})} & 1 & & \\ \vdots & & \ddots & \\ e^{j\omega_c(\tau_1-t_n-\Delta\tau_{n,1})} & & & 1 \end{bmatrix}. \quad (4.2.2)$$

A direct way to handle this issue is to all the combinations of the arrival times. Then run trough the enumeration to find the best result. The best result may vary due to the cost function may set case to case. Another way is to add compensation term in the steering matrix, however, it is not always functioning well, because the compensation term should be following some certain structures, but the time delay error of manual picked arrival time is not.

4.3 Peak search and enumeration-based MUSIC

For a time-domain signal, the most common way to determine the arrival time is to select the maximum amplitude position; however, for GPR signals, due to the strong attenuation, this method may cause errors. Besides, considering the multi-layer cases, if one layer has a close relative permittivity to its adjacent layers, the reflection will be weak and easily filtered out by the maximum amplitude judgment.

The proposed MUSIC algorithm contains a self-adaptive peak search method to avoid the loss of possible peaks. Instead of choosing the position with the largest amplitude, the process selects local maxima and

marks them as possible arrival times for each trace of the time-domain signal. The likely arrival time information will be stored in an arrival time matrix $J \in R^{L\times M}, L > M$. The procedure can be simply described as shown in Fig. 4 with M = 4 and L = 15.

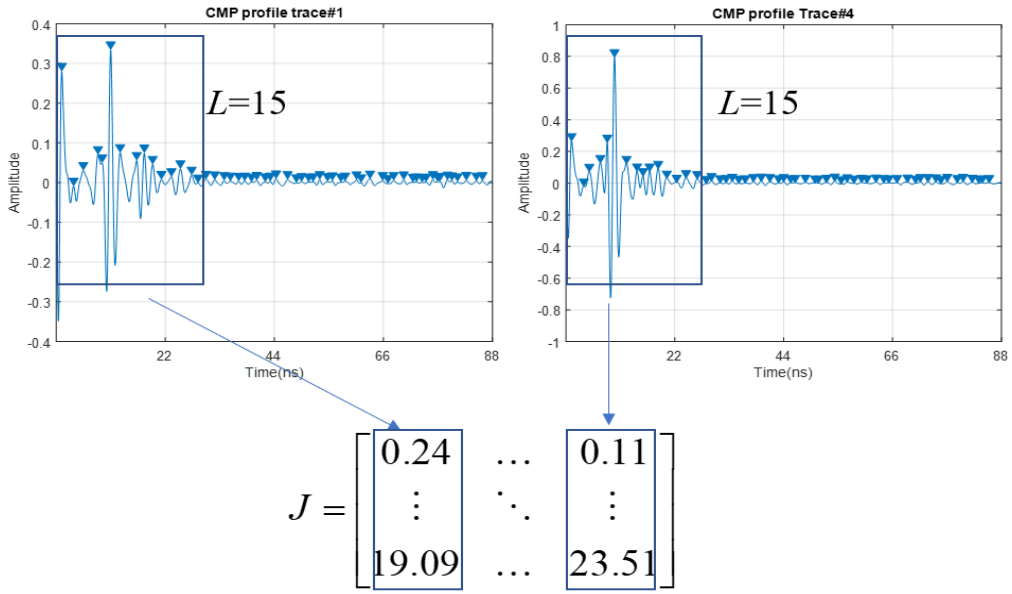

Fig.4.3.1. Selecting first L local maxima in all channels and recording their positions in an arrival time matrix.

The elements in J are enumerated to generate an array of arrival times T for use in the MUSIC algorithm,

$$T = [J_{1,i}, J_{2,j} \ldots . J_{M,k}] \tag{4.3.1}$$

where $i, j, \ldots, k \in N+, i, j, \ldots, k \le L$. Note that L should be set appropriately; a large L will make the computation time- consuming, whereas a small L may miss certain combinations of arrival times. It is better to reduce the number of desired peaks during the calculation. The procedure leads to two different way of utilizing the arrival time inputs one is to use entire T input and another is to use T use segment by segment. These two approaches will be discussed in the experiment section at the end of the chapter.

A simulation is carried out here to offer a general view of the algorithm. The simulation uses 4 antenna pairs transmitting and receiving the signal in 65 MHz to 1.5 GHz SFCW mode. The subsurface layer 1 is set to a 0.1 m depth and the signal transmission velocity is 0.15 m/ns. The subsurface layer 2 is set to a 0.2 m depth, and the signal transmission velocity is 0.08 m/ns. The system is in direct contact with the ground. There is no mutual coupling, and the SNR is set to 10 dB. The real part of the time domain signal is shown in Fig. 4.3.2.

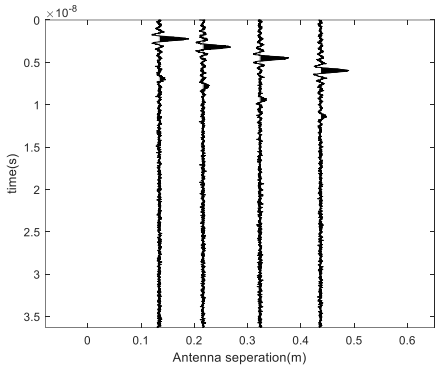

Fig. 4.3.2.CMP time-domain signal profile for the simulation.

Assuming no prior knowledge exists, we intentionally made the imaging area of the spectrum large, where the vertical and horizontal axes are set to 0~1m and 0.5~2m/ns. To detect the first layer, MUSIC must run the entire T with L = 20. Then a strong peak appears at 0.095m , thus, it is taken as the first layer, in this case, (3) and (4) can be solved by using the information from the first layer, then the second layer from 0.095m to 1m can be plotted.

Since spectrums for both layers are acquired, for comparing them with the conventional method, we combine these two spectrums by normalizing and using a threshold of 80% maximum amplitude. The results are shown in Fig.4.3.3. According to the results, the resolution of the proposed method is much higher than that of the standard method. Moreover, the second layer on the spectrum generated by the traditional method is weak and incorrectly located due to the negligence of the refraction.

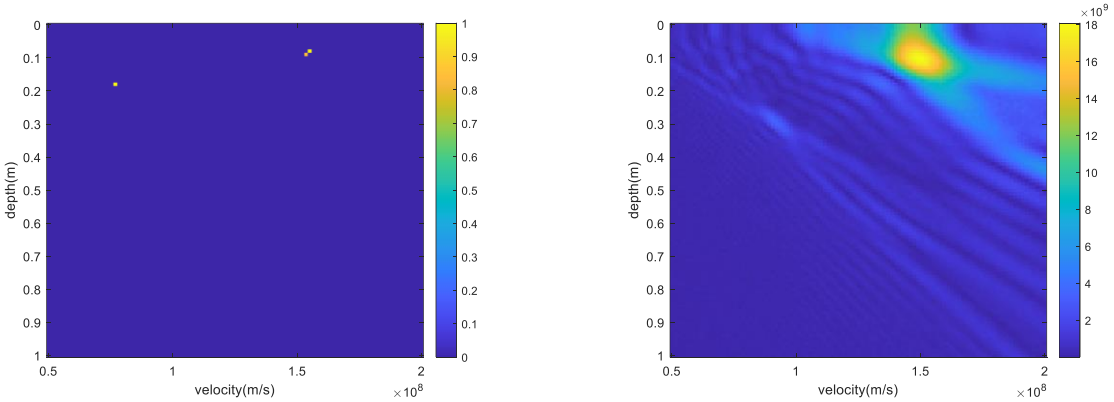

(a) Spectrum generated by The proposed method(b) Spectrum generated by The conventional method

Fig.4.3.3. Comparison between the velocity-depth spectra generated by(a) the proposed method. (b) the conventional method.

4.4 Optimization based MUSIC

This rewritten form will focus on the minimum value instead of the maximum in (4.1.5), explicitly, it follows the form as following.

$$F(r,\theta)=\begin{bmatrix}1 & \cdots & e^{-j\omega\tau_M}\end{bmatrix}\begin{bmatrix}a_{11} & \cdots & a_{1M}\\ \vdots & \ddots & \vdots\\ a_{M1} & \cdots & a_{MM}\end{bmatrix}\begin{bmatrix}1\\ \vdots\\ e^{-j\omega\tau_M}\end{bmatrix}^{*} \tag{4.4.1}$$

In a polynomial form, it donates

$$F(r,\theta)=a_{11}+a_{12}conj(e^{-j\omega\tau_2})+\ldots+a_{MM}e^{-j\omega\tau_M}conj(e^{-j\omega\tau_M}) \tag{4.4.2}$$

where M is the number of antenna elements, and τ_i can be expressed as

$$\tau_i=\frac{\sqrt{r^2+(i-1)^2d^2-2r(i-1)d\cos\theta}-r}{c}\quad . \tag{4.4.3}$$

Note that E_N is only related to the receiving signal because it is acquired from the eigenvalue decomposition of the array signal autocorrelation matrix and steering matrix has no more unknowns except r and θ after the array system is set, the exponential terms in (4.4.2) can be pre –calculated by enumeration all possible combinations of r and θ.

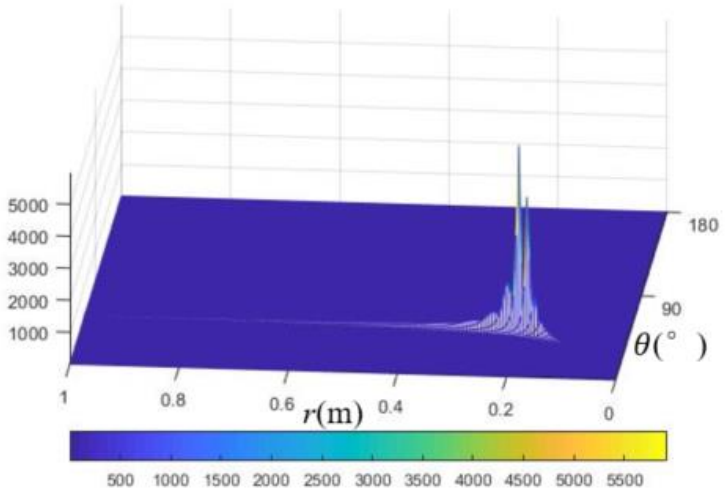

Fig.4.4.1 An example of 2D MUSIC result

The reason why the pre-calculation is necessary is because it saves the computational time and reveals the near field and far field condition for the system. Basing on (4.4.2), those exponential terms can be considered as 2D surfaces as same as F itself as shown in Fig.4.4.1.

It is clear that a ridge appears to be gradually vertical to the angle axis, which means the geometry arrangement between the system and the signal source are increasingly fitting the perfect far field condition. The fact is that there are totally $M(M\text{-}1)/2$ surfaces to be concerned, they have different shapes because of the geometry arrangement of the antenna elements and can all be plotted before the MUSIC processing. As previously mentioned, pre-calculation might cost time if the system contains a large number of elements, but it is just one time work. According to the surface shape in Fig.1, a simplified MUSIC can be raised, the calculation will be separate into two parts, far field part and near field part. In the far field part, the algorithm directly calculates the in a far field MUSIC case; meanwhile, in the near field part the algorithm also calculates in the near field case. In both step F are calculated and the smallest F corresponds the location of the target.

Note that the definition of far field and near field depends on the system itself, such as number of elements, aperture size and transmitting frequency, it should be discussed case by case. For the 2D MUSIC calculation in near field, due to the explicit form (4.4.4) is known and it is a real function because of the symmetrical feature of the Toeplitz matrix, this paper uses quasi-Newton method to solve an optimization problem instead of looping over range and angle combinations for the near field. The advantage if applying optimization techniques is that the far field information offers very rational initial guess. Mathematically. Eq.5 has a far field formulation when $r \geq r_{far\text{-}field}$.

$$F(\theta) = a_{11} + a_{12} conj(e^{j\frac{\omega d \cos\theta}{c}}) + ... + a_{MM} e^{j\frac{\omega(M-1)d\cos\theta}{c}} conj(e^{j\frac{\omega(M-1)d\cos\theta}{c}}) \tag{4.4.4}$$

So the initial guess is ($r_{far\text{-}field}$, $\theta_{far\text{-}failed}$) where

$$\theta_{far-field} = \min(F(\theta)). \tag{4.4.5}$$

The simulations are all carried out by using one single 2GHz CW signal source regardless to amplitude, the SNR is set to 10dB. The system is a 4 elements uniform linear array and the distance between two adjacent elements are 0.0375m. Note that the following result of the proposed method shows the $1/F$ so that the visualization follows the conventional way. For a 4 elements system, it has 6 exponential term to generate the surface plots. They are listed below.

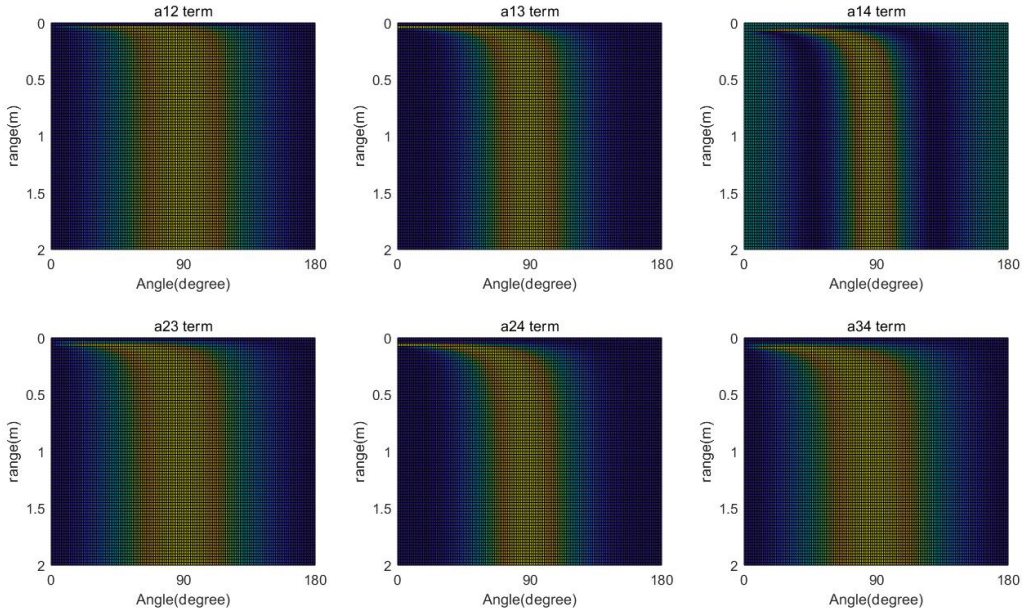

Fig.4.4.2 Surfaces generated by the exponential in (4.42).

The $r_{far\text{-}field}$ can be set to 0.6m, which is much further than the Fraunhofer distance $2D^2/\lambda$. The target is located in (0.3m, 60°), the conventional 2D MUSIC result is plotted with the proposed method, where green dots are iterations under the far field condition and red dots are iterations under the near field condition. It only takes 210 iterations to have a close result to the conventional MUSIC, but the computational time is almost negligible comparing to the conventional one.

To verify the accuracy of the proposed method, 1000 simulations with random source locations in the near field are made to exam the differences between the ground truth and the proposed method. The results are shown in Fig.4.4.4, all simulations are under 3cm Euclidean distance error.

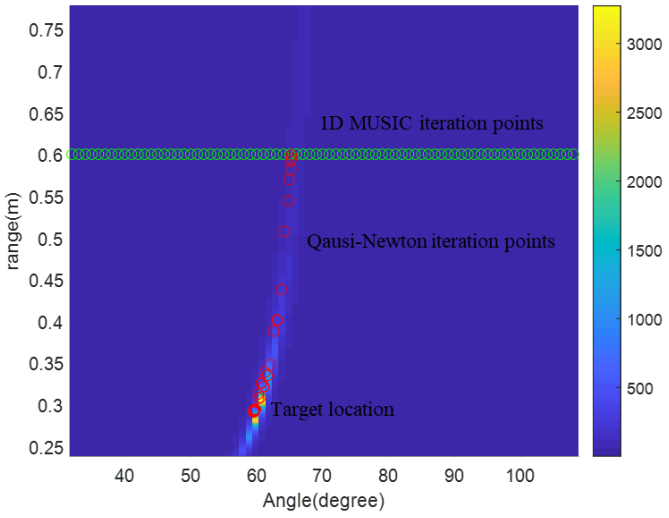

Fig.4.4.3 The simulation result.

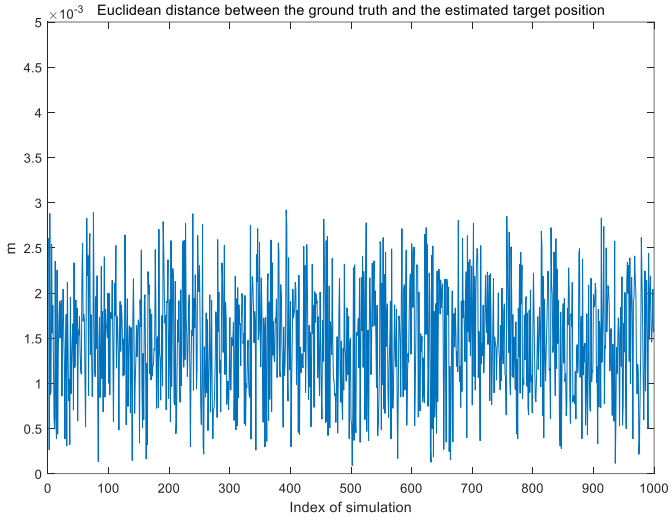

Fig.4.4.4 distance between the ground truth and the target position evaluated by the proposed methods

4.5 Resolution of MUSIC

This section aims to analyze the resolution of the fundamental MUSIC algorithm. Assuming that a peak in the MUSIC spectrum can be defined as a combination of two peaks

$$P_{\text{peak}} = (P(\theta_1) + P(\theta_2)) . \tag{4.5.1}$$

In the case of MUSIC, let θ_m be the mean of θ_1 and θ_2, then the scalar R can be written in the following form to describe the resolution

$$R(\Delta) = P_{\text{peak}} - P(\theta_m) \tag{4.5.2}$$

where $\Delta = |\theta_1 - \theta_2|$. When $R(\Delta) > 0$, $R(\Delta)$ can be distinguished and the azimuth resolution is Δ. When Δ is small, the spectral resolution can be explicitly written as

$$R(\Delta) = 1 - \frac{2\left|F\left(\frac{\Delta}{2}\right)\right|}{1 + |F(\Delta)|} \tag{4.5.3}$$

where

$$F(\Delta) = \frac{1}{M}\sum_{1}^{M} e^{-j\omega\xi} . \tag{4.5.4}$$

Knowing that ξ is the phase difference term, we can use $\frac{d\sin\theta}{c}$ to substitute the parameters of MUSIC into (4.5.4).

Thus, in the case of the far field MUSIC algorithm, the series can be easily calculated as azimuth angle is the only independent parameter.

$$\Delta \approx \lambda M d \pi \sqrt[4]{720}\,. \tag{4.5.5}$$

In the near field case, there are two independent variables, which makes F impossible to be simplified as it is in the far field case. Fig.4.5.1 shows the $|F(\Delta)|$ of 8 uniform linear elements array system with an element difference of 0.3m and a center frequency 1.5GHz.

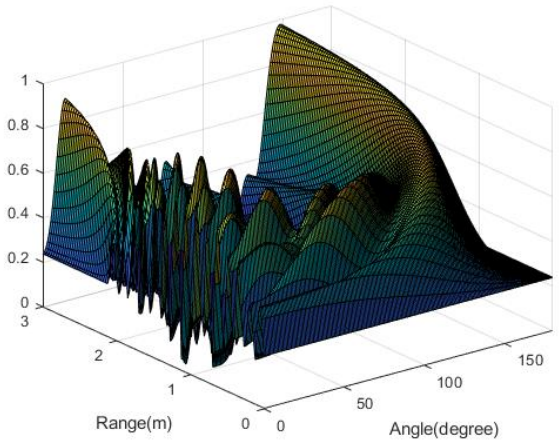

Fig. 4.5.1. simulation of $|F(\Delta)|$ in 3D view

The following figures demonstration the resolution of MUSIC algorithm resulted from the simulation with different system parameters.

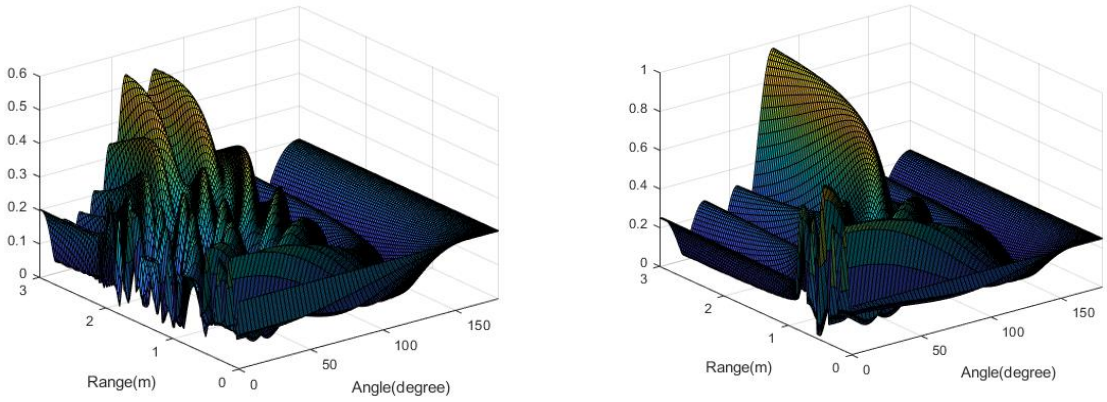

(a) 0.8GHz 8elemetns (b) 0.8GHz 4 elements

Fig. 4.5.2. simulation of $|F(\Delta)|$ in 3D view for 0.8GHz

The results indicate that there might be no approach to have a simplified form to describe resolution of the near field MUSIC. It also shows that the resolution of the near field MUISC are impacted by the target location when the system is fixed. In this case, like what we did to distinguish the near field and far field, we must calculate the required parameters before the system is fully assembled to ensure that the resolution fits the requirement of uses.

In the later section, Yakumo will be introduced, it is an SFCW system that has a 1GHz center frequency. The resolution of the system can be calculated by using the above procedure, but due to the antenna configuration, ξ must be modified.

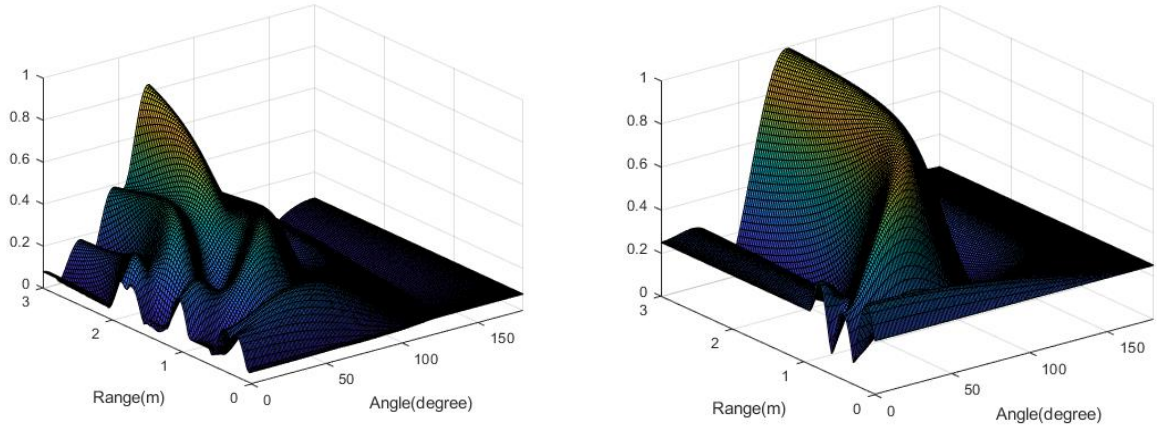

(a) 0.4GHz 8elemetns (b) 0.4GHz 4 elements

Fig. 4.5.3.simulation of $|F(\Delta)|$ in 3D view for 0.4GHz

Though the transmitter and receiver elements are designed and assembled as a ULA, the elements are utilized in the following way to be MIMO .

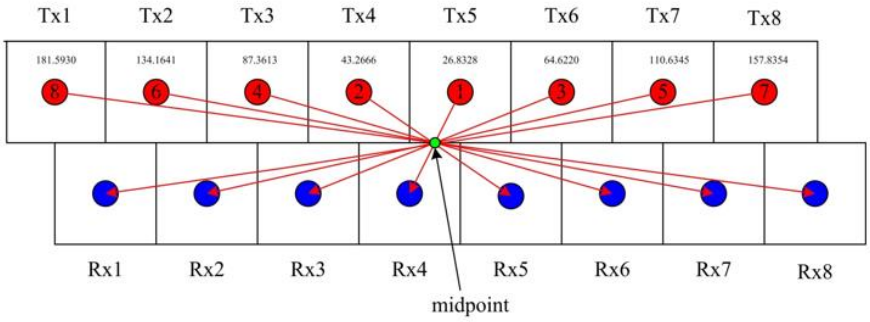

Fig. 4.5.4. Antenna configuration of Yakumo.

In this case, still following the law of cosine, we can rewrite ξ in $|F(\Delta)|$ as below

$$\xi = \sqrt{r^2 + x_i^{\,2} - 2rx_i \cos\theta} - r \tag{4.5.6}$$

where x_i is the offset length of *i*th channel. Thus, by using the offset length of the above configuration, we may have the $|F(\Delta)|$ of Yakumo system in Fig. 4.5.5.

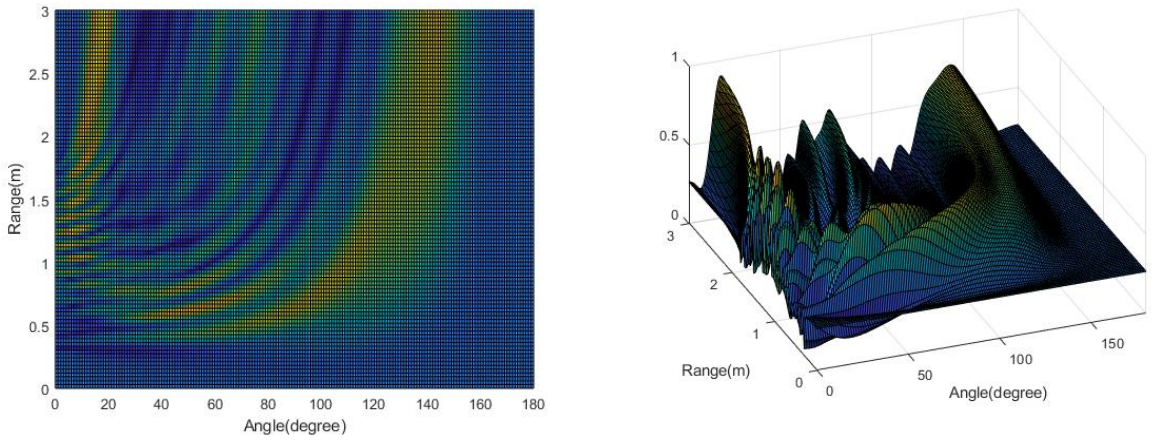

Fig. 4.5.5. $|F(\Delta)|$ of Yakumo.

Note that we have assumed Δ is small, so only a small range of $|F(\Delta)|$ needs to be concerned, the figures below shows the behavior of $|F(\Delta)|$ within 1°.

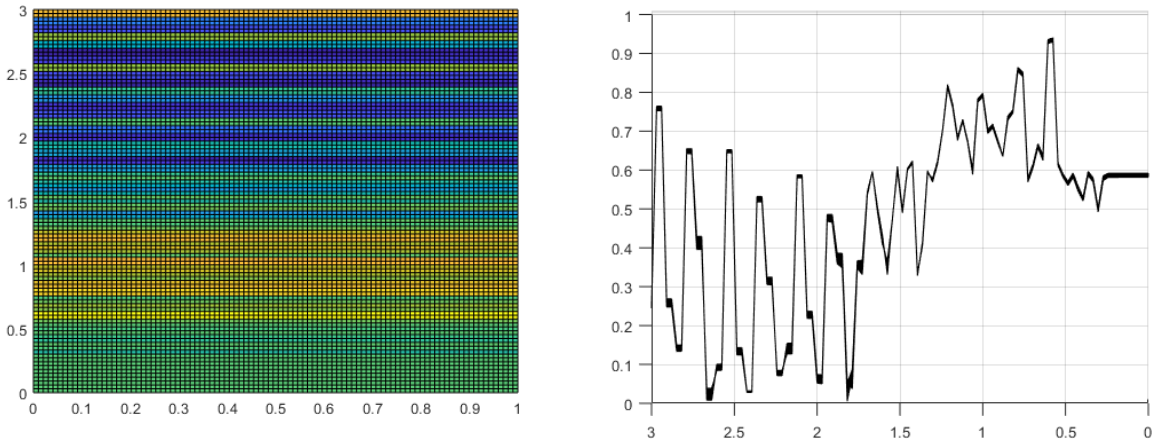

Fig. 4.5.6. $|F(\Delta)|$ of Yakumo within a small angle.

By observation, we know that the $|F(\Delta)|$ is not only related to the range parameters in a small value. However, no matter where the target is, the $R(\Delta)$ is always larger than 0, it means the resolution can be infinitely high(infinitely small angle),and it applies same to the range parameters.

The conclusion may be very anti-intuitive, however, the resolution of MUSIC estimator is directly linked with the approximation form of our covariance matrix, which means it can generate 0 error estimation because of the assumptions given.

Resolution discussion above is mainly based on the method given by the hypothesis of two closely located target. To achieve a more convincible proof, we will need Cramer-Rao Lower Bound (CRLB) to acquire a lower bound in terms of statistics to be our practical resolution for DOA estimation.[ref] gives a detailed math procedure of calculating the MUSIC algorithm's resolution in the far field.

Under the assumptions we stated in Chapter2, the CRB of θ and r are given by

$$\mathrm{CRB}(\theta)=\frac{\sigma}{2}\left\{\mathrm{Re}\left[X^{*}(t)D^{*}[I-\frac{AA*}{m}]DX(t)\right]\right\}^{-1} \tag{4.5.7}$$

and

$$\mathrm{var}(\sigma)=\frac{\sigma^{2}}{mN} \tag{4.5.8}$$

where D is a partial derivative matrix versus θ and r

$$D=\frac{\partial A(\theta,r)}{\partial\theta} \tag{4.5.9}$$

or

$$D=\frac{\partial A(\theta,r)}{\partial r}\ . \tag{4.5.10}$$

Under the far field assumptions r will be eliminated, thus the lower bound can be written as

$$\mathrm{CRB}_F \simeq \frac{6}{M(M-1)SNR}. \tag{4.5.11}$$

In this case, knowing that our assumptions contains 0 error in imaginary conditions. The CRB is infinitely high in the far field. And it applies to the near field cases as well.

4.6 Generalized EVD and Generalized SVD MUSIC

Using the same signal model, as mentioned, we can rewrite covariance matrix of *X*

$$S_1 = AQA^H + S_2 \tag{4.6.1}$$

where S_1 is the covariance matrix of the received signal and S_2 is the sum of all expected values related to *N*. According to conventional MUSIC, we first apply GEVD

$$S_1 z = \lambda S_2 z \ . \tag{4.6.2}$$

where λ and *z* are the GE value and GE vector of matrix pencil $\{S_1, S_2\}$, respectively. Then (4.6.1) can be rewritten as

$$S_1 z = (AQA^H + S_2)z \tag{4.6.3}$$

which yields

$$(1-\lambda)S_2 z = AQA^H z \ . \tag{4.6.4}$$

One important thing to note is the estimation of the covariance matrices S_1 and S_2. In the practice, the estimation is evaluated by $\frac{1}{L}XX^H$, where $X = X(t)$ and L is the snapshot length. However, it inevitably causes errors since the signal length is finite. According to Golub and Van Loan [15] ,one possible solution is to transform (4.6.3) into a GSVD-related subspace, which results in

$$\mathrm{span}\{k_{d+1},\ldots,k_M\} = \{k \mid XX^H k = \lambda_{\min} NN^H k\}. \tag{4.6.5}$$

Note that $\lambda_{\min}$ is also the square of the minimum singular value $\sigma_{\min}$ of matrices pencil $\{X, N\}$. Speiser and Van Loan also present an essential theorem, which allows the GSVD, in this case, to be expressed as

$$K^H(X^H X)K = diag(\alpha_1,...,\alpha_M)$$

and

$$K^H(N^H N)K = diag(\beta_1,...,\beta_M). \tag{4.4.6}$$

where the *i*th column vector of *K* is the GS vector matrix for the GS value $\sigma_i = \sqrt{\frac{\alpha_i}{\beta_i}}$, *i*=1,…*M*. Then the corresponding relations among generalized eigenvalue, generalized singular value, and generalized singular vector are established, and (13) can be approximated as

$$(1-\sigma_i)Nk_i = s(t)A(d,v)k_i. \tag{4.6.7}$$

However, to generate the velocity-depth spectrum, we must formulate a spectrum function such as (8), which requires the orthogonality of *A* and *k*. Clearly, $_{\sigma}$=1 can cause orthogonality, but it is trivial according to the feature of GSVD; in this case, one approach is to create an orthogonal basis from *K*. For example, Speiser and Van Loan propose an improved GSVD method that can reform *K* to an orthogonal basis. Compared to the traditional 2-step GSVD decomposition with QR and CS decomposition, it has another QR decomposition at the end.

According to (4.6.7), the mentioned procedure can be simplified by finding a nontrivial GSVD value close to 1 as an indicator of orthogonality. Mathematically, the spectrum function can be

$$P(d,v)=\frac{1}{\min\left|1-\sigma_i\right|} \tag{4.6.8}$$

where σ_i , $\sigma_i \neq 1$ and i = 1,2…M, is the ith Generalized Singular Value resulting from a GSVD operation for each iteration of *d* and *v*.

Finally, because the processing is based solely on phase information, selecting the arrival time is important. As mentioned, GPR profiles are usually cluttered and full of background noises. As a result, it is challenging to precisely select the first arrival time from the time-domain signal; thus, the arrival time can only be determined roughly, which requires the MUSIC algorithm to work in a high SNR condition with all kinds of noise concerned. It is for this reason that GSVD is proposed for use with the MUSIC method, as it avoids the evaluation of covariance matrices.

However, if we use the signal mode mentioned, the above algorithms may not work well, simply because of the ill-posed structure that our covariance matrix has. A solution of the covariance matrix that solely has the phase noise is to construct a identical matrix in a GEVD. Because in (4.5.2) when S_2=I, the GEVD will turn to be EVD that has an orthogonality as it is in conventional music.

Assume that matrix element-wise division can sperate the phase error as shown in (4.6.8)._

$$R_{xx}./\bar{R}_{xx}=\begin{bmatrix} 1 & e^{j\omega_c(\Delta\tau_{2,1})} & \cdots & e^{j\omega_c(\Delta\tau_{n,1})} \\ e^{j\omega_c(-\Delta\tau_{2,1})} & 1 & & \\ \vdots & & \ddots & \\ e^{j\omega_c(-\Delta\tau_{n,1})} & & & 1 \end{bmatrix} \tag{4.6.8}$$

The phase noise in the exponential term should be relatively smaller than the diagonal element 1. In this case, if the input covariance matrix and the ground truth are close to each other. We can perform a operation in (4.6.9) to approximately generate an identical matrix for GEVD without loss of the information of the phase error terms.

$$\begin{bmatrix} 1 & \Psi\Delta\tau_{1,2} & \cdots & \Psi\Delta\tau_{1,N} \\ -\Psi\Delta\tau_{1,2} & 1 & & \\ \vdots & & \ddots & \\ -\Psi\Delta\tau_{1,N} & & & 1 \end{bmatrix} \tag{4.69}$$

where Ψ is a scalar that has to be manually adjusted.

To demonstrate the procedure, a simulation is carried out to show that the different scalar Ψ will give different results. Only under a correct estimation, the orthogonality will appear.Assuming that we have a ground truth input array [3.578 4.68 6.33 8.21] ns which corresponds to a target in [0.15,0.1125x10^9] on MUSIC spectrum. Our observation data and input array will be [3.51,4.63,5.98,8.21] ns, and the goal of the processing is to have a same spectrum which has a target at [0.15,0.1125x10^9].

In this case, we will use the first input 3.51 as the reference phase to start the iteration. And the scalar in(4.69) will be set to 10^9 and 10^8

The results are shown in Fig.4.6.1 and Fig.4.6.2. And according to the amplitude the orthogonality only appears on the ground truth associated position on the spectrum. Though there is a ghost target.

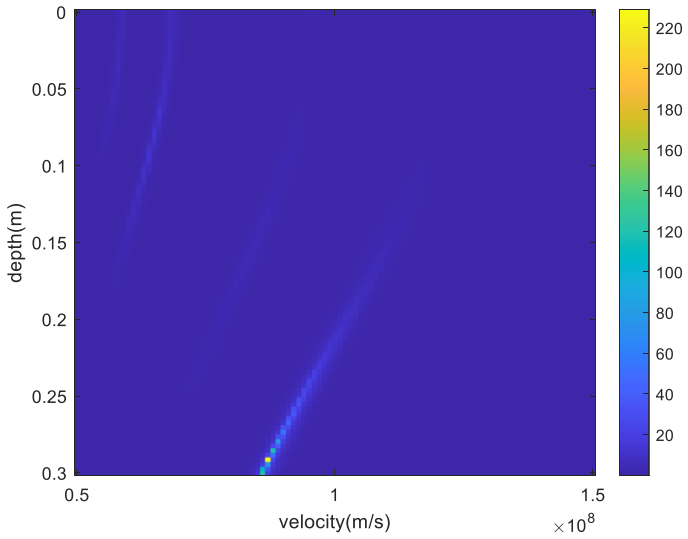

Fig.4.6.1 MUSIC spectrum generated by GEVD with a scalar $\Psi = 10^9$.

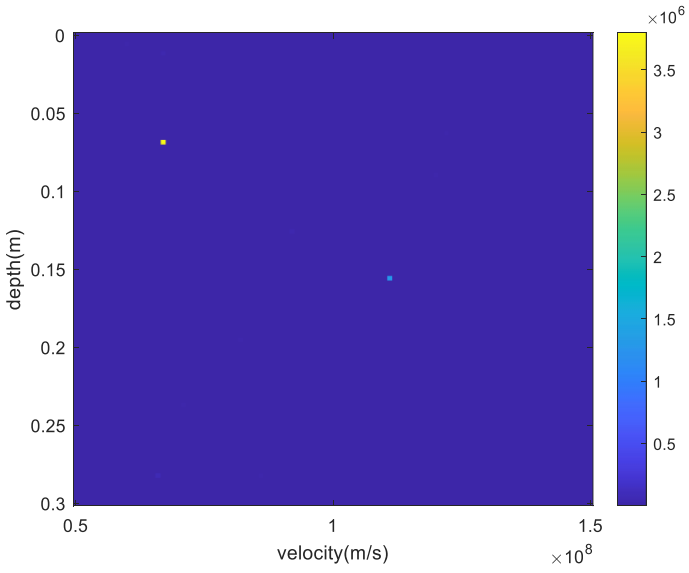

Fig.4.6.2 MUSIC spectrum generated by GEVD with a scalar $\Psi = 10^8$.

4.7 Experiments

Common MidPoint (CMP) method has been applied to Ground Penetrating Radar (GPR) surveys for decades, and it has proven to be successful in many fields, such as geoscience and civil engineering [8~10]. Specifically, GPR CMP surveys are efficient for subsurface layer detection since multi-static data can be used for further research, such as velocity-depth analysis[11,12]. The investigation reveals two essential parameters of a horizontal homogenous subsurface layer: layer depth and EM wave propagation speed. Conventionally, velocity-depth analysis is performed using Synthetic Aperture Radar (SAR)-based processing; however, it has many limitations due to its one-layer scenario and the correlation calculation that entirely relies on the amplitude. As a result, the accuracy of the estimation is insufficient. Therefore, various efforts have been made to introduce super-resolution techniques, for example, the MUSIC algorithm, to achieve better imaging quality for the CMP profile[13,14]. Nonetheless, the MUSIC algorithm requires arrival time information prior to processing, which means the arrival time must be manually determined. Consequently, it leads to two issues: the first is an error in arrival time determination, and the second is that reflection responses are hard to distinguish from one another. we applied near-field MUSIC combing with a self-adaptive peak detection introduced in the previous sections. Because the receivers are not receiving signal parallel, the far field condition cannot be fitted, in this case, there is one more parameter other than an arrival angle to be evaluated. A simulation of the two-layer structure and an on-site road pavement detection experiment are conducted. The results show that MUSIC-based approaches can generate a velocity-depth spectrum with higher resolution compared to conventional amplitude-based processing. Furthermore, the suggested method can reveal a layer that the traditional method cannot identify, by employing weak reflection from the time-domain signal.

Assuming there is only one homogenous subsurface layer, the propagation path of the EM wave can be simplified, as shown in Fig. 1.

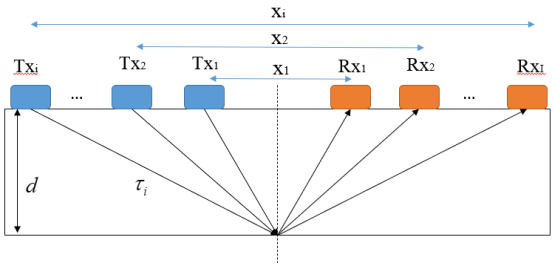

Fig.4.7.1. Schema of the layer and array configuration.

Here x_i is the offset of the ith antenna pairs, d is the layer depth, τ_i is the two-way arrival time of received signal for each antenna pair and v is the signal transmission velocity in the subsurface in the expression

$$\tau_i = \frac{2\sqrt{d^2 + \frac{x_i^2}{4}}}{v} \tag{4.7.1}.$$

Regarding multi-layer cases, for example, two-layer subsurfaces, a schema can be considered as in Fig. 2.

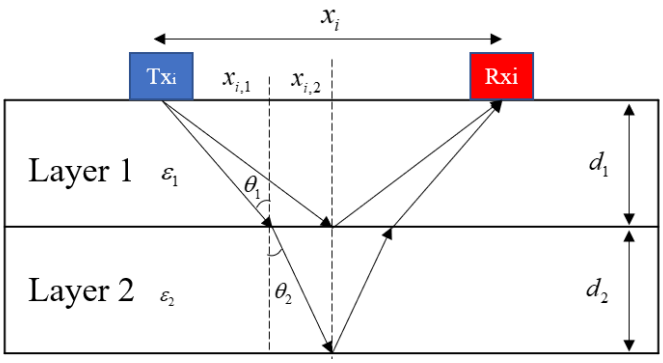

Fig4.7.2. Schema of the two-layer case.

In general, assuming there are Z layers, x_i can be sperated to sections, which donates $x_{i,q}$, where $i = 1, \cdots, M$ and $q = 1, \cdots, Z$. In this two-layer situation, there will be two arrival times for each channel concerned: one from the direct reflection from layer 1 and another from layer 2. The two-way arrival time of reflection from layer 2, τ'_i, can be expressed as

$$\tau'_i = \frac{2\sqrt{x^2_{i,1} + d_1^2}}{v_1} + \frac{2\sqrt{x^2_{i,2} + d_2^2}}{v_2} \tag{4.7.2}$$

where $x_{i,1}$ and $x_{i,2}$ numerically follows (4.7.3) and (4.7.4)

$$x'_{i,1} + x'_{i,2} = \frac{x_i}{2} \tag{4.7.3}$$

and

$$\frac{\sin\theta_1}{\sin\theta_2} = \sqrt{\frac{\varepsilon_2}{\varepsilon_1}} = \frac{v_1}{v_2}. \tag{4.7.4}$$

The expression follows the same approach when there are two or more layers.

4.7.1 Conventional CMP velocity-depth estimation

Conventional CMP velocity-depth estimation can be considered as taking correlations between the theoretical calculated arrival time and the measurement data arrival The technique is shown in Fig. 3. By iterating *v* and *d*, a 2D representation can be plotted, the so-called velocity-depth spectrum.

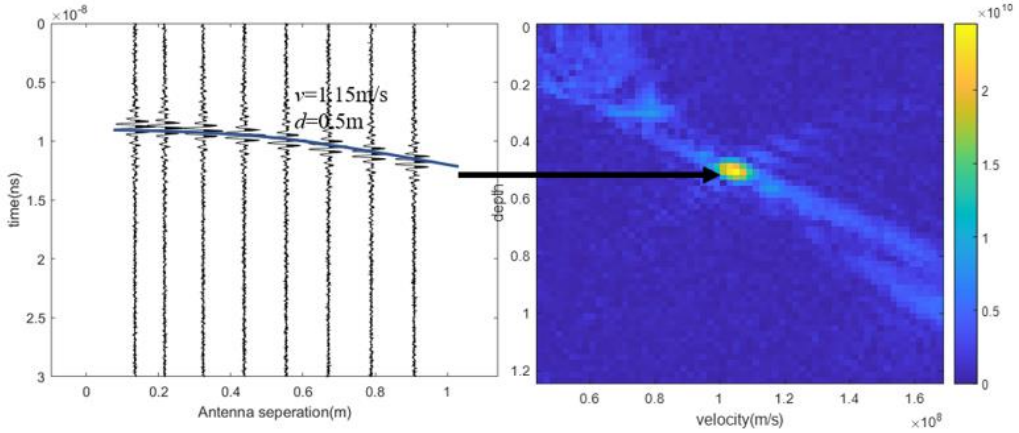

Fig.4.7.3. CMP profile in Wiggle plot and the process of transforming time-domain received data into a velocity-depth spectrum

Mathematically, the spectrum is a function of two variables *v* and *d*, which gives,

$$P(v,d)=\sum_{i=1}^{M} s_i(\tau_i(v,d)) \tag{4.7.5}$$

where *M* is the number of antenna pairs, s_i is the time-domain signal of the *i*th channel and τ_i has an explicit form as shown in (4.7.1).

There are two main advantages of conventional velocity-depth estimation. The first is that it requires only amplitude information. Another benefit is that the processing can be applied to complex or real signals, allowing it to operate on various commercial systems. However, as mentioned, this method has low resolution; moreover, the process does not account for the refraction from EM wave propagation. As a result, the estimation for the multi-layer subsurface contains errors.

4.7.2 MUSIC for CMP

We assume that the time domain signal for each channel has the following form

$$s(t)=De^{j\omega(t-\tau_i)} \tag{4.7.6}$$

where *D* is the amplitude and ω is the working frequency. It can be reformulated as a reference channel by multiplying with a phase difference term

$$s(t)=De^{j\omega(t-\tau_1)}e^{-j\omega(\Delta\tau_i)} \tag{4.7.8}$$

where

$$\Delta\tau_i=\frac{2(\sqrt{d_1^{\,2}+\frac{x_1^2}{4}}-\sqrt{d_1^{\,2}+\frac{x_i^2}{4}})}{v} \tag{4.7.8).}$$

If we only consider the first layer. According to the above equations, regardless of the amplitude, the received signal *X*(*t*) can be written by using a reference signal *s*(*t*) and the steering matrix *A*

$$X(t) = A(d,v)s(t) + N\,. \tag{4.7.9}$$

Using (4.1.5), the MUSIC algorithm can be applied, by calculating the covariance matrix of $X(t)$, and (4.1.4)can be formulated as follows

$$R_{xx} = A(d,v)QA(d,v)^H + \sigma^2 I \tag{4.7.10}$$

where R_{xx} is the covariance matrix of the received signal, Q is the covariance matrix of the reference signal. Then the velocity-depth spectrum F can be expressed by

$$P_{MUSIC}(d,v) = \frac{1}{\|A(d,v)E_n\|} \tag{4.7.11}$$

where E_n is the associated noise subspace eigenvectors [9]. A can be explicitly written as

$$A = [1, e^{j\omega \frac{2(\sqrt{d_1^2 + \frac{x_2^2}{4}} - \sqrt{d_1^2 + \frac{x_1^2}{4}})}{v}}, ..., e^{j\omega \frac{2(\sqrt{d_1^2 + \frac{x_M^2}{4}} - \sqrt{d_1^2 + \frac{x_1^2}{4}})}{v}}]\,. \tag{4.7.12}$$

For the multi-layer cases, for example, the two-layer structure. steering matrix A must be remodified, v_1 and d_1 must be determined before the iteration of v_2 and d_2 to solve $x_{i,1}$ and $x_{i,2}$, which gives

$$A' = [1, ..., e^{j\omega 2(\frac{\sqrt{x_{i,1}^2 + d_1^2}}{v_1} + \frac{\sqrt{x_{i,2}^2 + d_2^2}}{v_2} - \frac{\sqrt{x_{1,1}^2 + d_1^2}}{v_1} - \frac{\sqrt{x_{1,2}^2 + d_2^2}}{v_2})}] \tag{4.7.13}$$

where A' is the modified steering matrix designated for the second layer arrival time. Thus, the visualization must be completed layer by layer. There are many ways to achieve layer-by-layer visualization. One approach is to select the first few peaks located in the shallowest position on the velocity-depth spectrum and mark them as layer 1, then replot the spectrum using the information given by layer 1. Another way is to use prior knowledge to provide a rough estimation of the depth of the subsurface layer structure, which avoids the redundant judgment for identifying the peaks used in the previous method.

As mentioned, in the section 4.2 the imaging process must be done layer by layer; consequently, it is better to utilize T part by part to avoid miscalculating the multi-layer structure. However, if there is no approximate prior knowledge of the subsurface structure, performing the MUSIC algorithm with the complete enumeration of T is necessary to locate the first layer. In addition, compared to the original MUSIC, the proposed method includes an equation-solving procedure for $x_{i,q}$ for each iteration of v_i and d_i. The mentioned procedures apply the same to the third and fourth layers, and so on. In practice, it is preferable to integrate layers with close relative permittivity to avoid a significant computational load. The flowchart of the proposed method is shown in Fig. 5.

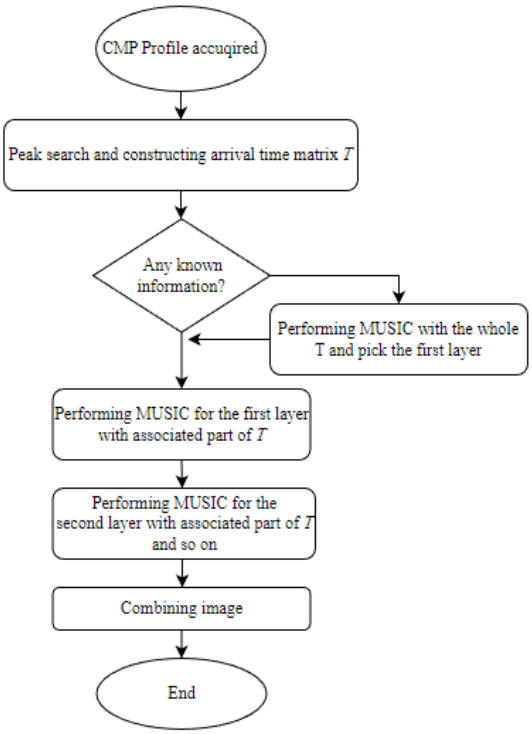

Fig.4.7.5. Flowchart of the proposed method.

This experiment employs an array GPR system for road pavement inspection. Fig. 4.7.6 shows the experiment setup. Fig.4.7.8 illustrates the array configuration. The array GPR system Yakumo is an SFCW system, operating from 65 MHz to 1.5 GHz. There are 8 antenna pairs, but because of the attenuation, we only use the 4 closest antenna pairs for processing. The arrival time is determined by the peaks of the real part of the signal and $L = 12$. To avoid as much noise and clutters as possible, 10 adjacent CMP profiles are added to the selected CMP profile before taking the average.

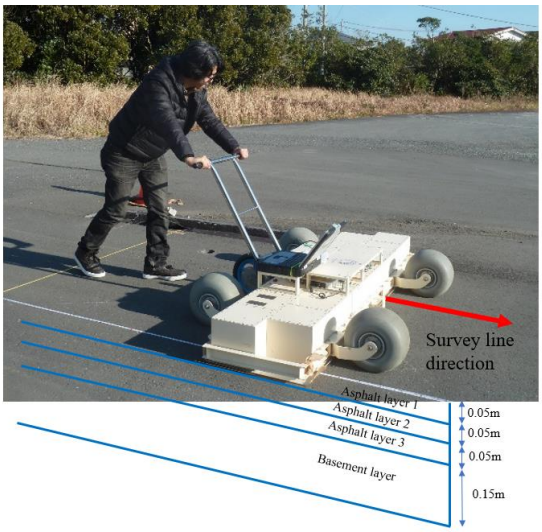

Fig.4.7.6. Road pavement inspection using Yakumo.

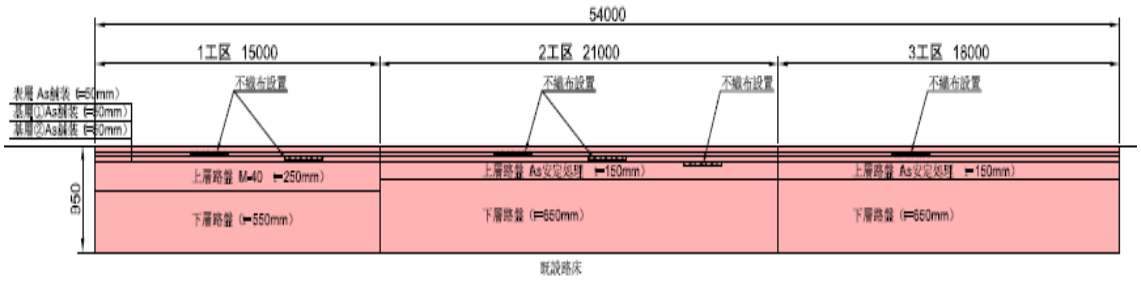

Fig. 4.7.7. Road pavement construction print.

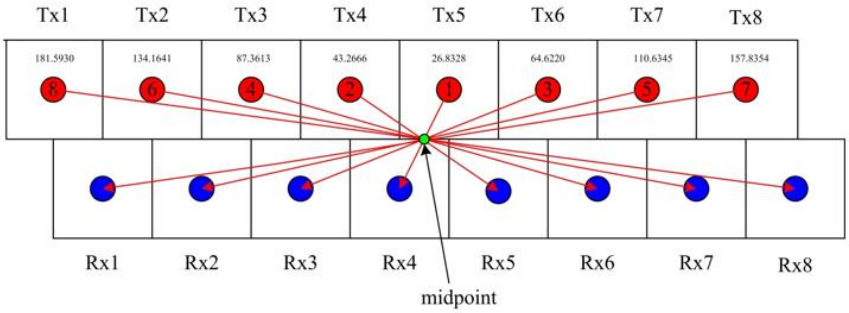

Fig. 4.7.8. Antenna configuration of Yakumo.

In this case, there are 3 asphalt layers on top of the base layer as drawn in Fig.4.7.6 and Fig.4.7.7; to avoid redundant calculation, we assume that the asphalt layers from 0m to 0.15m have a very close relative permittivity and can be merged into a single layer. The spectrum generated by the conventional method is shown in Fig. 10.

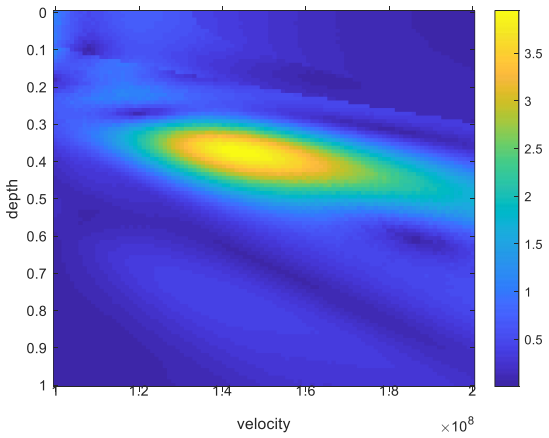

Fig.4.7.9. The Velocity-depth spectrum generated by the conventional method.

In contrast to the procedure presented in the simulation part, the subsurface structure is only approximately known here. Thus, the layer-by-layer imaging is set to be 0.2 m by 0.2 m. The first layer search can be done directly using the first few peaks because peaks located after a specific time are not possibly generated by the asphalt layer with a thickness of around 0.15 m. Therefore, the first 4 row vectors

of *J* are more than enough for this stage of the first layer detection. Then, by following the same procedure, the spectrums of the asphalt layer, the base layer and a combined spectrum can be plotted as shown in Fig. 10.Compared to the available information, the proposed method has an error of 10 % in thickness estimation. It may be caused by integrating the first 3 layers or the pavement construction itself. When compared to the conventional method, it produces a better result that clearly reveals 2 layers and provides useful velocity-depth information.

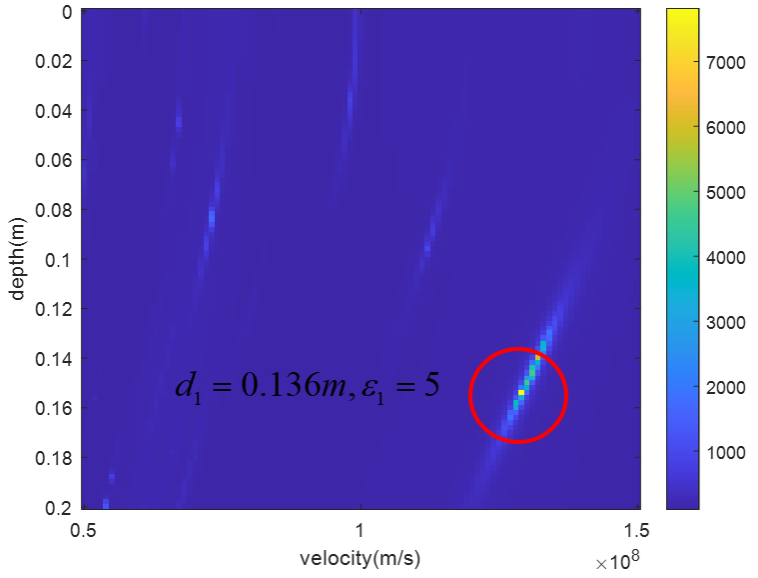

(a)

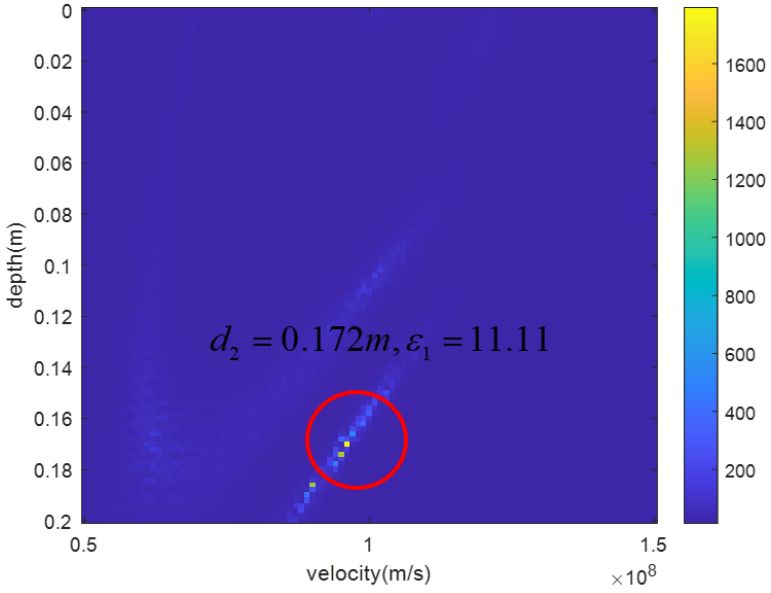

(b)

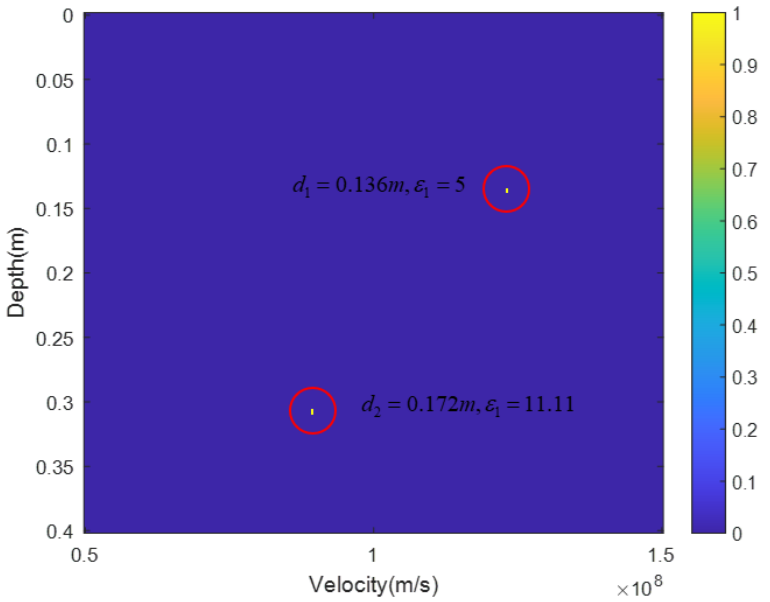

(c)

Fig.4.7.10. (a)The velocity-depth spectrum of the base layer. (b) The velocity-depth spectrum of the asphalt layer. (c) The combined velocity-depth spectrum of the pavement.

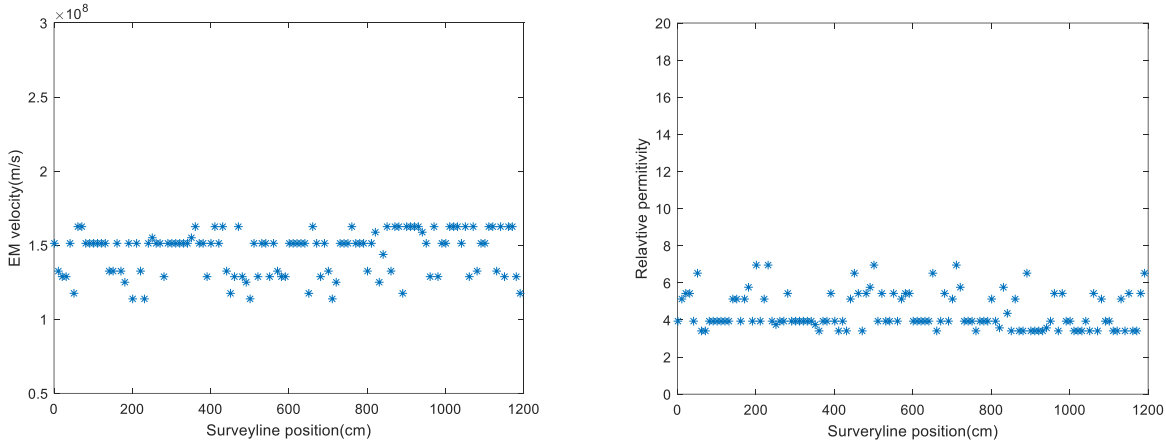

Fig.4.7.11. EM velocity and relative permittivity distribution of the first layer along the survey line

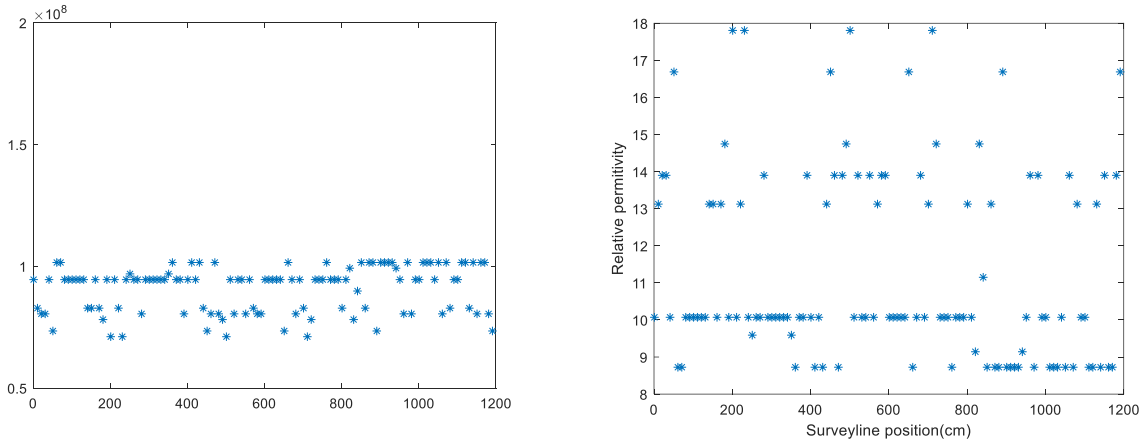

Fig.4.7.12. EM velocity and relative permittivity distribution of the second layer along the survey line

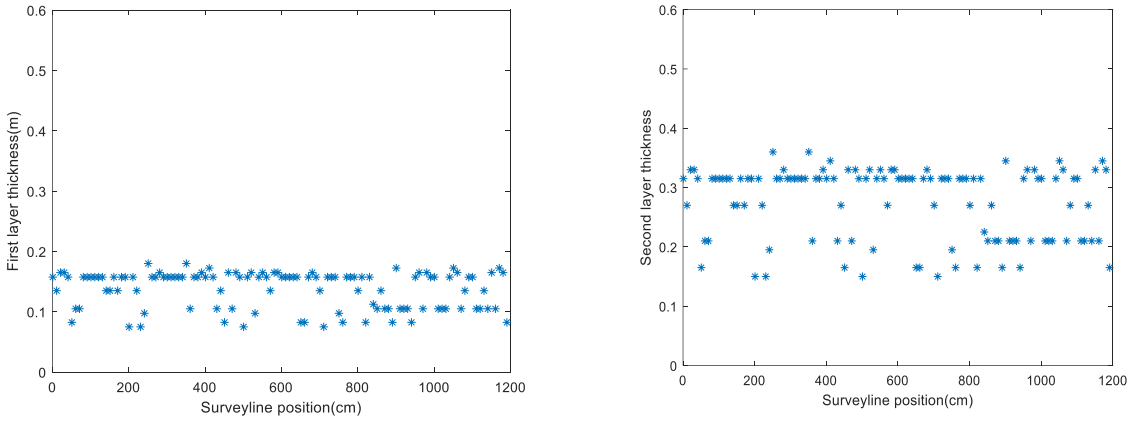

Fig.4.7.13.Thickness of the first layer and second along the survey line

In the previous section, the refraction is considered to achieve the arrival time selection as precise as possible. However, the calculation process is extremely complicated and time consuming. As previous mentioned, GEVD is another approach to solve the problem. In this section, different from the previous one, the first layer is our only target. The selected arrival time is [4.47 5.85 7.92 10.26] ns, and they are all located at the stationary points on each trace of signal.

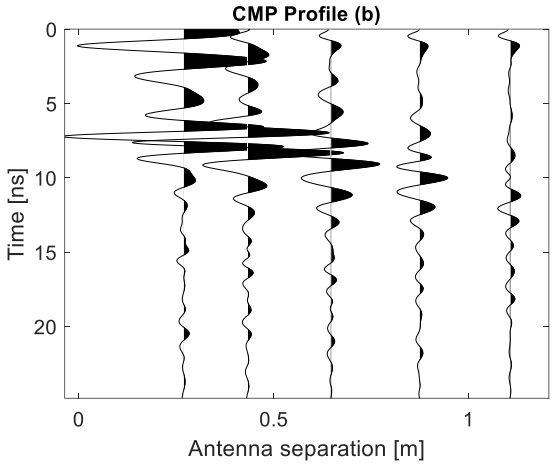

Fig.4.7.14. Time domain signal of the CMP Profile.

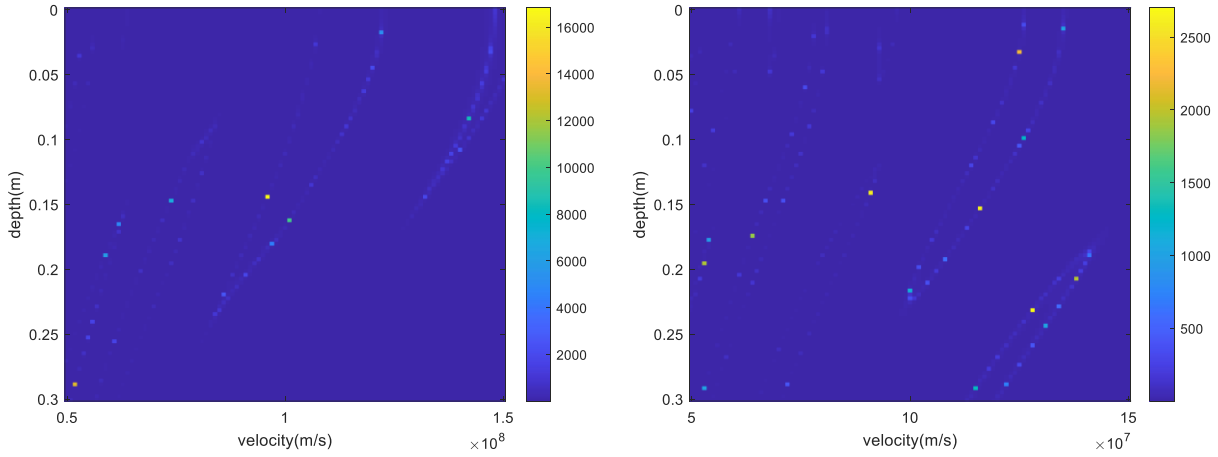

(a) Velocity depth spectrum when $\Psi = 3\times10^{8}$ (b) Velocity depth spectrum when $\Psi = 10^{9}$

Fig.4.7.15. The proposed method while the scalar is (a)3x10^{8} (b)10^{9}.

The results show that the proposed method is more robust compared to the original MUSIC. However, it is hard to judge which result is more correct in this experiment. Because the ground truth of the electric permittivity can hardly be stated, a conclusion can be drawn indicating that no matter what approach we use, the error of thickness of the first layer is around less than 10% and the relative permittivity is in a range between 5~10.

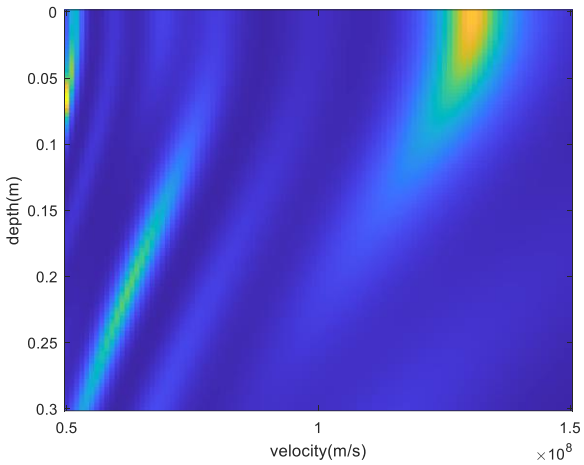

Fig.4.7.16 The result of the original MUSIC.

The main idea of this method is to solve the following problem

$$\arg\min_{v,d}\left\{\begin{bmatrix} 1 & \tau_2-\tau_1+\Delta\tau_{21} & \cdots & \tau_n-\tau_1+\Delta\tau_{n1} \\ \tau_1-\tau_2-\Delta\tau_{21} & 1 & & \\ \vdots & & \ddots & \\ \tau_1-\tau_n-\Delta\tau_{n1} & & & 1 \end{bmatrix}-\begin{bmatrix} 1 & \tau_2-\tau_1 & \cdots & \tau_n-\tau_1 \\ \tau_1-\tau_2 & 1 & & \\ \vdots & & \ddots & \\ \tau_1-\tau_n & & & 1 \end{bmatrix}\right\}. \quad (4.7.14)$$

Yet the problem may not have a clear answer, or in other words, there might be multiple stationary points.

4.7.3 Localization by using Software defined radio

In recent years, Software Defined Radio (SDR) attracted plenty of focus due to its compatibility that can be used for multiple purposes[18,19].The picture below is a typical commercial SDR RTL-SDR designed for receiving TV signal

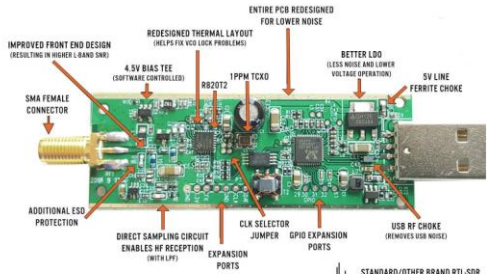

Fig.4.7.17 An example of commercial SDR.

In this experiment, we want to achieve subspace DOA estimation by assembling a ULA system using such commercial equipment .The design of the system contains only two parts: LASDR (Linear Array Software Defined Radio) with an external clock for time synchronization and computer for data processing and visualization. Fig.4.7.18 is the experiment setup. Fig. 4.7.19 shows the schematic diagram of the system setup

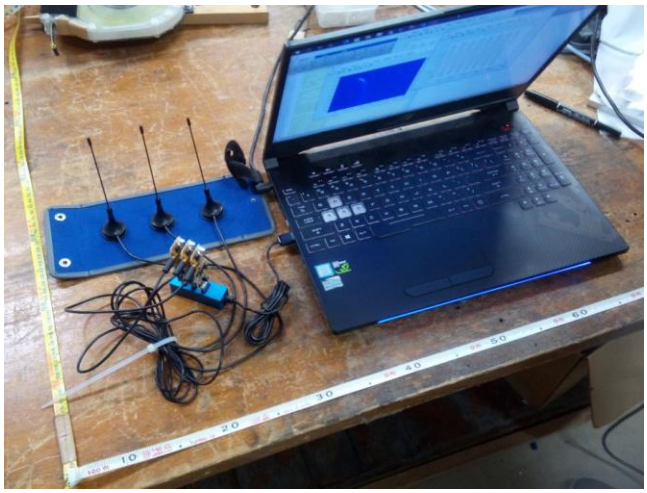

Fig.4.7.18. ULA SDR experiment setup.

For the target that is located within near field the reference SDR antenna, it will return a result with the range r and the angle θ of the target, and for the target located in the far field 2 wavelengths from the reference channel, the algorithm will return a result only containing the direction θ.

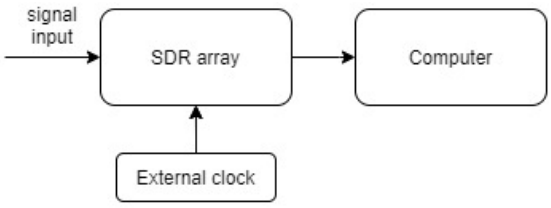

Fig.4.7.19 ULA SDR System setup.

we conducted laboratory experiment to verify the stability of the proposed method for measured data. All measurements use Vivaldi antenna for transmitter and receiver elements and all measurements are using a 4 elements ULA and an oscilloscope for data acquisition instead of using SDR units. The reference antenna is set to be the very left one. Fig.4.7.20.(a)shows the result of a single target measurement where the target is locating at r=0.23m, θ= 50°. Another experiment is carried out to verify the performance of algorithm for signal sources located in the far field wavelengths from the reference antenna. Fig.3.(b) shows the result when the target is at r=0.9m, θ= 60°. Both 2D MUSIC and optimized 2D MUSIC are applied and their performance are close. 2D MUSIC focuses the target along angle around 60°and the optimized MUSIC stop iteration at θ= 60° due to the divergence of the function value .

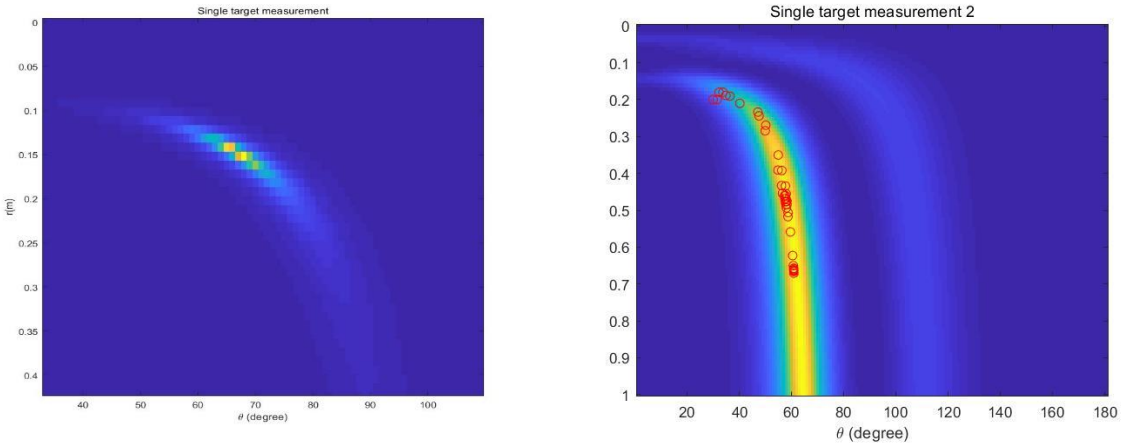

Fig.4.7.20. Experiment result for signal source in the near field and in the far field

These results prove the feasibility of the proposed algorithm. In addition, we also carried out the experiment with the SDR inbuilt clock and computer inbuilt clock, unfortunately, the acquired data is unable to be post-processed because the precision of the clocks are not suitable for the proposed algorithm. In the demonstration, the clocks on SDR will be removed and replaced with external clock for time synchronization for each SDR unit.

4.8 Summary

In this chapter, near field MUSIC is introduced. in addition, some improvements are made to solve two problems. The arrival time error caused by the manual selection. One possible way to tackle this problem is to take all the stationary points on all channel into consideration. The advantage is that some hidden information can be revealed; however, the disadvantage is obvious, the scale of computation is too large. Thus, it leads to the second problem, how to reduce the redundancy of the calculation? For the peak search process, we can reduce the selected points by following some certain rules, but it is somehow trivial, in this work, the novelty is that the proposed optimization methods can have the same result without performing a $O(N^2)$ scan process. Besides, this work also introduces some classical work based on the advanced matrix theory to solve the arrival time error problem by directly using the matrix decompositions. However, these methods are not as stable as they are when being applied under the designed conditions. We carried out both experiments and simulations to verify the feasibility of the proposed method, results show that the MUSIC based methods can be applied to the various fields by modifications.

In term of the theoretical finding, we exam the near field resolution of the MUSIC under the assumptions made in the previous chapters, the result proves that there is no explicit formulation to conclude the resolution of the MUSIC in a simplified form. Also, Section 4.3 indicates that the near field and far field has no clear borderline, or in other words, numerically, the far field is not located further than Fraunhofer distance.

References

[1] R. Schmidt, "Multiple emitter location and signal parameter estimation," in *IEEE Trans. Antennas Propag.*, vol. 34, no. 3, pp. 276-280, March 1986.

[2] A. L. Swindlehurst and T. Kailath, "A performance analysis of subspace-based methods in the presence of model errors. I. The MUSIC algorithm," in *IEEE Trans. Signal Process.*, vol. 40, no. 7, pp. 1758-1774, July 1992.

[3] J. Li, D. Li, D. Jiang and X. Zhang, "Extended-Aperture Unitary Root MUSIC-Based DOA Estimation for Coprime Array," in *IEEE Commun.s Lett.*, vol. 22, no. 4, pp. 752-755, April 2018.

[4] F. Wen, "Computationally Efficient DOA Estimation Algorithm for MIMO Radar With Imperfect Waveforms," in *IEEE Communications Letters*, vol. 23, no. 6, pp. 1037-1040, June 2019.

[5] X. Wang, L. Wan, M. Huang, C. Shen, Z. Han and T. Zhu, "Low-Complexity Channel Estimation for Circular and Noncircular Signals in Virtual MIMO Vehicle Communication Systems," in *IEEE Trans. Veh. Technol.*, vol. 69, no. 4, pp. 3916-3928, April 2020.

[6] X. Huang and B. Liao, "One-Bit MUSIC," in *IEEE Signal Process. Lett.*, vol. 26, no. 7, pp. 961-965, July 2019.

[7] A. Osman, M. M. E. Moussa, M. Tamazin, M. J. Korenberg and A. Noureldin, "DOA Elevation and Azimuth Angles Estimation of GPS Jamming Signals Using Fast Orthogonal Search," in *IEEE Trans. Aerosp. Electron. Syst.*, vol. 56, no. 5, pp. 3812-3821, Oct. 2020.

[8] L. Yi, K. Takahashi and M. Sato, "A fast iterative interpolation method in f-k domain for 3D irregularly sampled GPR data," in *IEEE J. Sel. Topics Appl. Earth Observ*. vol. 9, no. 1, pp. 9-17, Jan. 2016.

[9] H. Liu, Z.Shi, Jianhui Li, C. Liu, X. Meng, Y. Du and J. Chen, "Detection of Cavities in Urban Cities by 3D Ground Penetrating Radar," in *Geophysics*, vol. 86, no. 3, pp. A27-WB97, 2021.

[10] H. Liu, J. Zhong, F. Ding, X. Meng, C. Liu, and J. Cui, "Detection of Early-stage Rebar Corrosion Using a Polarimetric Ground Penetrating Radar System," in *Constr Build Mater.*, vol. 317, no. 24, pp. 1-10, Jan 2022

[11] X. Feng, M. Sato, Y. Zhang, C. Liu, F. Shi and Y. Zhao, "CMP Antenna Array GPR and Signal-to-Clutter Ratio Improvement," in *IEEE Geosci. Remote Sens. Lett.*,vol. 6, no. 1, pp. 23-27, Jan. 2009.

[12] H. Liu, K. Takahashi and M. Sato, "Measurement of Dielectric Permittivity and Thickness of Snow and Ice on a Brackish Lagoon Using GPR," in *IEEE J. Sel. Topics Appl. Earth Observ.*, vol. 7, no. 3, pp. 820-827, Mar. 2014.

[13] S. Zhao and I. L. Al-Qadi, "Super-Resolution of 3-D GPR Signals to Estimate Thin Asphalt Overlay Thickness Using the XCMP Method," in *IEEE Trans. on Geosci. Remote Sens.*, vol. 57, no. 2, pp. 893-901, Feb. 2019.

[14] C. Le Bastard, V. Baltazart, Y. Wang and J. Saillard, "Thin-Pavement Thickness Estimation Using GPR With High-Resolution and Superresolution Methods," in *IEEE Trans. on Geosci. Remote Sens.*, vol. 45, no. 8, pp. 2511-2519, Aug. 2007.

[15] Golub and C.F. Van Loan, *Matrix Computations*, Johns Hopkins Univ. Press, Baltimore, 1989

[16] R. G. Machado and A. M. Wyglinski, "Software-Defined Radio: Bridging the Analog–Digital Divide," *Proc.* of *the IEEE*, vol. 103, no. 3, pp. 409-423, March 2015

[17] J. Bonior, Z. Hu, T. N. Guo, R. C. Qiu, J. P. Browning and M. C. Wicks, "Software-Defined-Radio-Based Wireless Tomography: Experimental Demonstration and Verification," in *IEEE Trans. Geosci. Remote Sen*, vol. 12, no. 1, pp. 175-179, Jan. 2015.

Chapter 5. Estimation of Signal Parameters via Rotational Invariance Techniques

ESPRIT-like methods have garnered significant attention and have found widespread practical applications as one of the most significant approaches for DOA estimation. In recent years, ESPRIT are widely used in the field of MIMO processing at. el., proposed near field DOA estimation method by partially utilizing the ESPRIT method[1]. Except the amplitude and phase information, the polarization information is also significantly important, thus, Li et. al., proposed an improved technique for processing the polarization data with much lower complexity[2].Pan et. al., proposed an enhanced spatial smoothing (ESS) technique to make the full use of both the covariance matrices of individual subarrays and the cross-covariance matrices of different subarrays for solving the coherency[3]. In term of modifying the covariance matrices, Zhang et. al., modified the conventional estimation of the covariance metrics based on Forward and Backward Partial Toeplitz Matrices Reconstruction (FB-PTMR) to fully exploits half rows of the sample covariance matrix (SCM) to reconstruct the data matrix to overcome this weakness[4].

In this chapter, solving the DOA by using least square based techniques are more essential than the ESPRIT itself, because the near field ESPRIT problem is well-solved by Yuen and Friedlander with fourth-order cumulant matrix [5,6]. The reason why the chapter is distinguished from the previous one is because we try to transform the problem to a Least Square (LS) problem and we are trying to solve the DOA problem with the phase error. It is similar to the method that presented in section 4.6 where GSVD and GEVD are used to give an estimation base on the input with phase errors. While in this chapter, we want to solve the same problem with different approaches by constructing over-determined systems for the DOA estimations.

5.1 Original ESPRIT

Under the circumstanced described in Fig.2.5.4. The core of this method is to find a rotational parameter ζ ,which makes

$$X_2(t) = \zeta X_1(t) \tag{5.1.1}$$

where $X_1(t)$ and $X_2(t)$ are received signal matrix from subarray 1 and 2. Subarrays are selected combinations of channels from the received data $X(t)$ of the entire array.

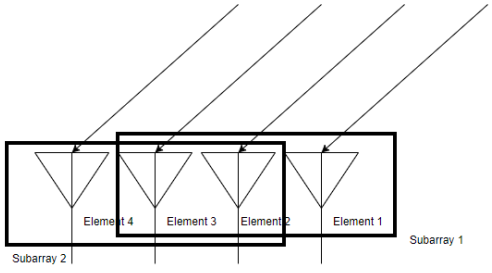

Fig.5.1.1. ULA subarray configuration.

In this configuration, (5.1.1) can be explicitly written as a diagonal matrix

$$X_2 = \begin{bmatrix} e^{j\omega_c d\sin\theta} & 0 & 0 \\ 0 & \ddots & 0 \\ 0 & 0 & e^{j\omega_c d\sin\theta} \end{bmatrix} X_1 . \tag{5.1.2}$$

The equation also can be transformed into multiplications between reference signal and steering matrix with the phase difference term $e^{j\omega_c d\sin\theta}$, which yields

$$X_2(t) = e^{j\omega_c d\sin\theta} A(\theta) x_1(t) \tag{5.1.3}$$

and

$$X_1(t) = A(\theta) x_1(t) . \tag{5.1.4}$$

Consequently, it leads back to (5.1.1), and the next step is to calculate the rotational term. Assuming that there is a kind of matrix decomposition $A(\theta)C = e^{j\omega_c d\sin\theta} C$, we may involve the covariance matrix R_{XX_1} and R_{XX_2} of $X_2(t)$ and $X_1(t)$,

$$R_{XX_2} C^{-1} \left[e^{j\omega_c d\sin\theta} \right]^{-1} C = R_{XX1} \tag{5.1.5}$$

The commonest approach is to use the matrix Least Square(LS) method directly between signal subspaces of R_{XX_1} and R_{XX_2} . Then because of the matrix similarity, the eigen value of the solution is the rotational term under the assumption made for the signal mode. The ESPRIT method has no spectrum function because the DOA parameters are directly solved, and it is one of its advantages over MUSIC; however, the spectrum of ESPRIT in the following sections are particularly designed to achieved the comparison to the MUSIC. Many works indicate that the ESPRIT has lower resolution compared to that of the MUSIC in the far-field case.

5.2 Near field Esprit

Considering Fig.5.2.1 , we know that there will be no rotational invariance term to “shift” the subarrays

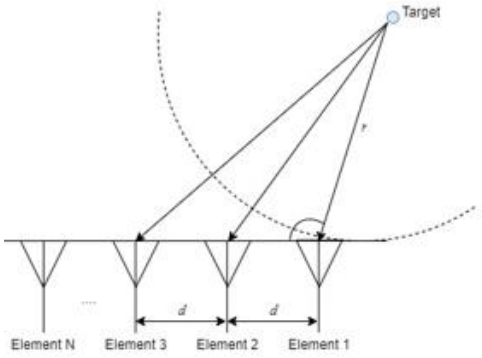

Fig.5.2.1. Near field configuration

As the subarray A_1 and A_2 have following expressions

$$A_1 = [1 \quad e^{\sqrt{r^2+d^2-2rd\cos\theta}-r} \quad \ldots \quad e^{\sqrt{r^2+(M-2)^2d^2-2rd(M-2)\cos\theta}-r}] \tag{5.2.1}$$

and

$$A_2 = [e^{\sqrt{r^2+d^2-2Rd\cos\theta}-R} \quad e^{\sqrt{r^2+4d^2-4rd\cos\theta}-R} \quad \ldots \quad e^{\sqrt{r^2+(M-1)^2d^2-2rd(M-1)\cos\theta}-r}] \tag{5.2.2).}$$

In this case, the received signal of subarrays can be shifted by a diagonal matrix that has different diagonal elements.

$$X_2 = \begin{bmatrix} e^{r-\sqrt{r^2+d^2-2Rd\cos\theta}} & & & 0 \\ & e^{\sqrt{r^2+4d^2-4Rd\cos\theta}-\sqrt{r^2+d^2-2Rd\cos\theta}} & & \\ & & \ddots & \\ 0 & & & e^{\sqrt{r^2+(M-1)^2d^2-2rd(M-1)\cos\theta}-\sqrt{r^2+(M-2)^2d^2-2rd(M-2)\cos\theta}} \end{bmatrix} X_1 \tag{5.2.3}$$

Unlike the approaches that use the matrix decomposition to reveal the rotational invariance term, we may transform the problem in to another one: solving a linear problem.

$$\phi_1 N_{Rxx_1} = \phi_2 N_{Rxx_2} = 0 \tag{5.2.4}$$

where N is the noise subspace vector of subarrays. Apparently, the equation system is formed by the important conclusion given in the last chapter. Thus, the near field ESPRIT can be considered as a kind of MUSIC algorithm which uses the segments of the input data in a way that is introduced in last chapter section.

A numerical example of a 4 elements ULA system is given to prove the feasibility of the system solving.

$$\begin{cases} a_{1,1}e^{r-r} + a_{2,1}e^{\sqrt{R^2+d^2+2rd\cos\theta}-r} + a_{3,1}e^{\sqrt{r^2+4d^2+4rd\cos\theta}-r} = 0 \\ a_{1,2}e^{r-r} + a_{2,2}e^{\sqrt{r^2+d^2+2rd\cos\theta}-R} + a_{3,2}e^{\sqrt{r^2+4d^2+4rd\cos\theta}-r} = 0 \\ b_{1,1}e^{\sqrt{r^2+d^2+2rd\cos\theta}-r} + b_{2,1}e^{\sqrt{r^2+4d^2+4rd\cos\theta}-r} + b_{3,1}e^{\sqrt{r^2+9d^2+6rd\cos\theta}-r} = 0 \\ b_{1,2}e^{\sqrt{r^2+d^2+2rd\cos\theta}-r} + b_{2,2}e^{\sqrt{r^2+4d^2+4rd\cos\theta}-r} + b_{3,2}e^{\sqrt{r^2+9d^2+6rd\cos\theta}-r} = 0 \end{cases}. \tag{5.2.5}$$

and

$$\begin{matrix} a_{i,j} \in N_{Rxx_1} \\ b_{i,j} \in N_{Rxx_2} \end{matrix}. \tag{5.2.6}$$

We do not have to solve θ and r explicitly trough the exponential term since they are constrained to a Known structure. We may simplify the above system to the one below with a vector $k \in C^{1\times 4}$.

$$\begin{cases} a_{2,1}k_2 + a_{3,1}k_3 = -a_{1,1} \\ a_{2,2}k_2 + a_{3,2}k_3 = -a_{1,2} \\ b_{1,1}k_2 + b_{2,1}k_3 + b_{3,1}k_4 = 0 \\ b_{1,2}k_2 + b_{2,2}k_3 + b_{3,2}k_4 = 0 \end{cases}. \tag{5.2.7}$$

Then the vector k represents the estimate result of $A(\theta)$. To solve the explicit θ and r, we might have various approaches. Enumeration is used in this example because of the visualization purpose. In practical uses, solving the problem may include the methods given in the previous chapter to accelerate the computation

To visualize the result, we use the following function to generate a spectrum

$$P(\theta, r) = \frac{1}{\left\| k - A(\theta, r) \right\|^2}. \tag{5.2.8}$$

Note that the method has higher sidelobe value and lower resolution compared to the near field MUSIC. A numerical simulation is given in Fig.5.2.2. to compare their performance under the same conditions in terms of target location, signal mode and antenna configuration.

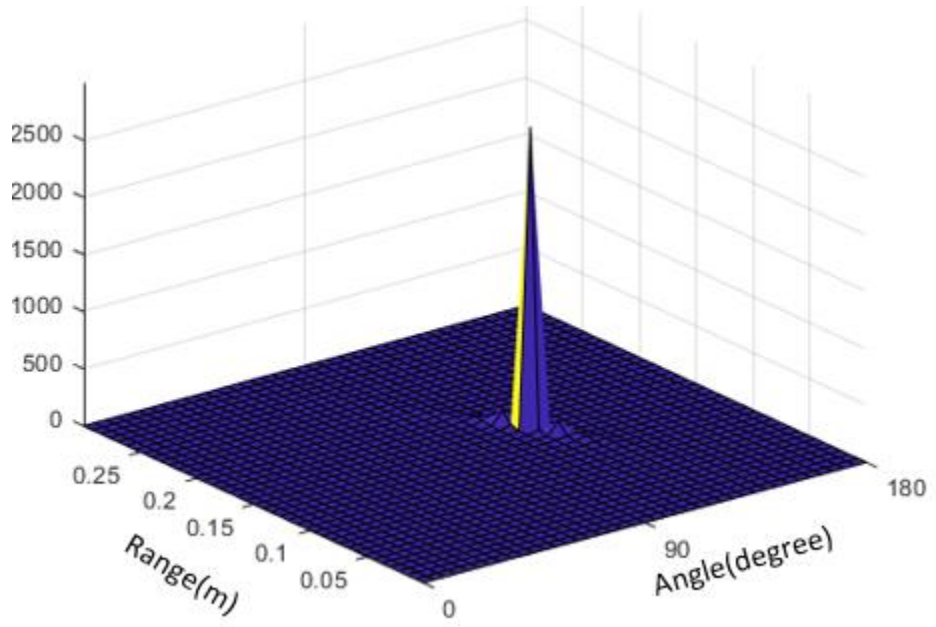

Fig.5.2.2. simulation result of near field MUSIC.

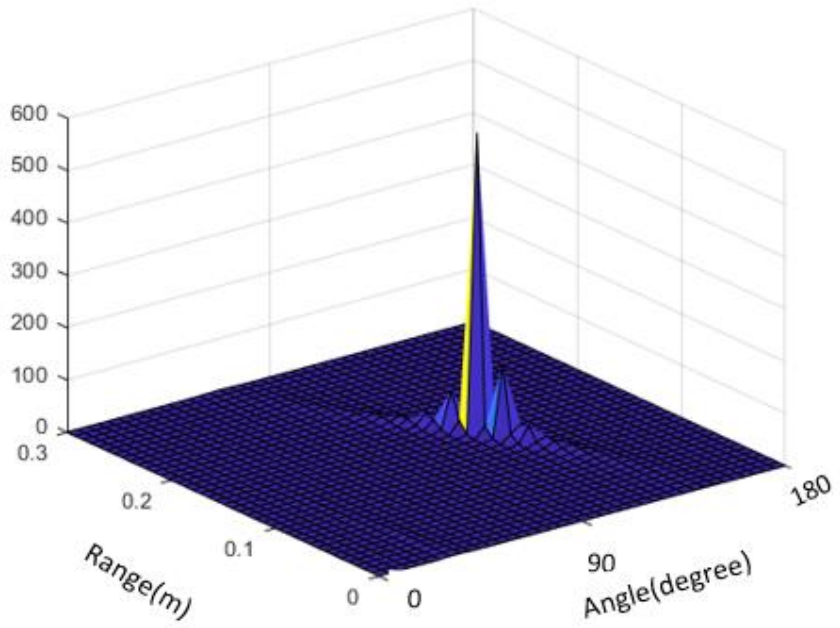

Fig.5.2.3.Simulation result of near field ESPRIT.

It is fundamentally using the core property of the MUSIC. The only difference is that introducing the subarrays will causes the system to be over-determined. Now, because the signal mode used in this section is a pure phase mode, the associated covariance matrix of x or in other words, approximated covariance matrix can be written as

$$R_{xx} = \begin{bmatrix} 1 & e^{j\omega_c(\tau_2-\tau_1)} & \cdots & e^{j\omega_c(\tau_n-\tau_1)} \\ e^{j\omega_c(\tau_1-\tau_2)} & 1 & & \\ \vdots & & \ddots & \\ e^{j\omega_c(\tau_1-t_n)} & & & 1 \end{bmatrix}. \tag{5.2.9}$$

This matrix contains information about the difference of arrival times we selected. And with certain subspace methods, we can accurately achieve DOA estimation. Under this specific condition, there is only one non-zero eigen value that equals to M.

Thus, the noise subspace can be considered as a spaced generated by solutions of the following linear system.

$$R_{xx}v = \begin{bmatrix} 1 & e^{j\omega_c(\tau_2-\tau_1)} & \cdots & e^{j\omega_c(\tau_n-\tau_1)} \\ e^{j\omega_c(\tau_1-\tau_2)} & 1 & & \\ \vdots & & \ddots & \\ e^{j\omega_c(\tau_1-t_n)} & & & 1 \end{bmatrix} v = 0\,. \tag{5.2.10}$$

However, as previous mentioned the problem is that the arrival times cannot be selected precisely with no error. Thus, the matrix will still be Toeplitz, but the elements inside may be impacted by the errors. In this case, we want to have an estimated covariance matrix to evaluate the DOA parameters and to make

the result as close as possible to the DOA parameters resulted from the covariance matrix of the ground truth.

5.3 TLS- ESPRIT.

The previous chapters explain how the phase error is generated and how it impacts the accuracy of the estimation. Along with the content that has been introduced in this chapter, we might have a mathematical expression of our linear system problem or least square problem in the previous section, where

$$(\mathrm{A}+\Delta\mathrm{A})\mathrm{x}=\mathrm{b}+\Delta\mathrm{b} \tag{5.3.1}$$

Where $\mathrm{A}\in\mathbb{R}^{M\times N}$, $\Delta\mathrm{A}\in\mathbb{R}^{M\times N}$, $\mathrm{b}\in\mathbb{R}^{M\times 1}$ and $\Delta\mathrm{b}\in\mathbb{R}^{M\times 1}$. This problem is called Total Least Square (TLS) problem Compared to the original least square problem, the expression has two more terms $\Delta\mathrm{A}$ and $\Delta\mathrm{b}$, according to the work done by ref, they are data error matrix and data error vector[7~9]. In our case, we consider error occurs on both sides of the linear system, in other words. we take the phase error into the concern to conduct biased estimation.

To solve the problem, we can establish a constrained optimization problem in such a way that

$$\begin{aligned}&\min_{\Delta\mathrm{A},\Delta\mathrm{b},\mathrm{x}}\|\Delta\mathrm{A}\|_F^2+\|\Delta\mathrm{b}\|_2^2\\&s.t.\quad(\mathrm{A}+\Delta\mathrm{A})\mathrm{x}=\mathrm{b}+\Delta\mathrm{b}\end{aligned}. \tag{5.3.2}$$

Then, the Lagrange function of the problem can be written as

$$L(\Delta\mathrm{A},\Delta\mathrm{b},\lambda)=\|\Delta\mathrm{A}\|_F^2+\|\Delta\mathrm{b}\|_2^2+2\lambda\left((\mathrm{A}+\Delta\mathrm{A})\mathrm{x}\text{-}\mathrm{b}\text{-}\Delta\mathrm{b}\right). \tag{5.3.3}$$

Thus, applying the Karush–Kuhn–Tucker(KKT) condition, we can have

$$\Delta\mathrm{b}=\frac{\mathrm{Ax}\text{-}\mathrm{b}}{\|\mathrm{x}\|^2+1}. \tag{5.3.4}$$

By substituting (5.3.1), we have

$$\Delta\mathrm{A}=\frac{(\mathrm{Ax}\text{-}\mathrm{b})\mathrm{x}^T}{\|\mathrm{x}\|^2+1}. \tag{5.3.5}$$

Consequently, the problem can be transformed to

$$\min_{\Delta\mathrm{A},\Delta\mathrm{b},\mathrm{x}}\frac{(\mathrm{Ax}\text{-}\mathrm{b})^2}{\|\mathrm{x}\|^2+1}. \tag{5.3.6}$$

By homogenizing the problem, we can have the following equivalent problem

$$\min_{\Delta\mathrm{A},\Delta\mathrm{b},\mathrm{x}}\left\{\frac{(\mathrm{AX}\text{-}t\mathrm{b})^2}{\|\mathrm{x}\|^2+\mathrm{t}}:t=1\right\}. \tag{5.3.7}$$

Then we define $z = [\mathrm{x}, t]^T$

$$f = \min_{z \in \mathbb{R}^{M \times N}} \left\{ \frac{z^T \mathrm{B} z}{\|z\|^2} : z_{n+1=1} \right\} \tag{5.3.8}$$

where B is

$$B = \begin{pmatrix} \mathrm{A}^T \mathrm{A} & -\mathrm{A}^T \mathrm{b} \\ -\mathrm{b}^T \mathrm{A} & \|\mathrm{b}\|^2 \end{pmatrix}. \tag{5.39}$$

Thus, to solve the TLS problem is to construct B from the data and to iterate the vector z. Fortunately, many works have proven the relationship between the smallest eigenvalue associated eigenvector and z in this problem. Or in other words, the iteration can be done by using the noise subspace. More detailly, there are two kind of solutions for the TLS problem can, least norm solution and optimized approximated solution [10,11].

5.4. Experiments

In this section we still use Yakumo to conduct the experiment, but the purpose is no more for GPR uses. Rather, we use Yakumo to achieve imaging to locate a metal sphere. The experiment schematic setup is as shown below.

Fig. 5.4.1 Yakumo sphere reflector experimental setup.

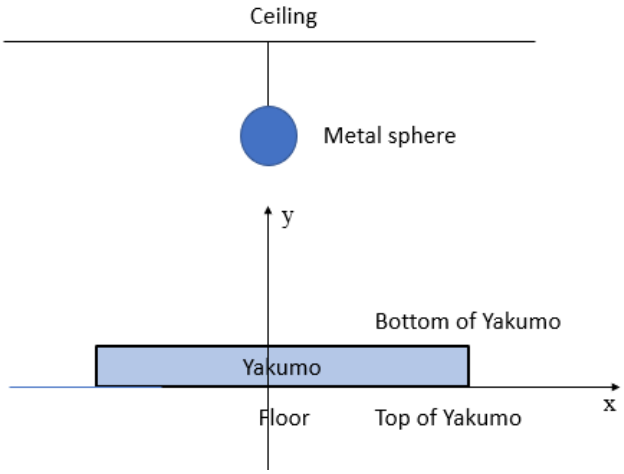

Fig5.4.2. Yakumo sphere reflector schematic setup.

The Yakumo is intentionally put upside down to and we use the combination of Tx1 and all Rx to conduct the SAR processing and the proposed ESPRIT processing. To visualize the result, we use the following function to generate a spectrum

$$P(\mathrm{x},\mathrm{y}) = \frac{1}{\left\| k - A(\mathrm{x},\mathrm{y}) \right\|^2} \tag{5.4.1}$$

where steering vector $A(\mathrm{x},\mathrm{y})$ can be explicitly written as

$$A(\mathrm{x},\mathrm{y},\mathrm{z}) = \left[e^{-i\omega_c \Delta\tau_1}, e^{-i\omega_c \Delta\tau_2}, \ldots e^{-i\omega_c \Delta\tau_n} \right]^* . \tag{5.4.2}$$

Instead, the phase difference can be written by using the Cartesian coordinate of the target $(\mathrm{x},\mathrm{y},\mathrm{z})$, *i*th transmitter element $(\mathrm{Tx}_i, \mathrm{Ty}_i, \mathrm{Tz}_i)$ and *j*th receiver element $(\mathrm{Rx}_j, \mathrm{Ry}_j, \mathrm{Rz}_j)$. As mentioned in this experiment, we use Tx1 and Rx1~Rx4, thus the phase difference has a specific expression

$$\Delta\tau_1 = \left[0, \ldots, \frac{\sqrt{(\mathrm{Tx}_1 - \mathrm{x})^2 + (\mathrm{Ty}_1 - \mathrm{y})^2} + \sqrt{(\mathrm{Rx}_n - \mathrm{x})^2 + (\mathrm{Ry}_n - \mathrm{y})^2}}{c} - \frac{\sqrt{(\mathrm{Tx}_1 - \mathrm{x})^2 + (\mathrm{Ty}_1 - \mathrm{y})^2} + \sqrt{(\mathrm{Rx}_1 - \mathrm{x})^2 + (\mathrm{Ry}_1 - \mathrm{y})^2}}{c} \right]. \tag{5.4.3}$$

To reduce the uncertainty of the experiment, we internally hang the sphere right above the origin of the yz plane, or in other words, we assume that x=0 for target coordinates.

From the result, both subspace methods have higher resolution. In speaking of the SAR processing, though the focus can be enhanced by using more inputs data, the resolution is still outmatched. The fact also proves the conclusion drawn from the last chapter, there is no lower limited for the subspace method regardless of the phase errors. Another important fact is that the ESPRIT method has multiple sidelobes and the peak is not as sharp as the MUSIC algorithm though their localization result is the same.

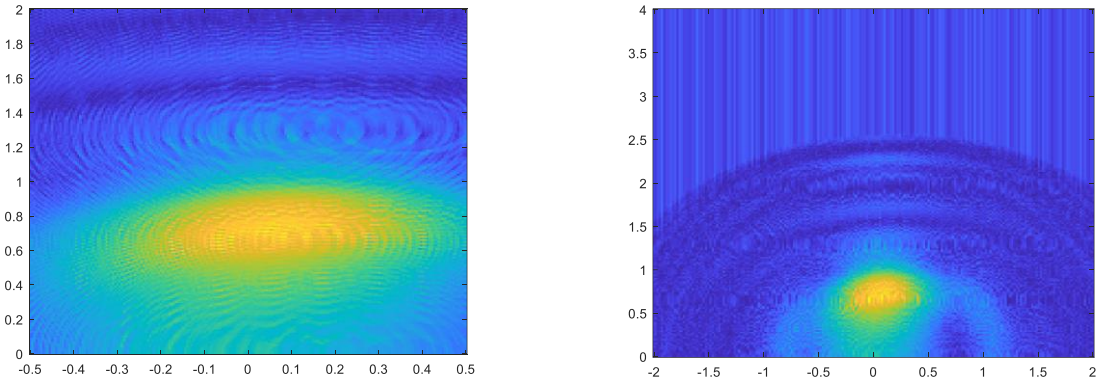

Fig.5.4.3. Metal sphere localization by using SAR processing.

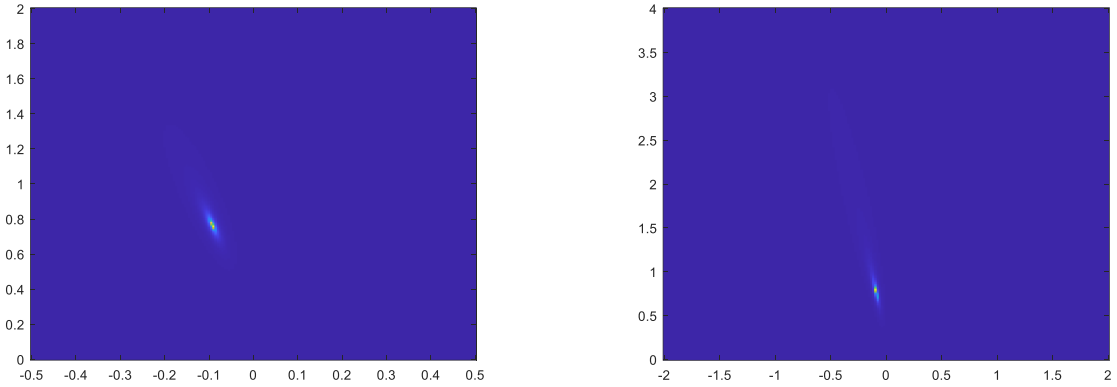

Fig. 5.4.4. Metal sphere localization by using near field MUSIC.

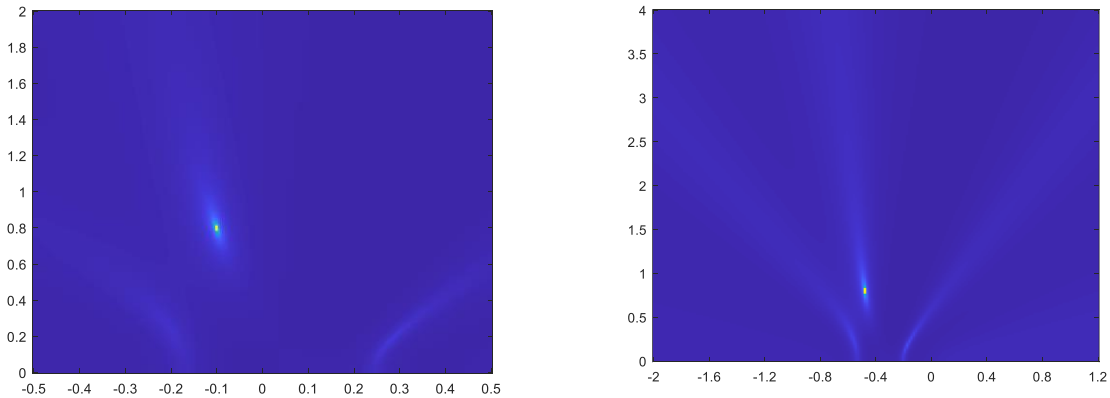

Fig.5.4.5. Metal sphere localization by using near field ESPRIT.

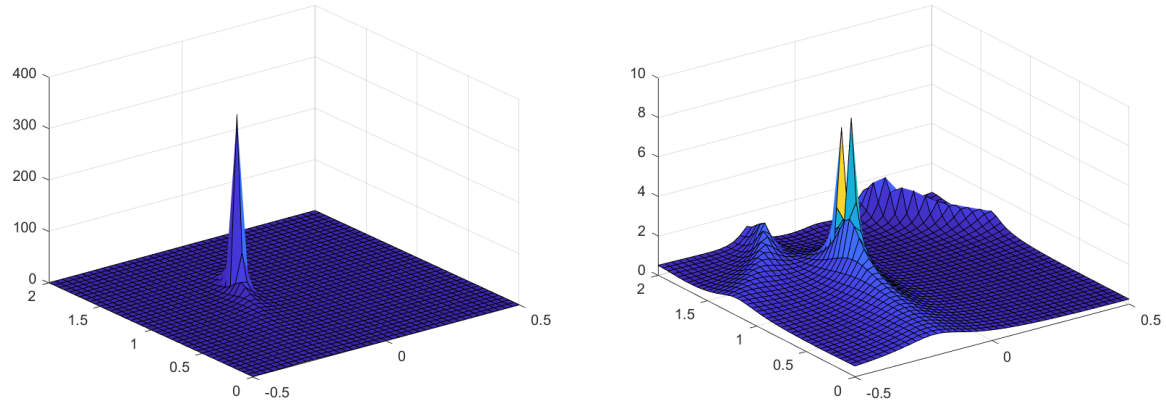

Fig.5.4.6 . Metal sphere localization by using near field ESPRIT.

Different from GPR uses, it seems that the signal is no longer suffering from the high attenuation in the subsurface medium. Thus, it is possible to process the data with the amplitude information by using the time domain signal form presented in (2.5.2). Knowing that the amplitude term cannot be shifted by just using feature of exponential multiplication, we might directly carry out element-wise division to the received signal, which yields

$$X(t) = S(t)_{\text{normilized}} ./ \left\{ 2\left[\frac{\sin(\frac{B}{2}(t-\tau(\text{x,y,z})))}{(t-\tau(\text{x,y,z}))} \right] \right\}_{\text{normilized}} . \qquad (5.4.4)$$

where $S(t)$ is the received time domain signal matrix and $X(t)$ is a pure phase representation of the signal . Thus, under ideal condition, the element-wise division should be done inside the enumeration process. Besides, $\{.\}_{\text{normilized}}$ stands for the normalization process.

Table5.4.1. Subspace method with amplitude information in ideal conditions

Input: Time domain received data matrix $S(t)$
1: for spectrum horizontal vector
2: for spectrum vertical vector
3: calculate $\tau(\text{x,y,z})$ **by current elements in axis vectors**
4: do (5.4.4) to remove the amplitude information
5: do either MUSIC or ESPRIT
9: end
10: end
Plot 2D spectrum
Output 2D Spectrum *P*

Note that the attenuation does exist in this condition, considering the distance from the system to the target. However, the time domain signal is not ideal as presented in the signal mode section, the following figure shows two traces of acquired data in the experiment.

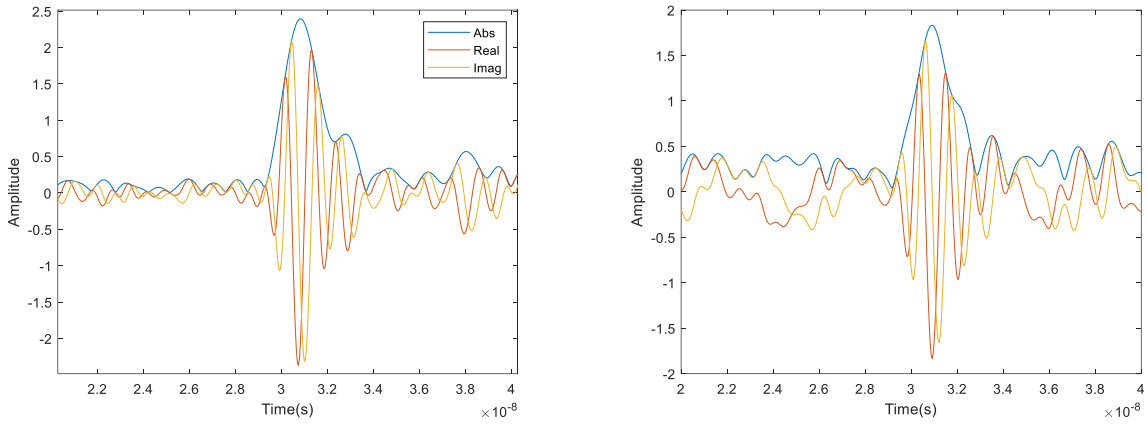

Fig.5.4.7. Examples of range profiles.

It apparently has the unwanted phase shift in all the received signal, or at least the correspondence between the global maxima of the envelope and the global maxima of the real and imaginary part is reversed. All these problems are caused by the property of the wideband signal. In this case, a classical solution, Incoherent Signal Subspace Method/MUISC (ISSM) is applied here to solve the problems.

The ISSM algorithm decomposes the wideband signal into narrowband components, and carries out the computation in each narrowband [11,12]. As the experiment is conducted by using SFCW system, for each frequency point acquired, we can still use arrival time difference to accomplish the description of different array, because the signal mode follows

$$s(f_q) = \exp(-i2\pi f_0 \tau)\exp\left[-i2\pi(q-1)\Delta f\,\tau\right] \tag{5.4.5}$$

where $s(f_q)$ is the receive signal in the frequency domain at qth frequency point, f_0 is the starting frequency , Δf is the frequency step and τ is the arrival time[13]. Consequently, we must run q times near field ESPRIT to evaluated the spectra on all frequency points and then perform the arithmetic mean value of the spectra. In this case, the acquisition in frequency domain has 256 points, which means 256 times proposed MUSIC has to be done. In each iteration MUSIC, the covariance matrix $\Theta_{i,j}$ is written as

$$\Theta_{i,j} = [s(f_q)_1 \quad \dots \quad s(f_i)_m]^H [s(f_q)_1 \quad \dots \quad s(f_q)_m] \tag{5.4.6}$$

where m is the length of the subarray chosen. Thus, the construction of the covariance is different from the that of the time domain MUSIC. However, after the evaluation of the covariance matrix, the procedure introduced in the previous section can be applied to this case.

The spectra of different channels are shown in Fig.5.4.8. The difference on each frequency point may be caused by the delay times and the reflection coefficient. Note that the metal sphere is not small enough to considered as a point target compared to its position an size to the aperture , though in the calculation, we see it as a point target. As a result, the inevitable error appears in our equation solving process and it is why TLS method is introduced to combine with ISSM algorithm

To have a TLS solution, we have to have identify by what judgement the solution is an optimized solution for the system as mentioned. Here we follow a classical work [14], and the only difference is that we are

trying to estimate the position of target instead of the frequency. Now, get to back to the TLS method itself and consider the complex signal in our case, we are given

$$\mathrm{x}_{\mathrm{TLS}} = (\mathrm{A}^{*}\mathrm{A} - \sigma_2^2 I)^{-1}\mathrm{A}^{*}\mathrm{b}\,. \tag{5.4.6}$$

where the structures of A and b are introduced in the previous section. The experiment result is shown in Fig.5.4.9. Compared to the proposed method given earlier, the performance is almost same though some artifacts appears along the vertical direction. They are mainly caused by the bad performance of some frequency points.

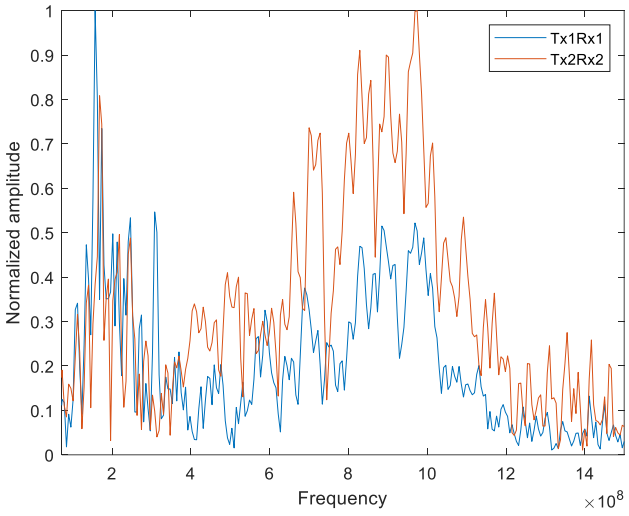

Fig.5.4.8 Frequency spectra difference between different channels (absolute value).

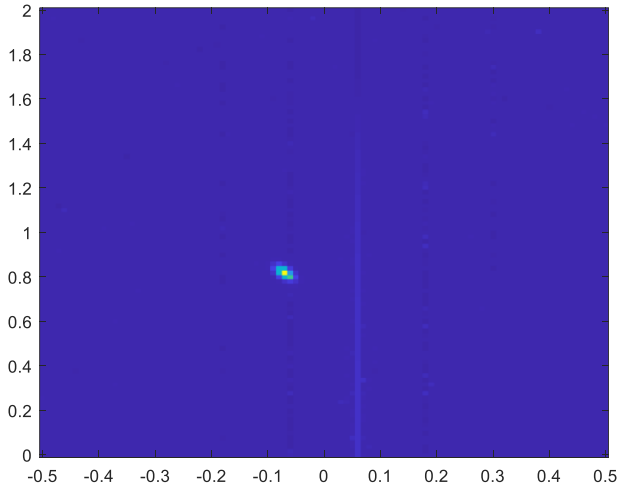

Fig.5.4.9. The result of near field ESPRIT based on ISSM method.

5.5 Summary

In these chapter, near field Esprit is presented by a simplified form based on the orthogonality of the MUSIC algorithm. While the focus is moved from the matrix operations to the classical linear system solving. As mentioned in the previous chapter, the phase error caused by the peak selection can be involved into the calculation while the traditional LS method does not compensate the error in it. Thus, TLS method is introduced to solve the problem by solving the constrained optimization problem. We conducted the experiment by using the wideband system to exam our proposed method. In addition, frequency domain signal processing is conducted for using frequency point to construct the covariance matrices, which is so-called ISSM, a classical method to transform wideband signal processing to narrow band signal processing. Two approaches are provided here, one uses the amplitude information, and one does not. From the results we can see that imaging performance is almost same.

References

[1] F. Wen, J. Shi and Z. Zhang, "Joint 2D-DOD, 2D-DOA, and Polarization Angles Estimation for Bistatic EMVS-MIMO Radar via PARAFAC Analysis," in *IEEE Trans. Veh. Technol.*, vol. 69, no. 2, pp. 1626-1638, Feb. 2020.

[2] B. Li, W. Bai and G. Zheng, "Successive ESPRIT Algorithm for Joint DOA-Range-Polarization Estimation With Polarization Sensitive FDA-MIMO Radar," in *IEEE Access*, vol. 6, pp. 36376-36382, 2018.

[3] J. Pan, M. Sun, Y. Wang and X. Zhang, "An Enhanced Spatial Smoothing Technique With ESPRIT Algorithm for Direction of Arrival Estimation in Coherent Scenarios," in *IEEE Trans. Signal Process.*, vol. 68, pp. 3635-3643, June 2020.

[4] W. Zhang, Y. Han, M. Jin and X. -S. Li, "An Improved ESPRIT-Like Algorithm for Coherent Signals DOA Estimation," in *IEEE Commun.s Lett.*, vol. 24, no. 2, pp. 339-343, Feb. 2020.

[5] N. Yuen and B. Friedlander, "Performance analysis of higher order ESPRIT for localization of near-field sources," in *IEEE Trans. Signal Process.*, vol. 46, no. 3, pp. 709-719, March 1998.

[6] R. N. Challa and S. Shamsunder, "High-order subspace-based algorithms for passive localization of near-field sources," *Conference Record of The Twenty-Ninth Asilomar Conference on Signals, Systems and Computers*, Pacific Grove, CA, USA, 1995, pp. 777-781.

[7] D. Feng, Z. Bao and L.Jiao, "Total least mean squares algorithm," in *IEEE Trans. Signal Process.*, vol. 46, no. 8, pp. 2122-2130, Aug. 1998.

[8] P. Lemmerling, B. De Moor and S. Van Huffel, "On the equivalence of constrained total least squares and structured total least squares," in *IEEE Trans. Signal Process.*, vol. 44, no. 11, pp. 2908-2911, Nov. 1996.

[9] S. Rhode, K. Usevich, I. Markovsky and F. Gauterin, "A Recursive Restricted Total Least-Squares Algorithm," in *IEEE Trans. Signal Process.*, vol. 62, no. 21, pp. 5652-5662, Nov.1, 2014.

[10] S.V. Huffel and J.Vandewalle, *The Total Least Squares Problem: Computational Aspects and Analysi,*. Frontiers in applied mathematics, 1991.

[11] M. Wax, T.-J. Shan and T. Kailath, "Spatio-temporal spectral analysis by eigenstructure methods", in *IEEE Trans. Acoust. Speech Signal Process.*, vol. ASSP-32, no. 4, pp. 817-827, Aug. 1984.

[12] K. Han and A. Nehorai, "Wideband gaussian source processing using a linear nested array", in *IEEE Signal Process. Lett.*, vol. 20, no. 11, pp. 1110-1113, Nov. 2013.

[13] W. Feng, “Title of thesis or dissertation,” Ph.D dissertation, Graduate school of environmental study, Tohoku University, Sendai, Miyagi, Japan, 2019.

[14] M. D. Rahman and Kai-Bor Yu, "Total least squares approach for frequency estimation using linear prediction," in *IEEE Trans. Signal Process.*, vol. 35, no. 10, pp. 1440-1454, October 1987.

Chapter 6 Subspace Tracking and Updating

Subspace tracking and subspace updating has limited differences and can be considered as a category of DOA estimation approaches. The original subspace tracking is based on the QR decomposition [1]. Compared to the MUSIC and the esprit, this method does not require any complicated decomposition such as EVD and SVD. The main idea is to use a permutation matrix to have some operations with the signal covariance matrix, then after QR decomposition, the noise subspace can be approximately acquired, then the parameter can be solved. The algorithm is designed to compensate the capability of computer computation in earlier years.

As personal computers vastly gain the capability of large scale computation. Many improved studies have been made without the limitation of large-scale matrix operation. While in recent years, most of the research is still focused on complexity reduction[2,3]. Valizadeh at. el., present a new subspace tracking algorithm with less computational cost based on constrained optimization[4]. Lassami at. el., proposed a low-complexity subspace tracking algorithm specifically for a sparsity constraint [5].

6.1 Conventional subspace tracking

Power method is the simplest form of subspace tracking. Originally, the power method is used for solving the maximum or minimum eigenvalue of a Hermitian matrix *A*. Given an initial vector x_0, we can have an iteration process by using a linear system

$$x_{k+1} = \frac{Ax_k}{Ax_k^H Ax_k} \ . \tag{6.1.1}$$

The iteration ends when x_k converges; meanwhile, the largest eigenvalue is the $Ax_k^H Ax_k$. A numerical example of $A \in C^{4\times 4}$ is given, as most of the related research use only real numbers for the demonstration

Numerical example is given to show the iterative calculation of the subspace tracking. we are using $[1,0,0,0]^T$ as a initial guess for the eigenvectors.

$$A = \begin{bmatrix} 17 & 15-9i & -2-9i & -14-29i \\ 15+9i & 18 & 3-9i & 3-33i \\ -2+9i & 3+9i & 5 & 17-4i \\ -14+29i & 3+33i & 17+4i & 61 \end{bmatrix} \tag{6.1.2}$$

In this example, the eigenvalue and eigenvectors are gradually converging to the part of result of the EVD. In many cases, for example the MUSIC and the ESPRIT method mentioned in the last two chapters, calculation of a full EVD or SVD is not necessary; sometimes, only few vectors are needed regarding to the limited number of channels we use for the simulation and experimentations.

Thus, it is very intuitive to have a method that can partially compute the components from the matrix decomposition. And during the process, we hope that some interested parameters of the signal can be evaluated. It leads to a category of modern DOA analysis, which is called subspace updating or subspace

tracking. Back to the iteration itself, it can also be categorized as a linear system optimization problem. Thus, this subspace updating problem is mainly focusing on how to modify the optimization in a more efficient to achieve the accurate result of the unknown parameters.

Table.6.1.1. Iteration results of the power method.

Iteration number	Dominant eigenvalue	Eigenvector	Error
1	17.4929	[0.9718 + 0.0000i 0.8575 + 0.5145i -0.1143 + 0.5145i -0.8003 + 0.5145i] ^{T}	16.4929
2	112.5108	[0.4862 - 0.0000i 0.4344 + 0.4314i -0.1433 + 0.2891i -0.7184 + 0.6956i] ^{T}	95.0180
3	94.7070	[0.3999 + 0.0000i 0.4021 + 0.4233i -0.1446 + 0.2716i -0.7091 + 0.7051i] ^{T}	17.8038
4	92.1732	[0.3867 - 0.0000i 0.3948 + 0.4215i -0.1450 + 0.2676i -0.7070 + 0.7073i] ^{T}	2.5338
5	91.7009	[0.3844 - 0.0000i 0.3937 + 0.4212i -0.1450 + 0.2670i -0.7066 + 0.7076i] ^{T}	0.4722
6	91.6237	[0.3840 + 0.0000i 0.3934 + 0.4212i -0.1450 + 0.2669i -0.7066 + 0.7076i] ^{T}	0.0772

In this example, the eigenvalue and eigenvectors are gradually converging to the part of the result of the EVD. In many cases, for example the MUSIC and the ESPRIT method mentioned in the last two chapters, calculation of a full EVD or SVD is not necessary; sometimes, only few vectors are needed regarding to the limited number of channels we use for the simulation and experimentations

Thus, it is very intuitive to have a method that can partially compute the components from the matrix decomposition. And during the process, we hope that some interested parameters of the signal can be evaluated. It leads to a category of modern DOA analysis, which is called subspace updating or subspace tracking. Back to the iteration itself, it can also be categorized as a linear system optimization problem. Thus, this subspace updating problem is mainly focusing on how to modify the optimization in a more efficient to achieve the accurate result of the unknown parameters.

As the most fundamental way of subspace tracking, the power method has many aspects to be improved. One of the most common aspects is the search direction. Having an appropriate step size and direction in each iteration can vastly reduce the computation and can avoid failures caused by the oversized or wrong directional step. However, following the simulation mode introduced in the last two chapters, we might have a specific problem because the largest eigenvalue is too dominant. Under this condition, the power method has only two iterations to give the correct result of the largest eigenvalue and its associated eigenvectors. Still, for the rest of the components, the method cannot converges. To tackle this problem, this work introduces a classical image-processing technique modified for DOA case and it is still under the structure of the subspace tracking algorithm

6.2 low rank-based subspace tracking

As mentioned, the acquired data by using the peak selection method will have a form with phase noise

$$\bar{R}=\begin{bmatrix} 1 & e^{j\omega_c(\tau_2-\tau_1)} & \cdots & e^{j\omega_c(\tau_n-\tau_1)} \\ e^{j\omega_c(\tau_1-\tau_2-\Delta t_{2,1})} & 1 & & \\ \vdots & & \ddots & \\ e^{j\omega_c(\tau_1-t_n-\Delta t_{n,1})} & & & 1 \end{bmatrix}. \tag{6.2.1}$$

The goal is to find an approach to recovery the above matrix to the ground truth covariance matrix as given in the assumptions.

$$R=\begin{bmatrix} 1 & e^{j\omega_c(\tau_2-\tau_1)} & \cdots & e^{j\omega_c(\tau_n-\tau_1)} \\ e^{j\omega_c(\tau_1-\tau_2)} & 1 & & \\ \vdots & & \ddots & \\ e^{j\omega_c(\tau_1-t_n)} & & & 1 \end{bmatrix}. \tag{6.2.2}$$

Before getting into the method, we should introduce the Augmented Lagrange Multiplier (ALM) method[6]. Unlike the optimization method introduced in the previous chapters for the non-constrained optimization, the method is widely used for solving constrained optimization problem that has a form.

$$\begin{aligned} &\min\ f(X) \\ &s.t.\quad h(X)=0 \end{aligned}. \tag{6.2.3}$$

To solve the above optimization problem, we first established the ALM function of the problem

$$L(X,Y,\mu)=f(X)+\langle Y,\quad h(x)\rangle+\frac{\mu}{2}\|h(x)\|_F^2 \tag{6.2.4}$$

where u is a positive scalar and Y is the Lagrange multiplier. The solving procedure can be considered as the gradient based method as previous introduced. Many developments have been made to this method and they generally try to modify the search step u and attempt to modified Y during the iteration for faster convergence and better precision. In a more general cases, the constrains are more than one, and the problem turns to

$$\begin{aligned} &\min\ f(X) \\ &s.t.\quad h_i(X)=0\quad ,\quad g_j(X)\le 0 \end{aligned} \tag{6.2.5}$$

where I=1, 2,…m and j=1,2,….n,and m and n are arbitrary positive number . Thus the ALM function is

$$L(X,Y,\mu)=f(X)+\langle Y,\quad h(x)\rangle+\langle Y,\quad g(x)\rangle+\frac{\mu}{2}\|h(x)\|_F^2+\frac{\mu}{2}\|g(x)\|_F^2\quad . \tag{6.2.5}$$

Then the duality is another issue needs to be discussed, because the duality can be used to avoid complicated iteration for the algorithm. In other words, we sometimes transform the optimization problem(primal problem) to its dual problem, then the result of the dual problem is the result that we want from the primal problem.

Originally, a dual function $D:\mathbb{R}^m\times\mathbb{R}^n\to\mathbb{R}$ can be defined as

$$
\begin{aligned}
D(\lambda,\mu) &= \inf_{x\subset\Omega} L(x,\lambda,\mu) \\
&= \inf_{x\subset\Omega}\left(f(x) + + \langle Y, \quad h(x)\rangle + \langle Y, \quad g(x)\rangle + \frac{\mu}{2}\|h(x)\|_F^2 + \frac{\mu}{2}\|g(x)\|_F^2 \right) .
\end{aligned} \tag{6.2.6}
$$

Reference work gives specific dual approach for solving the problem. It vastly improves the calculation speed of the algorithm as we do not have to update noise subspace in each iteration. Rather, only signal subspace is required to generate multiplier

$$
\begin{aligned}
&\max_{Y} \operatorname{tr}(D^T B) \\
&s.t \quad J(Y) < 1
\end{aligned} \tag{6.2.7}
$$

where in the covariance matrix assumed

$$
J(Y) = \max(\|Y\|_2, \lambda^{-1}) . \tag{6.2.8}
$$

Note that $\operatorname{Rank}(\hat{R}) = \operatorname{Rank}(R) = 2$. Under such circumstances, we use the a method called matrix completion to recovery $\hat{R}$ to R with the low rank structure of both covariance matrices kept. Mathematically, the problem can be written as

$$
\begin{aligned}
&\min_{A} \|A\|_* \\
&s.t. \quad A + E = D
\end{aligned} \tag{6.2.9}
$$

where $\|\cdot\|_*$ is the nuclear norm. A is a low rank matrix and E is a sparse matrix. Under the assumptions of this work, we may turn the problem into the following one

$$
\begin{aligned}
&\min_{E_{\hat{R}}} \|E_R - E_{\hat{R}}\| \\
&s.t. \quad A_R + E_R = R, A_{\hat{R}} + E_{\hat{R}} = \hat{R}
\end{aligned} . \tag{6.2.10}
$$

To sperate the covariance matrices, the referred works provide many approaches. Considering the computation speed, inexact augment Lagrange multiplier method is used. It is mainly because of the dual problem in the iteration

$$
(A_{k+1}^*, E_{k+1}^*) = \arg\min_{A,E} L(A, E, Y_k^*, u_k) . \tag{6.2.11}
$$

Because in the original RPCA problem, A and E are designed to be updated in A* and E* to improve the convergence rate. However, due to the convergences rate is $O(u_{k-1}^{-1})$, the algorithm converges slower if the multiplier is large.

Yet, to solve the optimization, all approach follows the same Lagrange function

$$
L(A, E, Y, \mu) = \|A\|_* + \lambda\|E\|_1 + \langle Y, \quad \hat{R} - A - E\rangle + \frac{\mu}{2}\|\hat{R} - A - E\|_F^2 . \tag{6.2.12}
$$

The pseudo algorithm is described in table 6.2.1.

Table. 6.2.1 Algorithm: Inexact ALM method.

Input: covariance matrix $S \in R^{M \times M}$ **, vectors of parameters**
1: $Y_0 = D / J(D), E_0 = 0, u_0 > 0, \rho > 0,\ k > 0$
2: while not converge do
4: $(U,S,V) = \text{svd}(D - E_k + u_k^{-1} Y_k);$
5: $A_k = U \Gamma_{u_k^{-1}}(S) V^T$
6: $E_{k+1} = \Gamma_{\lambda u_k^{-1}}[D - A_{k+1} + u^{-1} Y_k]$
7: $Y_{k+1} = Y_k + u_k (D - A_{k+1} - E_{k+1})$
8: $u_{k+1} = \rho u_{k+1}$
9: end while
Out put $A_k \quad E_{k+1}$

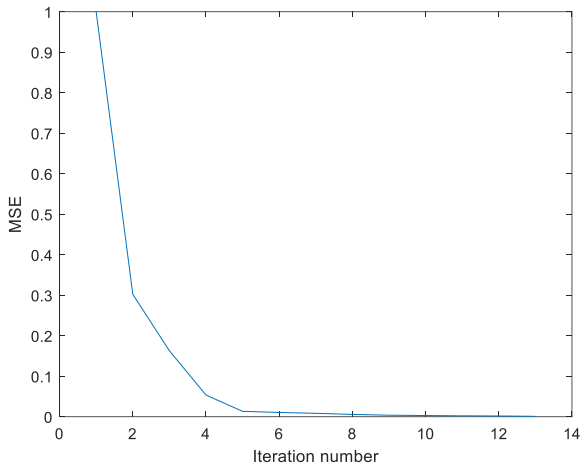

Fig.6.2.1 Convergency of the proposed method.

Simulations is conducted by using a Yakumo alike system. The only difference is antenna configuration. In the simulation, ULA is used with 0.133m element distance. Fig.6.2.1 shows the convergence of the second row in Fig.6.2.2.

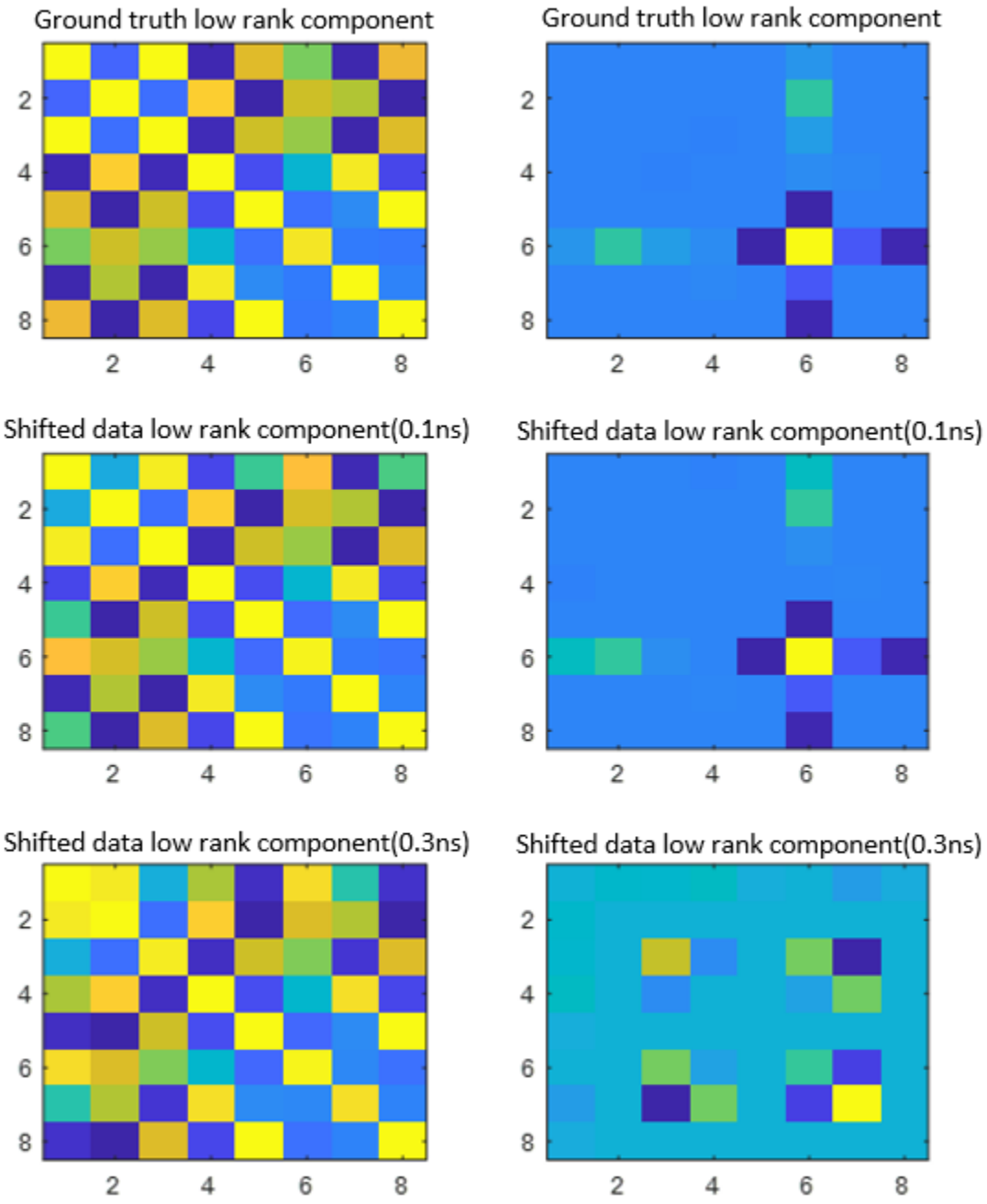

Fig.6.2.2 Simulation results of 8elements array under different phase error.

Fig.6.2.2 are resulted from the simulation by using 8 channel input data. We intentionally add phase shift to the selected arrival time in the time domain signal. And the behavior of the sparse matrices is changing due to the phase shift. Clearly, when phase shift of each channel gets larger, the difference gets larger.

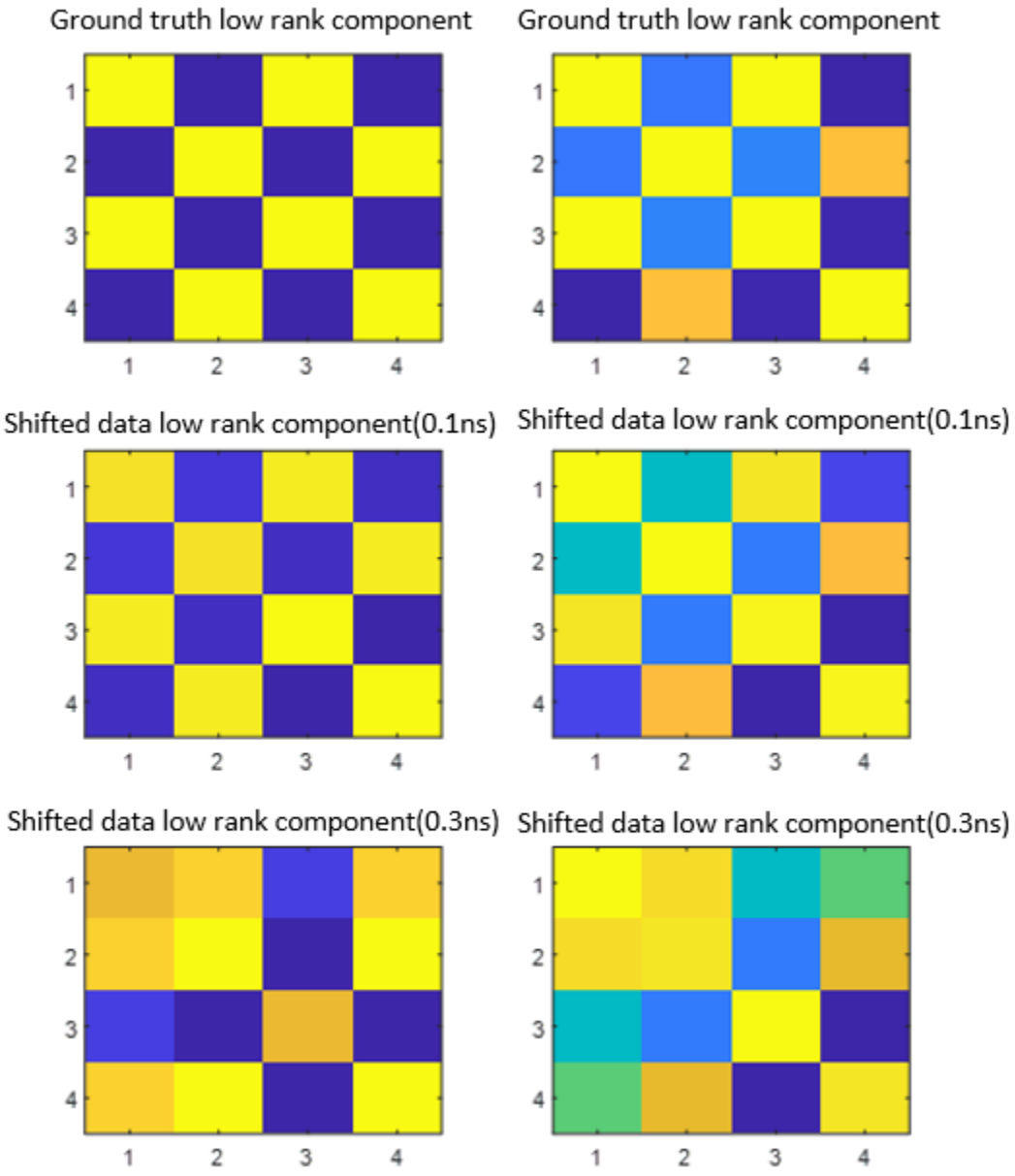

Fig.6.2.3 Simulation results of 4 elements array under different phase error.

The method is doubtful useful when number of channels is limited. In this 4-channel array case, we can clearly observe the difference of performance due to the arrival time shifted. However, the differenceS in the sparse matrices are not as obvious as they are in the previous example

A spatial spectrum generated by the above data is given as well. The goal is still to have the velocity depth estimation and the spectrum function is set to be

$$P(\theta,r)=\frac{1}{\left\|\bar{E}-E(\theta,r)\right\|^2} \tag{6.2.13}$$

where $E(\theta,r)$ is equal to E , and $\bar{E}$ is the sparse matrix generated by the acquired arrival time information. In this simulation .

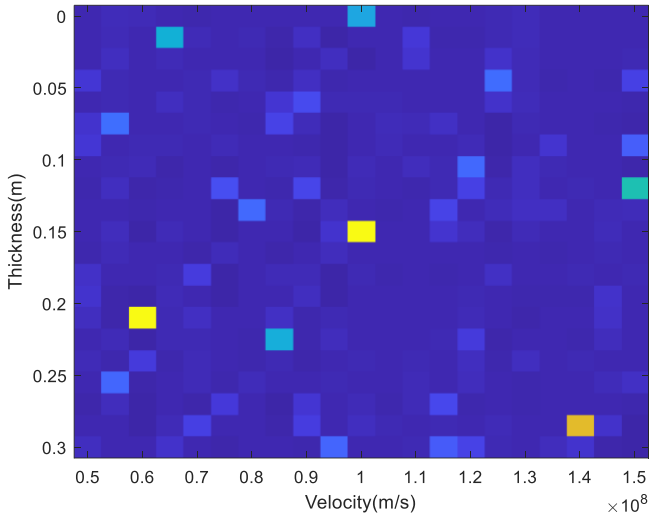

Fig.6.2.4. Velocity-depth spectrum generated by subspace tracking by using 8 channel input data.

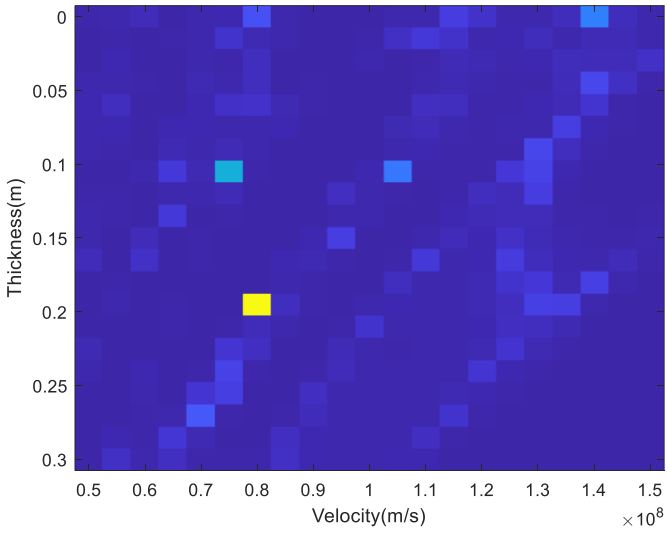

Fig. 6.2.5. Velocity-depth spectrum generated by subspace tracking by using 4 channel input data.

The above results assumes the phase shift on each channel has same value. However, random phase shifts on each channel could also appears. Instead of simulation of the velocity-depth analysis, we simulated an SFCW signal source located at [0.15m, 0.1m]. The simulated system has 8 channels and a working

frequency from 0.65mHz to 1.5GHz.To generate errors for the arrival time, additive gaussian white noise is directly added to the arrival time array.

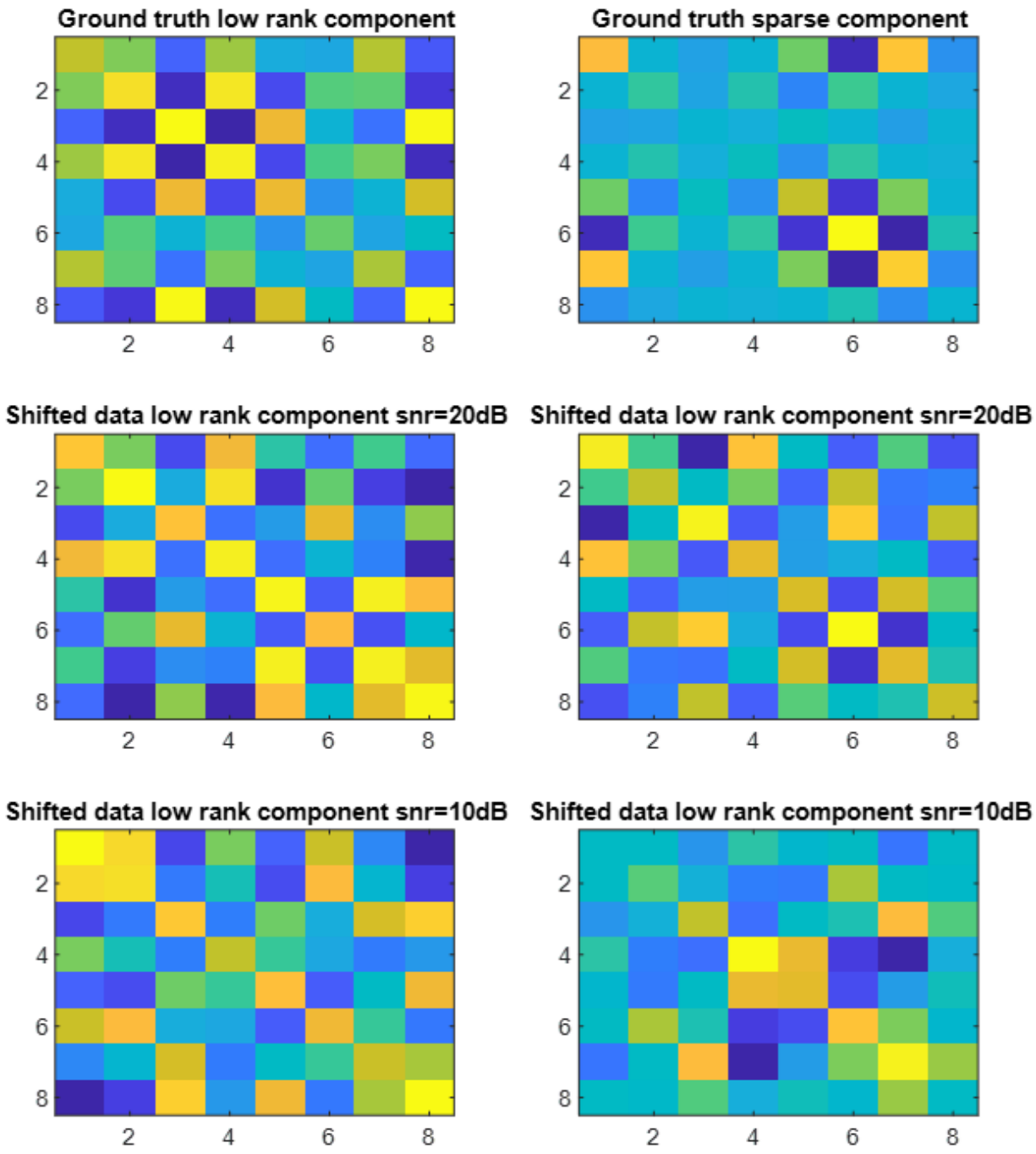

Fig.6.2.6. Simulation results of 8 elements array under different phase error for localization.

The results show that the more when the SNR rate is higher, or in other words selected arrival times are closer to the ground truth arrival time, and the low rank and sparse components are closer to the ground truth. The scale of the similarity can be calculated by using the norms following (6.2.13). Thus, the spatial spectrum can be plotted to localize the signal source after the nested loop of the testing vector. In this simulation, considering the computational speed, we lower the resolution of the spectrum to 0.1m and decrease the imaging range to 0~0.3 in both x and y directions. The result is shown in Fig.6.2.7.Compared to the spectrum generated by the conventional time domain MUSIC in Fig.6.2.8 , the proposed algorithm is more stable. Note the proposed method can achieve higher resolution spectrum but it is time-consuming because of the multiple nested loops.

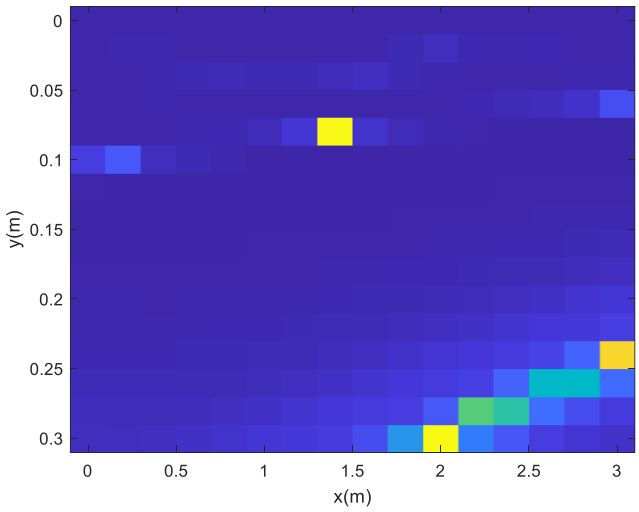

Fig.6.2.7. The spatial spectrum of low rank separation based DOA.

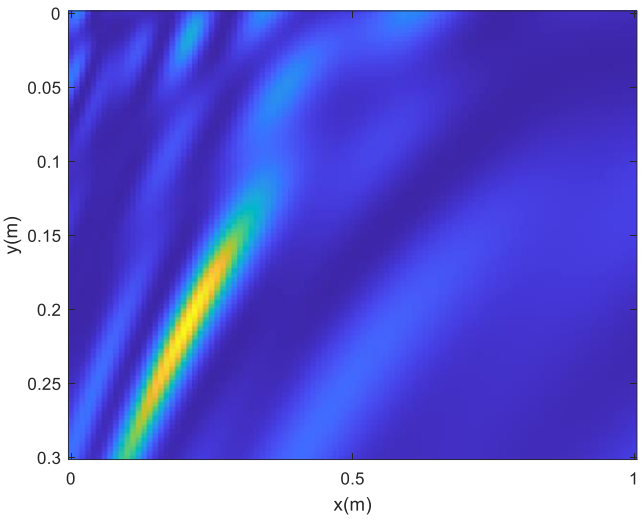

Fig.6.2.8. the spatial spectrum of original MUSIC.

6.3 Edge detection based subspace tracking related to GPR profile in a more general case

From the previous section, we noticed that the algorithm can be used even if the received signal is received by an array as the algorithms are originally introduced for the imaging processing. In other words, as long as the received data are acquired by a span of vectors in time-series, we may have chance to perform such kind of techniques. Thus, GPR B-scan is a perfect example for this method to be applied[7~9].While the main problem encountered in the topic is that the GPR data is initially high rank due to the attenuation and noise compared to the photo-graphic data. In this section, Sobel edge detection technique is introduced to perform the rank deduction first, which makes the subspace tracking algorithm much more easier to be performed.

Different from the conventional pick search method in time domain, the edge detection may use all surrounding elements for the detection[10]. Here a general explanation of edge detection by using the Sobel operator is written as

$$G_x = \begin{bmatrix} -1 & 0 & 1 \\ -2 & 0 & 2 \\ -1 & 0 & 1 \end{bmatrix} * A$$
$$G_y = \begin{bmatrix} 1 & 2 & 1 \\ 0 & 0 & 0 \\ -1 & -2 & -1 \end{bmatrix} * A \qquad (6.3.1)$$

For each 3x3 segment A, the gradient G_{xy} then can be written as

$$G_{xy} = \sqrt{G_x^{\,2} + G_y^{\,2}} \ . \qquad (6.3.2)$$

The final step is to compare the calculated gradient with a threshold manually set prior to the processing. It means that judging if an element is on edge in the GPR profile requires not only the adjacent elements on the same trace but also the adjacent elements from the adjacent trace of the time domain signal. However, in practical uses, GPR A-scan traces may not have such a strong relationship as adjacent elements from the photographic image do due to the sampling division. And it is the reason why the method is not a very hot topic in the field of GPR imaging processing. An experiment result is given here to demonstrate the process of the algorithm

First ,edge detection with the Sobel operator is applied to a GPR B-scan data as shown in Fig.6.3.1, and the target is kept. The process eliminates some weak targets from the original profile, which is the main advantage of edge detection.

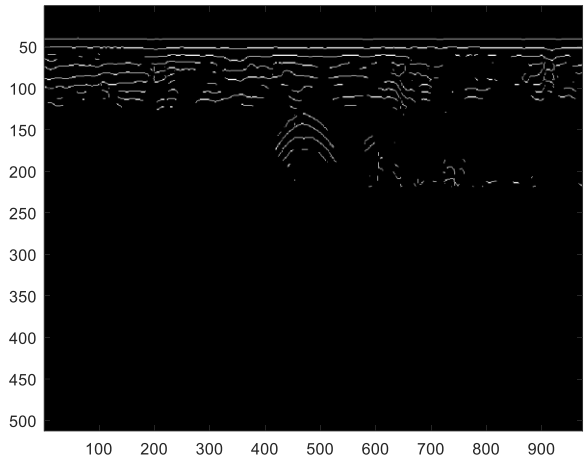

Fig.6.3.1.GPR B-scan data for pipe detection.

Then, subspace tracking algorithm presented in the last chapter is carried out. The only difference in this case is that we use B-scan data instead of the covariance matrix generated by the array signal. The result is shown in Fig,6.3.2. The result shows that the target response is clearly distinguished from the low rank components while it cannot be done by directly using the low rank separation procedure.

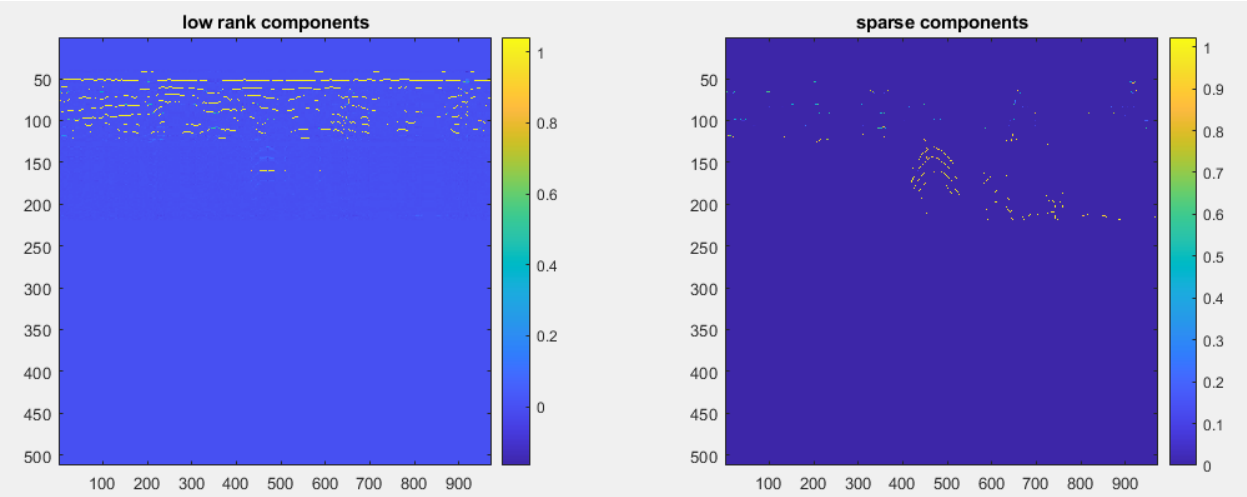

(a) Low rank components (b) Sparse components

Fig.6.3.2.GPR B-scan data for pipe detection(a)Low rank components of the GPR B-scan (b) Sparse components of the GPR B-scan.

6.4 Summary

In this section, we present a new subspace tracking technique that utilizes the popular constrained optimization technique ALM, which has been widely studied in the field of imaging processing as a means

of low rank matrix recovery. While the research fields may differ, the fundamental ideas behind these approaches are quite similar, as they both involve iterative decomposition of matrix components. Unlike the methods discussed in previous chapters, subspace tracking methods require larger input sizes, as smaller matrices may not adequately reveal the signature of the sparse component. Furthermore, the ALM-based techniques proposed here are well-suited for processing regular GPR profiles through a series of rank reduction steps, using a Sobel operator-based edge detection approach in this chapter. Experimental results demonstrate the significant potential of subspace tracking techniques for various applications.

References

[1] W.W. Bradbury, R.Fletcher. “New iterative methods for solution of the eigenproblem.” *Numer. Math.* vol. 9, pp.259–267.1966.

[2] F. Wang, C. Yu, S. Li, M. Su and Y. Liu, "An Adaptive Regularized Subspace Pursuit based Variable Step-size Method for Power Amplifier Sparse Model Selection," *Proc. of 2021 IEEE MTT-S International Wireless Symposium* , Nanjing, China, 2021, pp. 1-3.

[3] M. Chagmani, B. Xerri, B. Borloz and C. Jauffret, "The constrained stochastic matched filter subspace tracking," *Proc. of the 10th International Symposium on Image and Signal Processing and Analysis*, Ljubljana, Slovenia, 2017, pp. 205-209.

[4] Valizadeh, R. Mohammadian, A. Rafiei and A. Rafati, "A novel algorithm for signal subspace tracking based on a new subspace information criterion," *Proc. of 2007 6th International Conference on Information, Communications & Signal Processing*, Singapore, 2007, pp. 1-4.

[5] N. Lassami, K. Abed-Meraim and A. Aïssa-El-Bey, "Low cost subspace tracking algorithms for sparse systems," *Proc. of 2017 25th European Signal Processing Conference*, Kos, Greece, 2017, pp. 1400-1404.

[6] I.T.Jolliffe, *Principal Component Analysis*. Springer-Verlag .1986.

[7] F. H. C. Tivive, A. Bouzerdoum and C. Abeynayake, "GPR Target Detection by Joint Sparse and Low-Rank Matrix Decomposition," in *IEEE Trans. Geosci. Remote Sens.*, vol. 57, no. 5, pp. 2583-2595, May 2019.

[8] H. Zhou, Z. Mo, Y. Wang and R. Duan, "Low rank reconstruction algorithm for ground penetrating radar linear inverse imaging," *Proc. of IET International Radar Conference 2015*, Hangzhou, 2015, pp. 1-4.

[9] F. H. C. Tivive, A. Bouzerdoum and C. Abeynayake, "GPR signal classification with low-rank and convolutional sparse coding representation," *Proc. of 2017 IEEE Radar Conf.*, Seattle, WA, USA, 2017, pp. 1352-1356.

[10] C. C. Lee, "Elimination of redundant operations for a fast Sobel operator," in *IEEE Trans. Syst. Man Cybern. A Syst. Hum.*, vol. SMC-13, no. 2, pp. 242-245, March-April 1983.

Chapter 7. Conclusions

This work focuses on the near field modified subspace methods following two problems:

- Compensation for the arrival time /phase errors.
- Complexity deduction.

In Chapter 4, this work uses the stationary points search method to run through all possible combinations of the arrival time from each channel. In other words, the proposed method fully relies on the steering matrix of the MUSIC algorithm and assumed that only certain combinations could generate the orthogonality, which is our target on the spectrum. This method has obvious advantages and disadvantages; the advantage is shown in the road pavement experiment, where the hidden layer can be revealed and the accuracy of the proposed method is much higher than the conventional method. However, because all the stationary points are considered to be related to the possible arrival time, the computation complexity is extremely high, which leads to the second problem as mentioned. To tackle this problem, optimization techniques are applied to avoid the two-dimensional scan process in the near field MUSIC. However, an initial guess is required for the optimization techniques, to solve this problem, we utilize the boundary between the near field and far field as a rational range to generate the initial guess to allow the optimization-based MUSIC to be executed automatically.

Besides, GSVD and GEVD based MUSIC are discussed in this work as they are classical approaches for handling the abnormal covariance matrix with phase errors as we assumed. In this work, some modifications are made to simplify the process of using these advanced and time-consuming matrix decompositions. In addition, the resolution of the near field MUSIC is discussed. However, due to the special assumptions we made, the resolution has no upper limit if the arrival time information is precisely evaluated. Thus, it can be considered in such a way that super-resolution imaging can be achieved by using relatively weaker hardware platform, as proof, we bring an SDR array experiment to verify the idea, which shows the feasibility of the study.

In Chapter 5, near field ESPRIT method is introduced as an opening to the LS method.
The problems are transformed from the non-constrained optimizations to the constrained ones, and the Lagrange multiplier is first introduced in this chapter. Unlike the approaches we used in the previous chapter, the TLS based ESPRIT mathematically considers the error in the covariance matrix and tries to obtain an approximation solution to the ground truth. A classical sphere reflector experiment is performed and both the near-field MUSIC and TLS near field MUSIC are tested. Note that, we applied conventional ISSM MUSIC approaches for the wideband signal, and the results show that both algorithms outperform conventional SAR imaging in terms of the localization purpose.

In Chapter 6, following the constrained optimization techniques mentioned previously, subspace tracking or updating techniques are introduced. With the concern of the novelty, this work introduces a recent trending imaging processing technique low-rank matrix recovery to solve the conventional subspace tracking problem for the DOA estimation. Because, fundamentally, the kernel iterations of the ALM based low rank matrix recovery process is highly like subspace tracking. Numerical simulations are carried out, and they show the versatility of the ALM based algorithm. Moreover, as a bonus work, we use edge detection techniques to reduce the rank of the GPR profile, and it allows the implementation of the proposed method not only for the array signal processing but for more universal uses.

In conclusion, two important points can be made. Firstly, to compensate for the phase errors caused by signal arrival, techniques based on TLS method are preferable. This is because they have a mathematical proof for handling contaminated elements in the matrix A when solving the system Ax=b. Secondly, optimization techniques are a more efficient approach compared to the conventional, time-consuming spectra plotting for DOA purposes. However, it is worth noting that this study focuses specifically on the near field case. It is important to consider that the some techniques used in this work may be outdated compared to the latest theories and practices in the optimization field.

Publication list

Journals

[1] C. Zhou and M. Sato, "MUSIC-Based Super-Resolution CMP Velocity-Depth Analysis for Multilayer Cases," in *IEEE Geoscience and Remote Sensing Letters*, vol. 20, pp. 1-5, 2023. (Chapter 4, Section 4.7.3)

[2] Changyu Zhou, Motoyuki Sato, "Simplex based MUSIC for solving coherent signal," *IEICE Communications Express*, vol.10, no. 9, p. 641-646, 2021. (Chapter 4, Section 4.4).

Conference

[1] Changyu Zhou, Motoyuki Sato, "MUSIC-Based Super Resolution CMP Velocity-depth Analysis for Multi-layer Cases" presented in *URSI-JRSM* , Tokyo, Japan, Sep.1-2,2022.(Oral presentation. Chapter 4, Section 4.7.3)

[2] Changyu Zhou, Motoyuki Sato "An Novel MUSIC based CMP analysis" in *URSI AT-AP RASC 2022*, Gran Canaria, Spain, May. 29-Jun. 3, 2022.(Online presentation. Chapter 4, Section 4.6)

[3] Changyu Zhou, Tomohiro Kondo "Simplex based 2D MUSIC for Localization of RF sources" presented in *ISAP 2020*, Osaka, Japan, Jan. 25-28, 2021. (Online presentation. Chapter 4, Section 4.7.4)

Awards

[1] First prize, Changyu Zhou, Tomohiro Kondo "Simplex based 2D MUSIC for Localization of RF sources," in Student paper contest RF source localization section, International Symposium on Antennas and Propagation (ISAP) 2020,Osaka,Japan.

[2] Best presentation award, Changyu Zhou, Tomohiro Kondo "Simplex based 2D MUSIC for Localization of RF sources," in Student paper contest, International Symposium on Antennas and Propagation (ISAP) 2020, Osaka, Japan.

Acknowledgement

I would like to express my deep gratitude to my advisor, Professor Sato Motoyuki, for his guidance, support, and encouragement throughout my graduated level studies in all these years. His wisdom, passion and experience have been invaluable, and I am deeply honored to have had such a stage provided by him to be trained and educated.

I would also like to say thank you to all my committee members Professor Takahashi Hiroshi, Professor Okamoto Atsushi, Chen Qiang, and Professor Yamada Hiroyoshi. Their expertise, and informative feedback on my work gives it vast improvement.

I am grateful to the JST SPRING, Grant Number JPMJSP2114 for providing financial support for my research.

I would like to extend a special thanks to my family and friends for their love and support throughout the years.

Lastly, I would like to express my appreciation to my fiancée Ding Yi. Till now, I cannot believe that I am this blessed to have such a lover in my life. I hope this dissertation can be the record of our love, a flower of eternity.

Without the help and support of all these individuals and organizations, this dissertation would not have been possibly accomplished.